NASA Technical Paper 2234

December 1983

Effect of Thrust Reverser Operation on the Lateral-Directional Characteristics of a Three-Surface F-15 Model at Transonic Speeds

E. Ann Bare and
Odis C. Pendergraft, Jr.

NASA

25th Anniversary
1958-1983

NASA
Technical
Paper
2234

1983

Effect of Thrust Reverser Operation on the Lateral-Directional Characteristics of a Three-Surface F-15 Model at Transonic Speeds

E. Ann Bare and
Odis C. Pendergraft, Jr.

Langley Research Center
Hampton, Virginia

NASA
National Aeronautics
and Space Administration

**Scientific and Technical
Information Branch**

1983

SUMMARY

An investigation was conducted in the Langley 16-Foot Transonic Tunnel to determine the lateral-directional aerodynamic characteristics of a fully metric 0.047-scale model of the F-15 three-surface configuration (canards, wing, horizontal tails) with twin nonaxisymmetric or two-dimensional (2-D) nozzles and twin axisymmetric nozzles installed. The effects of 2-D nozzle in-flight thrust reversing and rudder deflection were also determined. Test data were obtained at static conditions and at Mach numbers from 0.60 to 1.20 over an angle-of-attack range from -2° to 15°. Reynolds number varied from 2.6×10^6 to 3.8×10^6. Angle of sideslip was set at approximately 0° and -5° for all configurations and at approximately -10° for selected configurations.

Results of the investigation indicate that thrust reversing had only small effects on lateral-directional stability and directional control at the subsonic/transonic flight speeds tested. The configuration with axisymmetric nozzles was slightly more stable than the configuration with two-dimensional convergent-divergent nozzles.

INTRODUCTION

Recent studies of twin-engine fighter aircraft (refs. 1 to 5) have identified a number of potential advantages of nonaxisymmetric nozzles as compared to conventional round or axisymmetric nozzles. One important benefit of nonaxisymmetric nozzles is the adaptability of the design to include thrust vectoring and reversing with less weight penalty than conventional axisymmetric nozzles (refs. 5 and 6). The addition of thrust reversing capabilities to most current and future fighter aircraft would greatly enhance short field take-off and landing (STOL) performance. Also, the use of in-flight thrust reversing has the potential to improve airplane agility during air-to-air combat.

The performance of nonaxisymmetric nozzle thrust reversers at static and subsonic flight conditions has been determined in several experimental investigations (refs. 7 to 12). These results indicate that highly efficient nonaxisymmetric nozzles with thrust reversers can be designed. However, use of the in-flight thrust reverser could cause significant changes in airplane tail loads, particularly for twin-vertical-tail configurations (ref. 13) and could also degrade the control effectiveness of horizontal-tail (ref. 11) and rudder surfaces (ref. 14).

A 0.047-scale sting-mounted aerodynamic model of the F-15 three-surface configuration (canards, wing, horizontal tails) with the correct inlet shape and mass flow was previously tested in the 16-Foot Transonic Tunnel, and the results are reported in reference 15. Aerodynamic force and moment corrections for the sting-mounted aerodynamic model (canards off) data to account for axisymmetric nozzle-exhaust flow can be found in reference 16. Sting interference and aft-end distortion corrections for the aerodynamic model without canards can be found in reference 17, and the effects of aft-end modifications on the same aerodynamic model, such as vertical tail size and dorsal fin addition, can be found in reference 18. The longitudinal aerodynamic data and the static nozzle performance data for the subject model (three-surface F-15) of this report are presented in reference 19.

The purpose of the present investigation was to determine the effect of thrust reversing on the lateral-directional aerodynamic characteristics of a three-surface F-15 propulsion model (canards, wing, horizontal tails) having faired-over inlets. The model was tested with axisymmetric nozzles installed and with two-dimensional convergent-divergent (2-D C-D) nozzles installed. Each nozzle type was tested in the positive-thrust mode, and the 2-D C-D nozzles were also tested in partial and full reverse-thrust modes.

This investigation was conducted in the Langley 16-Foot Transonic Tunnel at static conditions and at Mach numbers from 0.60 to 1.20. Reynolds number varied from 2.6×10^6 to 3.8×10^6; angle of attack was varied from -2° to 15°. Angle of sideslip was set at approximately 0° and -5° for the axisymmetric nozzle configuration and at approximately 0°, -5°, and -10° for several of the 2-D C-D nozzle configurations. Nozzle pressure ratio was varied from jet off (1.0) to about 6.5 depending on Mach number. Differential thrust reversing and the effect of rudder deflection were also investigated. Further information on the installation of two-dimensional nozzles on the F-15 can be found in reference 20.

SYMBOLS

A_e nozzle-exit area, cm^2

A_t nozzle-throat area, cm^2

b wing span, 0.612 m

$\bar{c}$ mean aerodynamic chord, cm

C_Y side-force coefficient, $\frac{\text{Total side force}}{q_\infty S}$

C_{Y_β} side-force parameter, $\frac{\Delta C_Y}{\Delta \beta}$ (from pitch tests at $\beta \approx 0°$ and -5°), per deg

C_l rolling-moment coefficient, $\frac{\text{Total rolling moment}}{q_\infty Sb}$

C_{l_β} lateral-stability parameter, $\frac{\Delta C_l}{\Delta \beta}$ (from pitch tests at $\beta \approx 0°$ and -5°), per deg

C_n yawing-moment coefficient, $\frac{\text{Total yawing moment}}{q_\infty Sb}$

C_{n_β} directional-stability parameter, $\frac{\Delta C_n}{\Delta \beta}$ (from pitch tests at $\beta \approx 0°$ and -5°), per deg

$C_{n_{\delta_R}}$ rudder power, $\frac{\Delta C_n}{\Delta \delta_R}$ (from pitch tests with $\delta_R = 0°$ and -10°), per deg

M free-stream Mach number

p_a ambient static pressure, Pa

q_∞ free-stream dynamic pressure, Pa

S wing reference area, 0.124 m^2

α angle of attack, deg

β angle of sideslip, deg

δ_R rudder deflection angle (negative right), deg

δ_{REV} nozzle thrust-reverser flap angle, deg (fig. 10)

Abbreviations:

ASME American Society of Mechanical Engineers

B.L. butt line, cm

C-D convergent-divergent

F.S. fuselage station, cm

L.E. leading edge

L.H. left hand

NPR nozzle pressure ratio, $\frac{\text{Jet total pressure}}{\text{Tunnel static pressure}}$

R.H. right hand

W.L. waterline

2-D two-dimensional (nonaxisymmetric)

APPARATUS AND PROCEDURE

Wind Tunnel

This investigation was conducted in the Langley 16-Foot Transonic Tunnel, which is a single-return, continuous-flow, atmospheric wind tunnel with a slotted, octagonal test section measuring 4.8 m diametrically to midflat center line. With the aid of a compressor system, which draws air out through slots in the test section for $M > 1.05$, the test-section airspeed is continuously variable between Mach numbers of 0.20 and 1.30. Further details on dimensions and the operating characteristics of the Langley 16-Foot Transonic Tunnel can be found in reference 21.

Support System

The model was supported in the tunnel by the sting-strut support system shown in figure 1. High-pressure air lines and all instrumentation were routed through this support system. The complete model was mounted on an internal, six-component strain-gage balance through an adapter to the sting strut. A yaw clutch mechanism (see fig. 2) attached to the strut top was used to yaw the model on the strut.

Propulsion Simulation System

The facility high-pressure air system provided a continuous flow of clean, dry, heated air to the model. This high-pressure air is transferred from a common high-pressure plenum in the front of the model to the nozzles by means of dual flow-transfer assemblies. A sketch of the assembly is shown in figure 2. The two sets of flexible metal bellows (longitudinal) in conjunction with the two side-mounted metal bellows (lateral) serve to minimize pressurization tares while still maintaining sufficient flexibility for proper force balance operation in all six components.

Model

The model used for this investigation was a 0.047-scale model of an F-15 three-surface configuration (canards, wing, horizontal tails). This model is a fully metric jet-effects model with faired-over inlets to allow propulsion simulation. A sketch of the model is shown in figure 3. Figure 4 shows a photograph of the model installed in the Langley 16-Foot Transonic Tunnel. Model geometric characteristics are given in table I. The configuration is characterized by boom-mounted twin vertical tails (toe angle, L.E. out, of 2°), aft-located boom-mounted horizontal tails, closely spaced twin engines, and forward inlet-mounted canards. For this investigation, the canards were set at a nominal angle of -6° (leading edge down) - the minimum drag angle for subsonic cruise flight as determined from unpublished wind-tunnel data. The internal transition duct (from round to rectangular cross section for the 2-D C-D nozzles) was terminated at fuselage station 91.592, which was the common connect point for all two-dimensional nozzles. External hardware interfairings were added to adapt the model afterbody for smooth integration of the rectangular nozzle shape with 2-D C-D nozzles installed. The axisymmetric nozzles used an externally tapered ring to fair between F.S. 93.259 and F.S. 94.488.

Baseline axisymmetric nozzles.- A sketch of the dry-power axisymmetric nozzle showing its geometry is given in figure 5. A sketch and the coordinates of the fixed shroud around the nacelle ahead of the movable nozzle boattails (movable on flight hardware only) are given in figure 6. For this investigation, only the dry-power nozzle flap positions were tested, using fixed nozzle hardware.

Two-dimensional convergent-divergent nozzles.- The 2-D C-D nozzle design used for the current test simulates a variable-area internal expansion nozzle. The throat area and the exit area of the full-scale hardware would be independently controlled by the separate actuation of the convergent and divergent nozzle flaps. Thrust reversal would be accomplished by actuation of the convergent flaps, closing the throat area while simultaneously opening the reverse flow ports upstream. For a complete description of this nozzle mechanism, see reference 8.

A photograph of the two-dimensional convergent-divergent nozzles installed on the F-15 model is shown in figure 7. A sketch of the forward-thrust, dry-power 2-D C-D nozzle is shown in figure 8. The nozzle has fixed, straight (parallel inside surface) sidewalls which represent sidewalls that do not change shape as the nozzle power setting changes. Thus, when the nozzle boattail flaps (top and bottom) are closed down to cruise or dry-power setting, the sidewalls form channels over the flap surfaces. (See photograph in fig. 7.) A variable geometry sidewall would be required to eliminate these channels.

Figure 9 is a photograph of the fully deployed 2-D C-D thrust reversers installed on the F-15 model. Sketches of the two reverser deployments tested are shown in figure 10. The partially deployed reverser ($\delta_{REV} = 90°$) was designed to spoil all forward thrust, while the fully deployed reverser ($\delta_{REV} = 130°$) was designed to produce approximately 50 percent reverse thrust at $M = 0$.

Instrumentation

Model forces and moments, including nozzle thrust contributions, were measured by an internal six-component strain-gage balance. Internal cavity pressures were measured at two locations forward and two locations aft of the yaw clutch. The mass-flow rate (both nozzles) was measured by a turbine flow meter (external to the tunnel). The flow conditions in each nozzle were determined by two total-pressure probes - one from the top and one from the side of each tailpipe - and one total-temperature probe in each nozzle. All pressures were measured with individual pressure transducers.

Tests

Test data were taken at Mach numbers of 0.60 and 0.90 for all configurations and at 1.20 for selected configurations. Angle of attack was varied from -2° to 15° depending upon Mach number; nozzle pressure ratio varied from approximately 1.0 (jet off) to about 6.5 depending upon Mach number. Data were taken at a nominal sideslip angle β of 0° for all configurations and at -5° and -10° for selected configurations. The model was preset at a selected sideslip angle before each run by fixing the model on the yaw clutch mechanism. Basic data were obtained by holding nozzle pressure ratio constant and varying angle of attack. Undeflected rudders were tested with all configurations, and selected configurations were tested with the rudders deflected at -10°.

Boundary-layer transition was fixed on the model by means of 0.25-cm-wide strips of No. 120 carborundum grit. These strips were located 1.91 cm aft (streamwise) of the nose and the inlet fairings. Transition strips were also located on all lifting surfaces at 5 percent of the local chord. The methods described in references 22 and 23 were used to determine the locations of these strips and the grit size.

Data Reduction

All data for both the model and the wind tunnel were recorded simultaneously on magnetic tape. For each data point, approximately 50 frames of data, taken at a rate of 10 frames per second, were used to obtain average recorded data. The average data were used to compute standard force and moment coefficients using wing area and span for reference area and length. Corrections were made to the force data to account for bellows/balance interaction tares (refs. 7 and 11). In addition, balance corrections were also made to account for internal cavity pressure/area tares.

Model angle of attack and sideslip were corrected by applying sting deflection terms caused by bending under aerodynamic load. A flow angularity adjustment of 0.1°, which is the average upflow angle measured in the Langley 16-Foot Transonic

Tunnel, was applied to angle of attack. No sideflow angle adjustment was made; however, past experience has shown sideflow in the 16-Foot Transonic Tunnel to be generally 0.1° or less.

Mass-flow rate through the nozzles was determined by using total-pressure and total-temperature measurements in the flow-transfer assemblies and flow constants determined from pretest calibrations with ASME standard nozzles.

Jet total-pressure profiles were determined for axisymmetric nozzles and the 2-D C-D nozzles with straight sidewalls by use of movable Kiel probes (total pressure). Each internal total-pressure probe was corrected to the integrated value of jet total pressure at the nozzle throat.

PRESENTATION OF RESULTS

The results of this investigation are presented in plotted coefficient form. Unless otherwise noted on the figures, data are for the baseline configuration with boom-mounted twin vertical tails (toe angle, L.E. out, of 2°) and boom-mounted horizontal tails at 0° deflection.

The basic lateral-directional performance data for all configurations are presented in the following figures:

DISCUSSION

Basic Data

Forward-thrust mode.- The lateral-directional characteristics of the three-surface F-15 configuration with the nozzles in the forward-thrust mode are presented in aerodynamic coefficient form, including thrust contributions if any, in figures 11 to 17. Data are shown at $\beta = 0°$ in figures 11, 13, 16, and 17, at $\beta = -5°$ in figures 12 and 14, and at $\beta = -10°$ in figure 15. The data are plotted versus angle of attack at constant sideslip angle and at various nozzle pressure ratios. For $\beta = 0°$ a symmetrical model (left to right) with the lateral-directional control surfaces set at 0° should have lateral-directional force and moments of zero. However, for this configuration (figs. 11 and 13), the data show that small values were measured for each lateral-directional component. Possible reasons for these values are small differences in model symmetry or slight misalignment. Since most of the conclusions of this study are based on incremental data from $\beta = 0°$, it is believed that these small values will not affect the results.

For the baseline axisymmetric nozzle configuration, operation of the jet had little or no effect on the lateral-directional coefficients for $\beta = 0°$ (fig. 11) or $\beta = -5°$ (fig. 12). Since there was little or no effect, these data also indicate

that the axisymmetric nozzles were properly aligned and of equal thrust. For the forward-thrust 2-D C-D nozzle configuration, jet operation produced similar results, that is, little or no effect on the basic lateral-directional characteristics at $\beta = 0°$ (fig. 13), $\beta = -5°$ (fig. 14), and $\beta = -10°$ (fig. 15).

Comparing the data in figures 13 to 15 shows increasing side-force coefficient, more negative yawing moment (except at $M = 0.90$ above $\alpha = 10°$), and more positive rolling moment as the sideslip angle becomes more negative. This would be expected for a laterally and directionally stable aircraft.

The effect of NPR on the lateral-directional characteristics of the configuration with 2-D C-D nozzles and rudder deflected -10° is shown in figure 16. Jet operation had only small effects on all parameters, as was previously noted for the other configurations with 2-D C-D nozzles and undeflected rudders. Comparing figure 16 with figure 13 shows, as would be expected, that deflecting the rudder produces more negative side force and a large positive increase in yawing-moment coefficient.

Data for the configuration with 2-D C-D nozzles and vertical tails removed are presented in figure 17. The effects of jet operation are similar to those already noted for the same configuration with vertical tails installed (fig. 13). Note that removing the vertical tails causes a change in sign of the yawing-moment coefficient. (Compare fig. 17 with fig. 13.) This yawing-moment shift can be largely attributed to a misalignment of the vertical tails since the vertical-tails-off, side-force data are nearer zero. This would also explain the small lateral-directional force and moments at $\beta = 0°$ noted earlier.

Reverse-thrust mode.- Lateral-directional characteristics of the configuration with 2-D C-D nozzles with partially deployed thrust reversers ($\delta_{REV} = 90°$) are presented in figures 18 and 19. Jet operation of the partially deployed thrust reversers at $\beta = 0°$ has little effect on the rolling-moment and side-force coefficients. Yawing-moment coefficient shows little effect at $M = 0.60$; however, the yawing-moment coefficient is reduced at $M = 0.90$ and $M = 1.20$. As sideslip angle is decreased to -5°, there is a greater effect of NPR on yawing moment. At sideslip the inboard surface of the windward vertical tail is sheltered from the free-stream flow, and the decrease in yawing moment is probably due to the impingement of the reverse flow plume on this inboard surface of the vertical tail. Side-force coefficient is unaffected by operation of the jet, and there is a slight reduction in rolling moment.

The effect of fully deployed thrust reversers ($\delta_{REV} = 130°$) on the lateral-directional characteristics of the configuration with 2-D C-D nozzles is presented in figures 20 to 22. As shown by figure 20, full deployment increases the effect of jet operation on yawing moment at $\beta = 0°$. (Compare with fig. 18.) There is also some small effect on rolling-moment and side-force coefficients. However, as angle of sideslip is decreased to -5° (fig. 21), there is no corresponding increase in the effect of reverser operation on yawing moment as was noted for reverser partially deployed ($\delta_{REV} = 90°$). In fact, there is a decrease in the magnitude of the effect of NPR on yawing moment at $\beta = -5°$. The trend of yawing moment with angle of attack is also different with thrust reverser fully deployed. At higher angles of attack (above 12° at $M = 0.60$, and above 8° at $M = 0.90$), yawing moment increases with increasing NPR. At a sideslip angle of -10° (fig. 22), the crossover in yawing moment occurs at $\alpha = 0°$. At $\beta = -5°$, jet operation caused a slight decrease in side-force coefficient and a significant reduction in rolling-moment coefficient

(fig. 21). The effect increases with decreasing angle of sideslip (fig. 22), particularly on rolling-moment coefficient. These trends indicate that the jet plumes from the fully deployed thrust reversers ($\delta_{REV} = 130°$) influence the vertical tails and afterbody, and also the wing.

The effects of differential reversing on the lateral-directional characteristics are presented in figure 23. Differential reversing was simulated by operating the left-hand nozzle in the forward-thrust mode ($\delta_{REV} = 0°$) and by operating the right-hand nozzle with thrust reverser fully deployed ($\delta_{REV} = 130°$). Data are shown at $M = 0$ in figure 23(a) to indicate the magnitude of the static thrust contribution to each lateral-directional component as a function of NPR. Side-force coefficient varied from approximately 0, jet off, to a maximum of -0.0016 at NPR = 5.0; yawing-moment coefficient increased from 0 to 0.0024 at NPR = 6.2. Rolling-moment coefficient remained essentially 0. At static conditions ($M = 0$), computed coefficients are based on the ambient static pressure since the dynamic pressure is 0 at $M = 0$; for example,

$$C_{n|M=0} = \frac{\text{Total yawing moment}}{p_a Sb}$$

The values of jet total pressure equivalent to the operating NPR at $M = 0.60$ and $M = 0.90$ are indicated in figure 23(a). At $M = 0.60$ (fig. 23(b)), differential thrust reversing causes an increase in side force and rolling moment and a decrease in yawing moment. The trends of yawing moment and side force are opposite those expected from the static thrust contributions. In addition, no effect on rolling moment would be expected. Thus, the trends observed at $M = 0.60$ indicate an interaction of the differential reverse flow with the external aerodynamics which more than offsets the thrust contribution. At $M = 0.90$ (fig. 23(c)), differential thrust reversing has a larger effect on yawing moment and a smaller effect on side force than observed at $M = 0.60$, thus indicating that the jet-plume/free-stream flow interactions are very Mach number dependent.

The lateral-directional characteristics of the configuration with deflected rudders ($\delta_R = -10°$) and deployed thrust reverser are shown in figure 24 ($\delta_{REV} = 90°$) and figure 25 ($\delta_{REV} = 130°$). Operation of the thrust reversers with deflected rudders (figs. 24 and 25) produced trends similar to those discussed previously for the same configurations with $\delta_R = 0°$ (figs. 18 and 20). Side-force and rolling-moment coefficients are only slightly affected. The reduction in yawing moment for reverser partially deployed is slightly greater than noted for undeflected rudder ($M = 1.20$); however, a greater reduction in yawing-moment coefficient occurred at all Mach numbers with the reverser operating in its fully deployed position.

Figures 26, 27, and 28 present the effects of removing empennage surfaces (vertical tails only, horizontal tails only, and both vertical and horizontal tails) for the configuration with thrust reversers fully deployed ($\delta_{REV} = 130°$). With the vertical tails removed (fig. 26), operation of the jet has very little effect on the lateral-directional characteristics at either $M = 0.60$ or $M = 0.90$. This was also the case for all tails removed (fig. 28). When the horizontal tails are removed (fig. 27), the lateral-directional characteristics are very similar to those with all tails in place. (Compare fig. 27 with fig. 20.) This would indicate that most of the thrust reversing effects on the lateral-directional characteristics are associated with the reverse-thrust jet-plume interaction with the flow field and that there is some misalignment in the installation of the vertical tails.

Comparison and Summary Data

Static stability derivatives.- Figures 29 and 30 show the effect of jet operation on the static stability derivatives for the configuration with axisymmetric nozzles and with 2-D C-D nozzles. In general, jet operation shows no effect on the dihedral effect $\left(C_{l_\beta}\right)$. Directional stability $\left(C_{n_\beta}\right)$ shows little or no effect of jet operation at $M = 0.60$. At $M = 0.90$, there is a small increase in the directional stability with jet operation.

Figure 31 shows the effect of afterbody/nozzle shape on static stability derivatives. Dihedral effect is unaffected, while the configuration with axisymmetric nozzles is more directionally stable at both $M = 0.60$ and $M = 0.90$.

Figures 32 and 33 show the effects of jet operation on the static stability derivatives of the 2-D C-D configurations with thrust reversers deployed. As would be expected, jet operation had a larger effect with reverser deployed than with reverser stowed. The impact of reverser operation is particularly evident on the directional-stability derivative C_{n_β}. Directional stability is generally increased by thrust reverser operation at low angles of attack. At higher angles of attack, jet operation produces a smaller increase in directional stability to the point that the jet-on curve crosses the jet-off curve and a decrease in directional stability occurs (figs. 32(b) and 33). The crossover point of the jet-on and jet-off directional-stability curves tends to move to a lower angle of attack with increasing Mach number and increasing reverser deployment. In figure 32(a) the curves do not cross, but it is expected that at a higher angle of attack they probably would. The increase in directional stability at low angles of attack is probably due to a blockage of the free-stream flow by the reverse flow plume which causes an increase in vertical-tail side force (ref. 20). This is particularly evident (fig. 32) for the reverser partially deployed ($\delta_{REV} = 90°$) as most of the reverse flow is contained between the vertical tails. With increasing angle of attack, directional stability (jet off and jet on) decreases as a smaller area of the vertical tail is exposed to the free-stream flow. During reverser operation, there is also increasing impingement by the reverse flow plume inboard of the windward vertical tail which causes an even sharper loss in stability. The configuration becomes directionally unstable with the reverser fully deployed at $M = 0.90$ and $\alpha > 12°$.

There is a slight decrease in the dihedral effect with the operation of the thrust reversers partially deployed (fig. 32). There is a somewhat larger decrease in dihedral effect with the thrust reversers fully deployed (fig. 33). The reverser exhaust exit ports are located a short distance aft of the wing trailing edge. The results shown in figures 32 and 33 indicate interference effects of the reverse flow plume on the wing flow field causing a loss in lift on the windward wing. As would be expected, the effect of jet operation increases with increasing reverser deployment.

Figure 34 summarizes the effect of thrust reverser deployment on the lateral-directional stability derivatives at operating NPR. The same effects already noted are seen when partially and fully deployed thrust reversers are compared with reverser stowed at operating NPR.

Rudder directional-control effectiveness.- A major concern of using in-flight thrust reversers is the effect of the reverse flow on control surfaces, such as the rudder or vertical tail, and horizontal tails. (See ref. 7.) When rudders are deflected on the twin vertical tails, one is deflected inboard between the vertical

tails and one is deflected outboard of the vertical tail. Figures 35 to 37 show the effect of jet operation on rudder control power. Jet operation with the reverser stowed caused an increase in rudder power at $M = 0.60$ but had only small effects at $M = 0.90$ and 1.20. With thrust reversers partially and fully deployed, jet operation causes a decrease in rudder power. As might be expected, the effect of jet operation tends to increase with increasing reverser deployment. Figure 38 summarizes the effect of thrust reversing on rudder directional-control effectiveness at operating NPR. Since the reverser exhaust exit ports are located forward of the rudder, there should be no reverser exhaust flow impingement on the rudder. Any effect of the thrust reverser on rudder control effectiveness probably results from blockage of the free-stream flow by the reverse flow plumes. As would be expected, the largest loss in rudder effectiveness occurred at the lowest Mach number, 0.60, with essentially no effect at $M = 1.20$. The loss in rudder effectiveness due to thrust reversing, though noticeable, would probably not greatly affect the handling qualities of the F-15. There is also no indication of the total loss in the control-surface effectiveness, as was noted in reference 7, for a general research afterbody model with the vertical tails located forward of the reverser exit ports.

CONCLUSIONS

An investigation has been conducted in the Langley 16-Foot Transonic Tunnel to determine the lateral-directional aerodynamic characteristics of a fully metric 0.047-scale model of the F-15 three-surface configuration (canards, wing, horizontal tails) with twin two-dimensional (2-D) nozzles and twin axisymmetric nozzles installed. The effects of 2-D nozzle in-flight thrust reversing and rudder deflection were also determined. Test data were obtained at static conditions and at Mach numbers from 0.60 to 1.20 over an angle-of-attack range from -2° to 15°. Angle of sideslip was set at approximately 0° and -5° for all configurations and at approximately -10° for selected configurations. Results from this investigation indicate the following:

1. Differential reversing (left-hand reverser stowed, right-hand reverser fully deployed) reduced yawing moment for Mach 0.60, an opposite effect from that expected from the static thrust contribution. This indicates that the effect of the jet-plume flow interacting with the free-stream flow on external aerodynamics more than offsets the thrust contribution for each component.

2. The configuration with axisymmetric nozzles was slightly more directionally stable than the configuration with two-dimensional convergent-divergent nozzles.

3. Directional stability is generally increased by jet operation with thrust reverser deployed at low angles of attack. The increase in stability becomes small at increasing angles of attack until the jet-on curve crosses the jet-off curve and a decrease in directional stability occurs. This crossover point tends to move to a lower angle of attack with increasing Mach number.

4. Dihedral effect is decreased slightly by thrust reverser deployment.

5. Directional control power is reduced by jet operation with thrust reversers deployed, but probably not enough to be significant in aircraft handling qualities.

Langley Research Center
National Aeronautics and Space Administration
Hampton, VA 23665
October 18, 1983

REFERENCES

1. Martens, Richard E.: F-15 Nozzle/Afterbody Integration. J. Aircr., vol. 13, no. 5, May 1976, pp. 327-333.

2. Hiley, P. E.; Wallace, H. W.; and Booz, D. E.: Nonaxisymmetric Nozzles Installed in Advanced Fighter Aircraft. J. Aircr., vol. 13, no. 12, Dec. 1976, pp. 1000-1006.

3. Berrier, Bobby L.; Palcza, J. Lawrence; and Richey, G. Keith: Nonaxisymmetric Nozzle Technology Program - An Overview. AIAA Paper 77-1225, Aug. 1977.

4. Capone, Francis J.: The Nonaxisymmetric Nozzle - It Is for Real. AIAA Paper 79-1810, Aug. 1979.

5. Miller, Eugene H.; and Protopapas, John: Nozzle Design and Integration in an Advanced Supersonic Fighter. AIAA Paper 79-1813, Aug. 1979.

6. Stevens, H. L.: F-15/Nonaxisymmetric Nozzle System Integration Study Support Program. NASA CR-135252, 1978.

7. Capone, Francis J.; and Maiden, Donald L.: Performance of Twin Two-Dimensional Wedge Nozzles Including Thrust Vectoring and Reversing Effects at Speeds up to Mach 2.20. NASA TN D-8449, 1977.

8. Capone, Francis J.: Static Performance of Five Twin-Engine Nonaxisymmetric Nozzles With Vectoring and Reversing Capability. NASA TP-1224, 1978.

9. Hiley, P. E.; Kitzmiller, D. E.; and Willard, C. M.: Installed Performance of Vectoring/Reversing Nonaxisymmetric Nozzles. J. Aircr., vol. 16, no. 8, Aug. 1979, pp. 532-538.

10. Pendergraft, O. C.: Comparison of Axisymmetric and Nonaxisymmetric Nozzles Installed on the F-15 Configuration. AIAA Paper 77-842, July 1977.

11. Capone, Francis J.; and Berrier, Bobby L.: Investigation of Axisymmetric and Nonaxisymmetric Nozzles Installed on a 0.10-Scale F-18 Prototype Airplane Model. NASA TP-1638, 1980.

12. Re, Richard J.; and Berrier, Bobby L.: Static Internal Performance of Single Expansion-Ramp Nozzles With Thrust Vectoring and Reversing. NASA TP-1962, 1982.

13. Bare, E. Ann; Berrier, Bobby L.; and Capone, Francis J.: Effect of Simulated In-Flight Thrust Reversing on Vertical-Tail Loads of F-18 and F-15 Airplane Models. NASA TP-1890, 1981.

14. Capone, Francis J.; Re, Richard J.; and Bare, E. Ann: Thrust Reversing Effects on Twin-Engine Aircraft Having Nonaxisymmetric Nozzles. AIAA-81-2639, Dec. 1981.

15. Henderson, William P.; and Leavitt, Laurence D.: Stability and Control Characteristics of a Three-Surface Advanced Fighter Configuration at Angles of Attack up to 45°. NASA TM-83171, 1981.

16. Berrier, Bobby L.; and Maiden, Donald L.: Effect of Nozzle-Exhaust Flow on the Longitudinal Aerodynamic Characteristics of a Fixed-Wing, Twin-Jet Fighter Airplane Model. NASA TM X-2389, 1971.

17. Maiden, Donald L.; and Berrier, Bobby L.: Effects of Afterbody Closure and Sting Interference on the Longitudinal Aerodynamic Characteristics of a Fixed-Wing, Twin-Jet Fighter Airplane Model. NASA TM X-2415, 1971.

18. Maiden, Donald L.; and Berrier, Bobby L.: Effect of Airframe Modifications on Longitudinal Aerodynamic Characteristics of a Fixed-Wing, Twin-Jet Fighter Airplane Model. NASA TM X-2523, 1972.

19. Pendergraft, Odis C., Jr.; and Bare, E. Ann: Effect of Nozzle and Vertical-Tail Variables on the Performance of a Three-Surface F-15 Model at Transonic Mach Numbers. NASA TP-2043, 1982.

20. F-15 2-D Nozzle System Integration Study. Volume I - Technical Report. NASA CR-145295, 1978.

21. Corson, Blake W., Jr.; Runckel, Jack F.; and Igoe, William B.: Calibration of the Langley 16-Foot Transonic Tunnel With Test Section Air Removal. NASA TR R-423, 1974.

22. Braslow, Albert L.; Hicks, Raymond M.; and Harris, Roy V., Jr.: Use of Grit-Type Boundary-Layer-Transition Trips on Wind-Tunnel Models. Conference on Aircraft Aerodynamics, NASA SP-124, 1966, pp. 19-36. (Also available as NASA TN D-3579.)

23. Braslow, Albert L.; and Knox, Eugene C.: Simplified Method for Determination of Critical Height of Distributed Roughness Particles for Boundary-Layer Transition at Mach Numbers From 0 to 5. NACA TN 4363, 1958.

TABLE I.- MODEL GEOMETRIC CHARACTERISTICS

Overall model length, m	0.93
Wing:	
Span, m	0.612
Area, m^2	0.124
Root chord (theoretical), m	0.33
Tip chord (theoretical), m	0.082
Mean geometric chord, m	0.228
Aspect ratio	3.0
Taper ratio	0.25
Sweepback of leading edge, deg	45
Airfoil section	NACA 64A-series with modified conical camber L.E.
Horizontal tail (exposed each side):	
Span, m	0.113
Area, m^2	0.012
Root chord (theoretical), m	0.165
Tip chord (theoretical), m	0.055
Sweepback of leading edge, deg	50
Airfoil section	NACA 64-series
Vertical tail (exposed each panel):	
Span, m	0.146
Area, m^2	0.013
Root chord, m	0.137
Tip chord, m	0.037
Sweepback of leading edge, deg	36.57
Toe-out angle (baseline only), deg	2
Airfoil section	NACA 64-series
Canard (exposed each panel):	
Span, m	0.088
Area, m^2	0.006
Root chord, m	0.113
Tip chord, m	0.028
Sweepback of leading edge, deg	50
Airfoil section	NACA 64-series
Dihedral angle, deg	20
Rudder (each panel):	
Area, m^2	0.002

L-80-2042

Figure 1.- Photograph showing sting-strut arrangement of 0.047-scale F-15 propulsion model installed in Langley 16-Foot Transonic Tunnel.

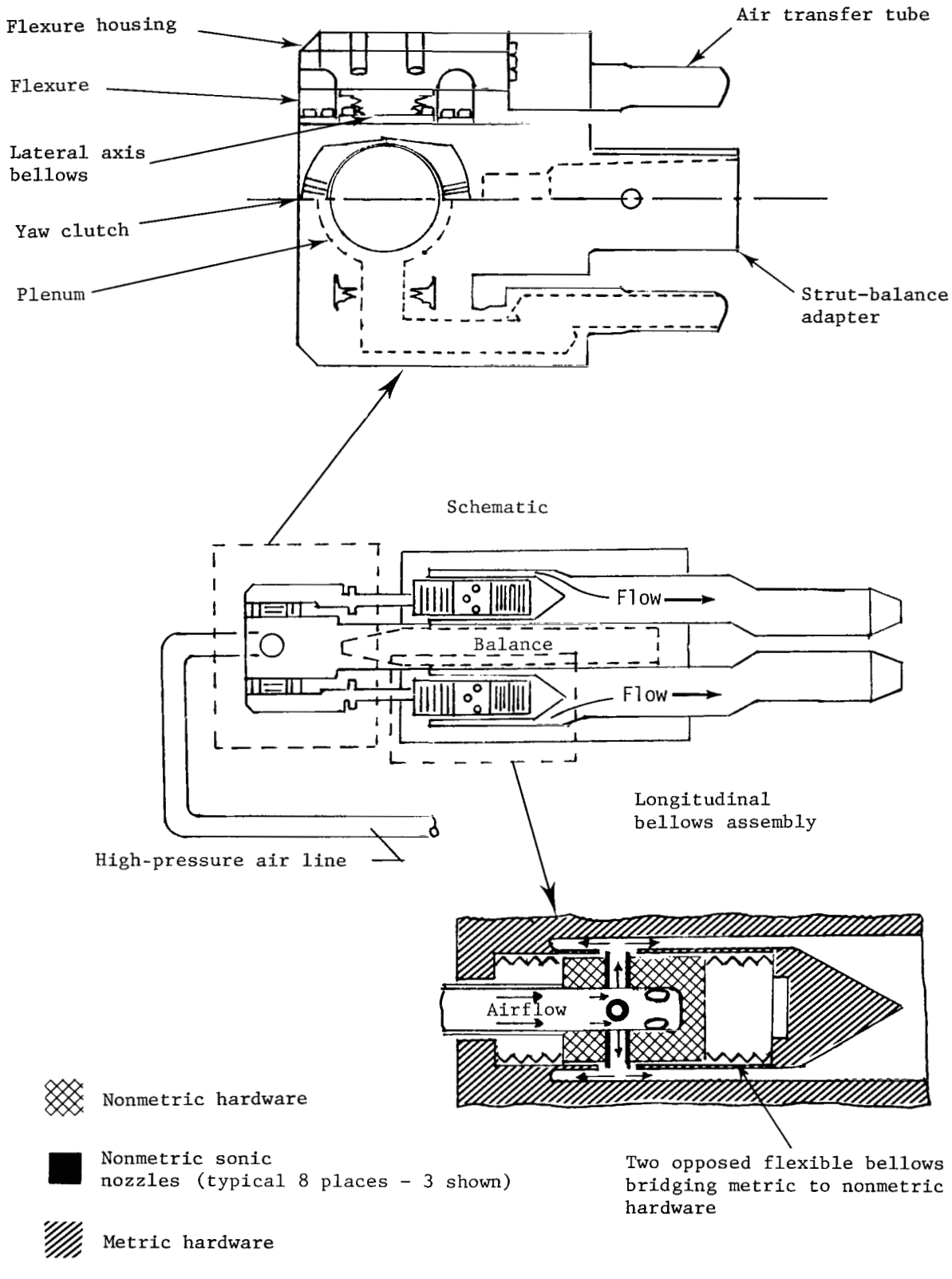

Figure 2.- Sketch showing high-pressure air transfer methods of propulsion system.

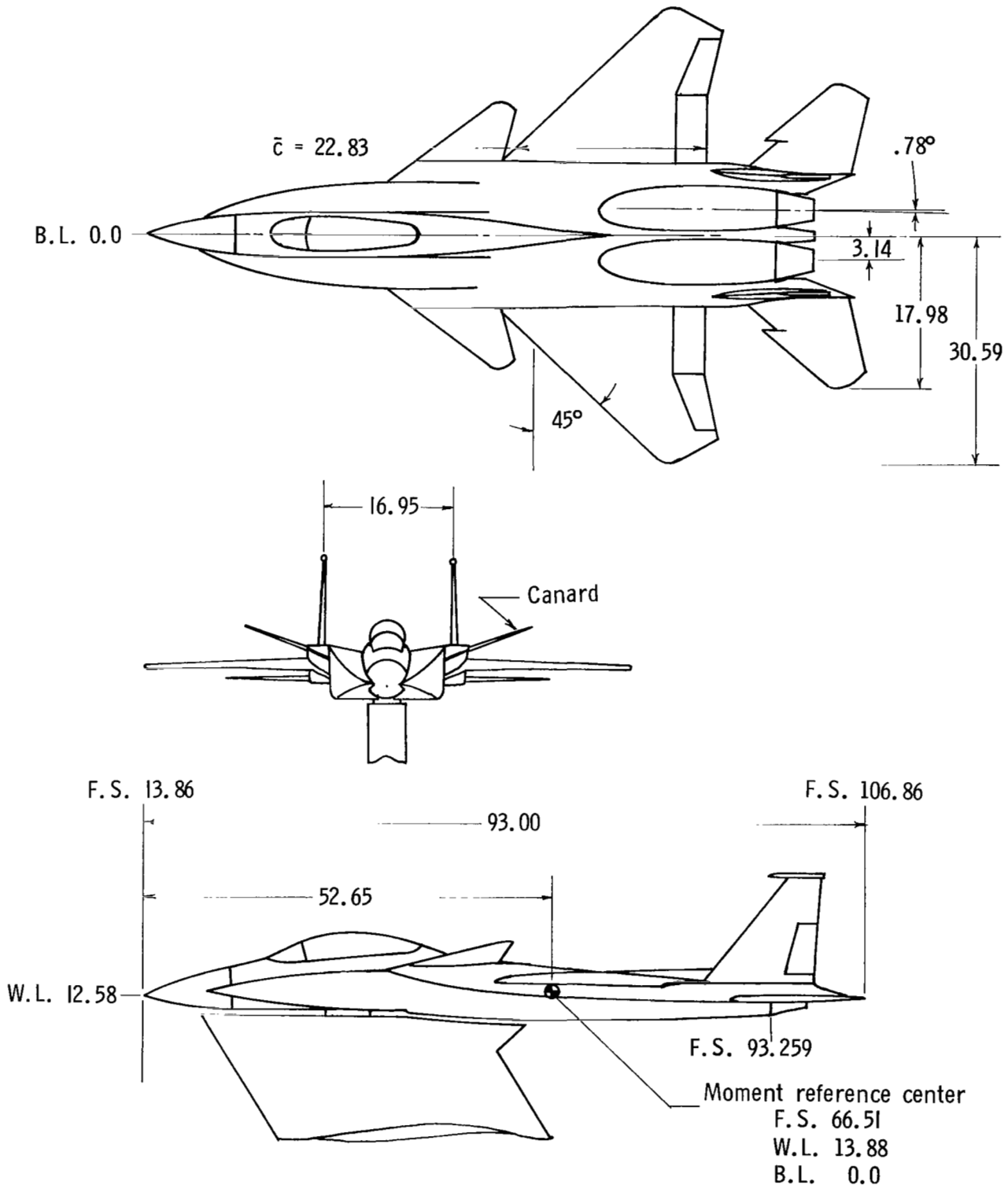

Figure 3.- Sketch of 0.047-scale three-surface F-15 model. All dimensions are in centimeters unless otherwise noted.

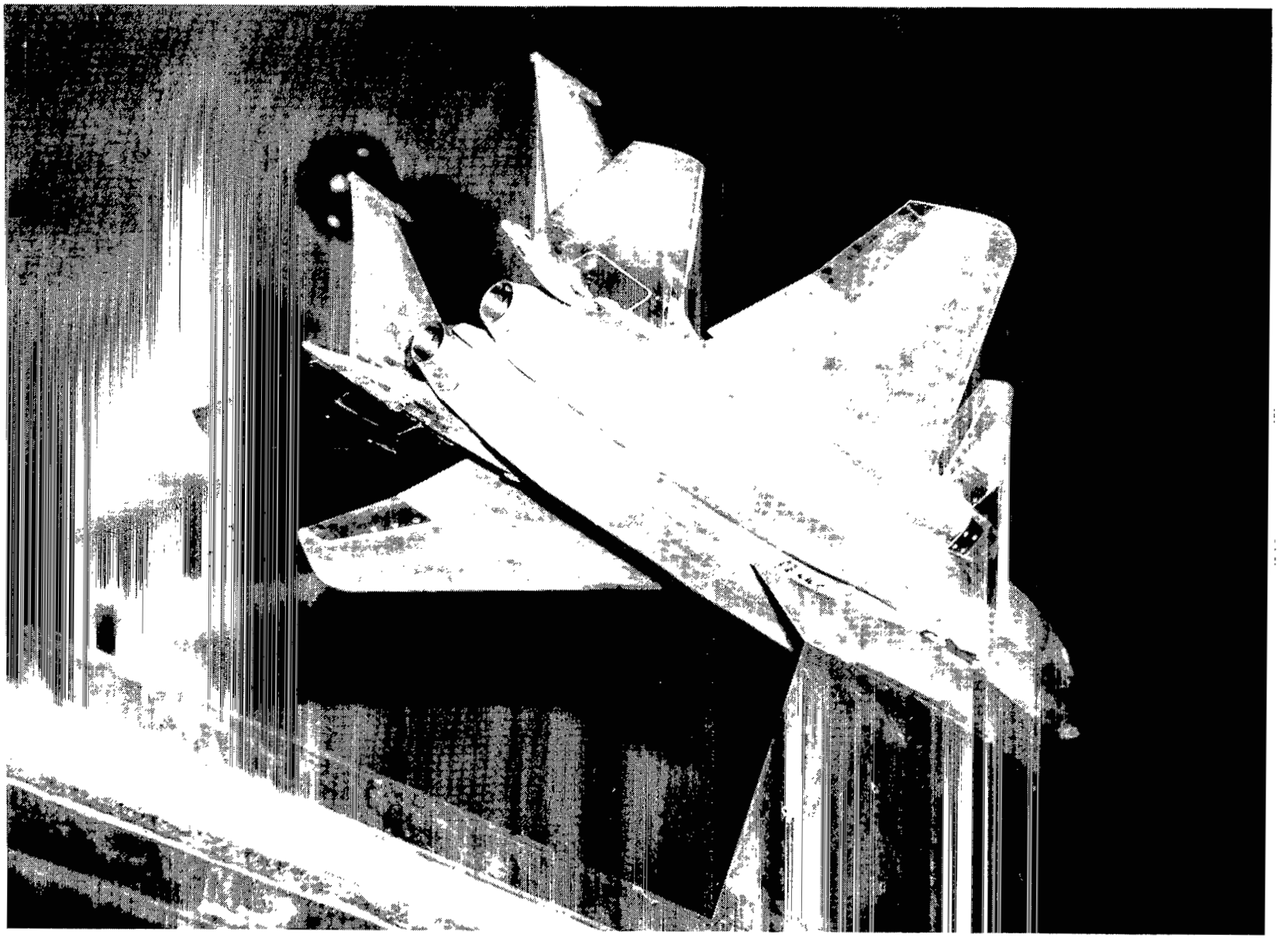

L-80-2019

Figure 4.- Photograph of baseline three-surface F-15 model with axisymmetric dry-power nozzles.

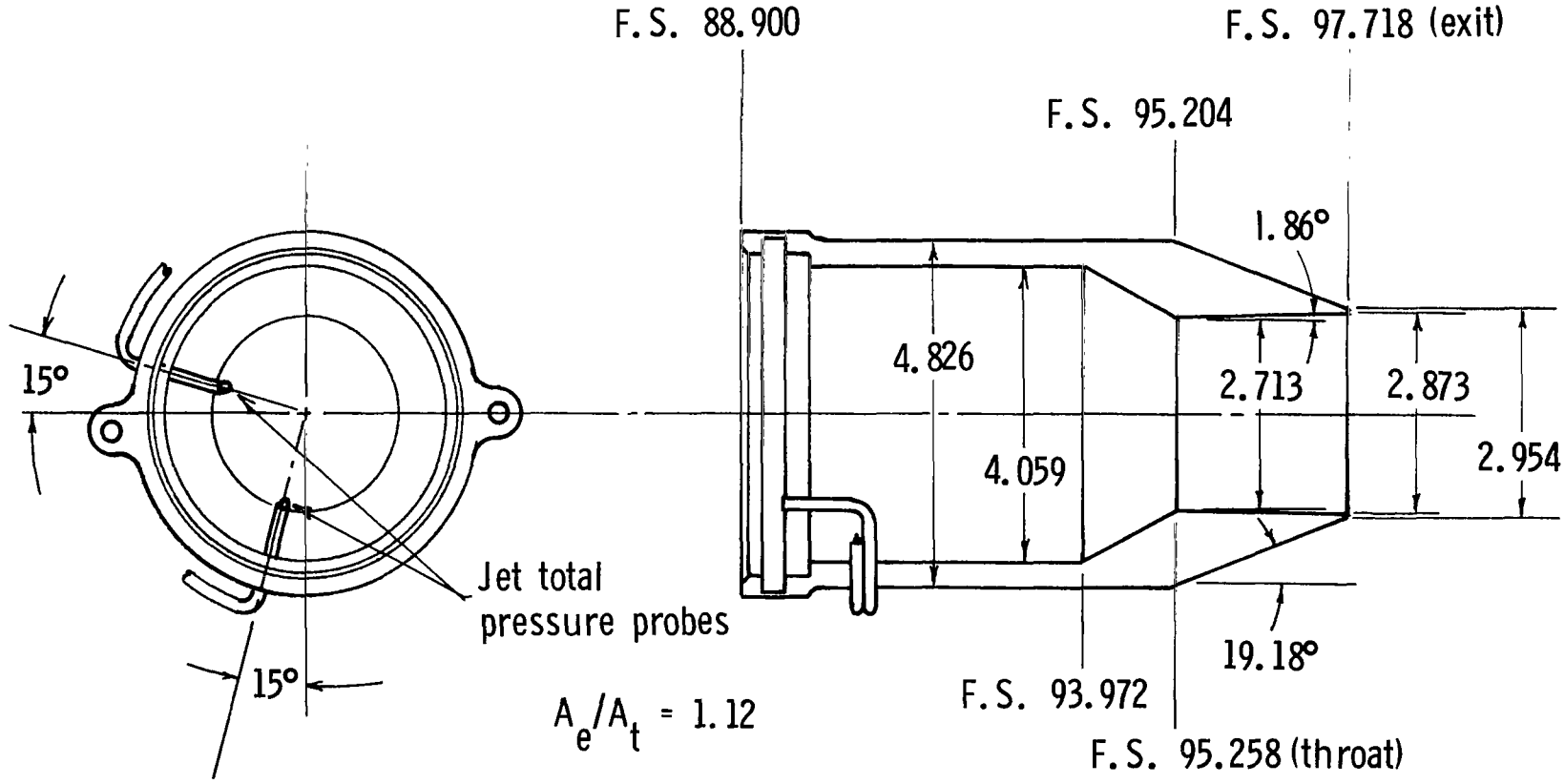

Figure 5.- Sketch of axisymmetric nozzle. All dimensions are in centimeters unless otherwise noted.

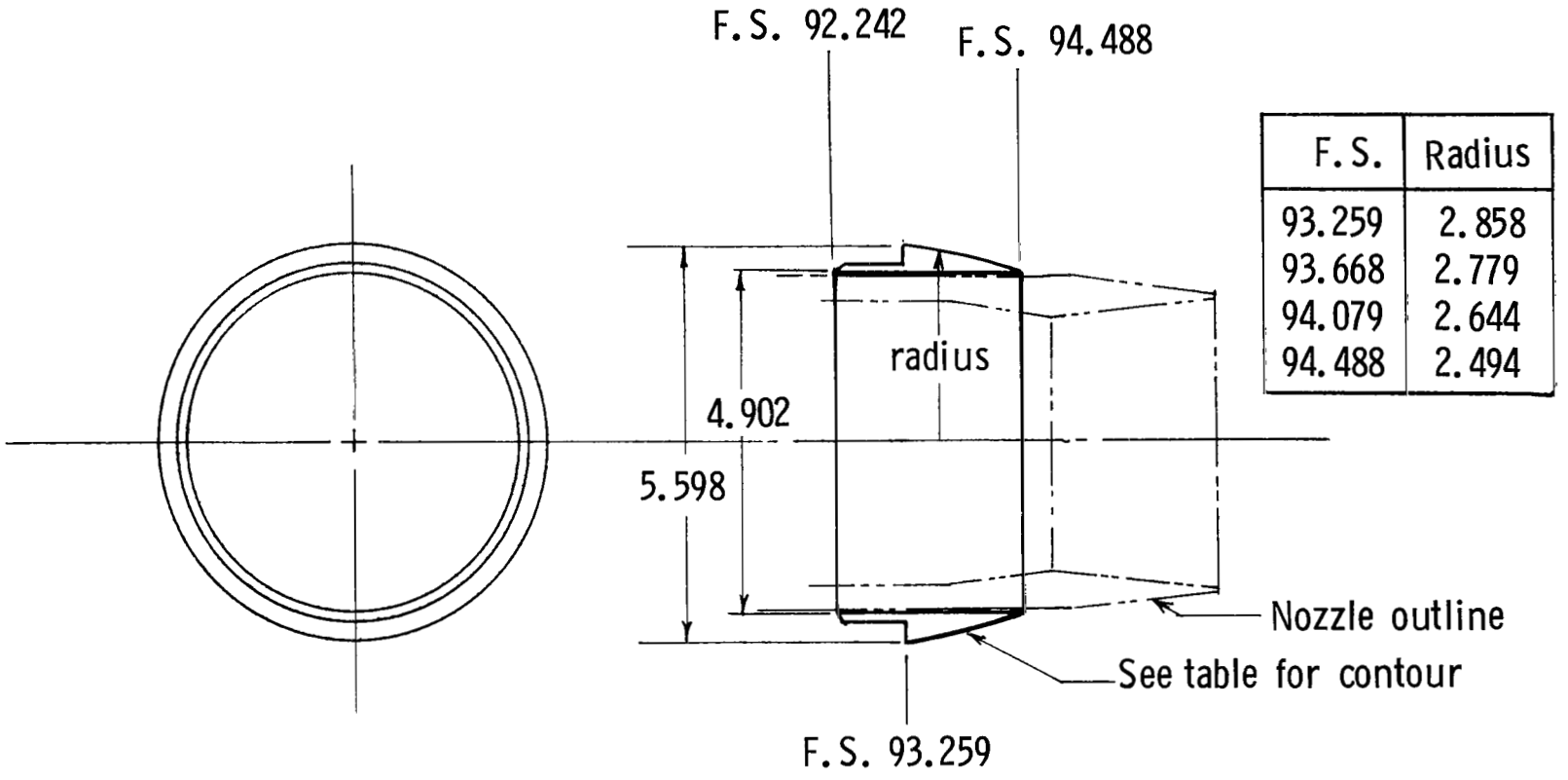

F.S.	Radius
93.259	2.858
93.668	2.779
94.079	2.644
94.488	2.494

Figure 6.- Sketch of axisymmetric external nozzle shroud. All dimensions are in centimeters.

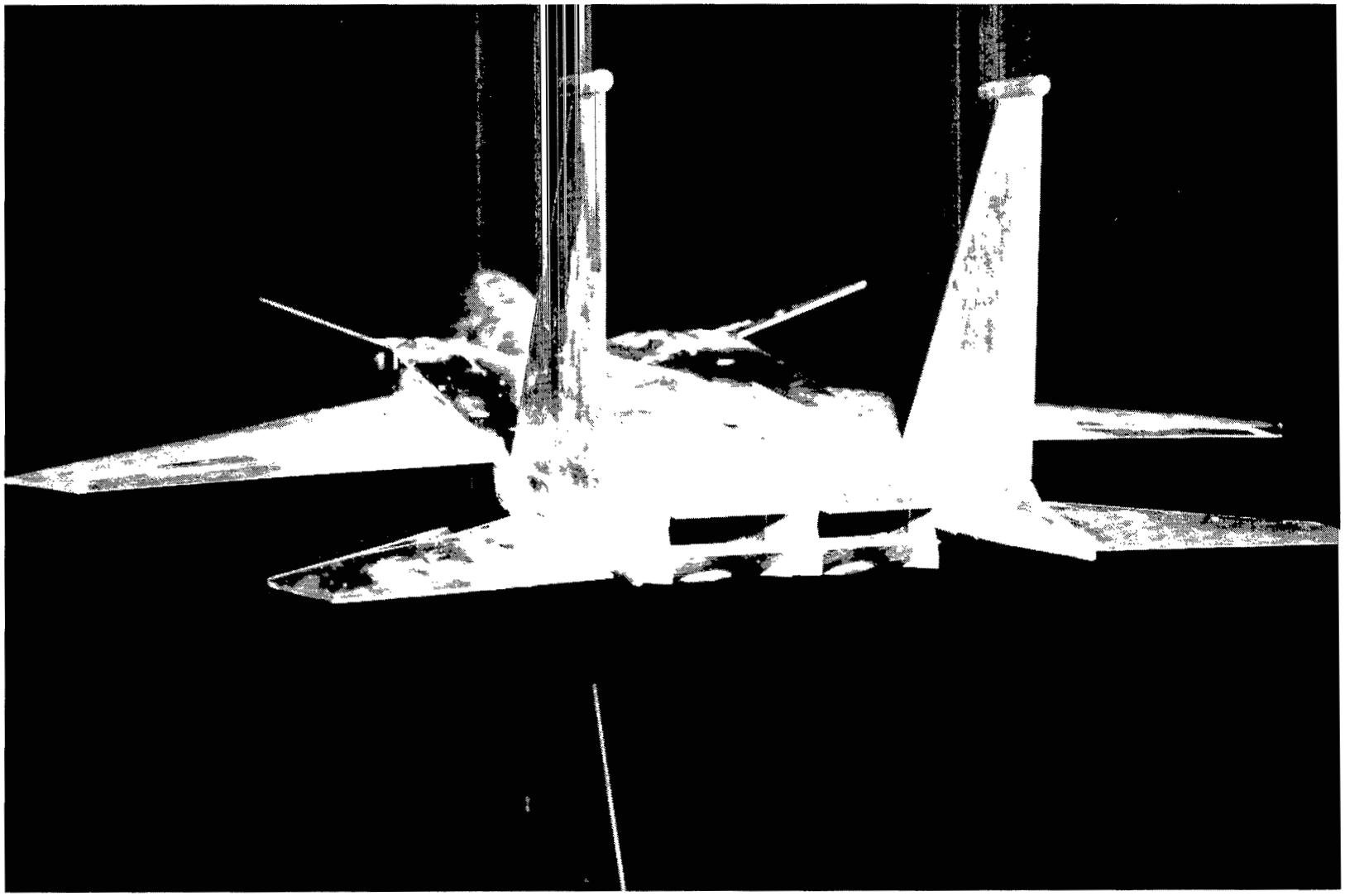

L-80-2038

Figure 7.- Photograph of model with two-dimensional convergent-divergent (2-D C-D) straight-sidewall dry-power nozzles installed.

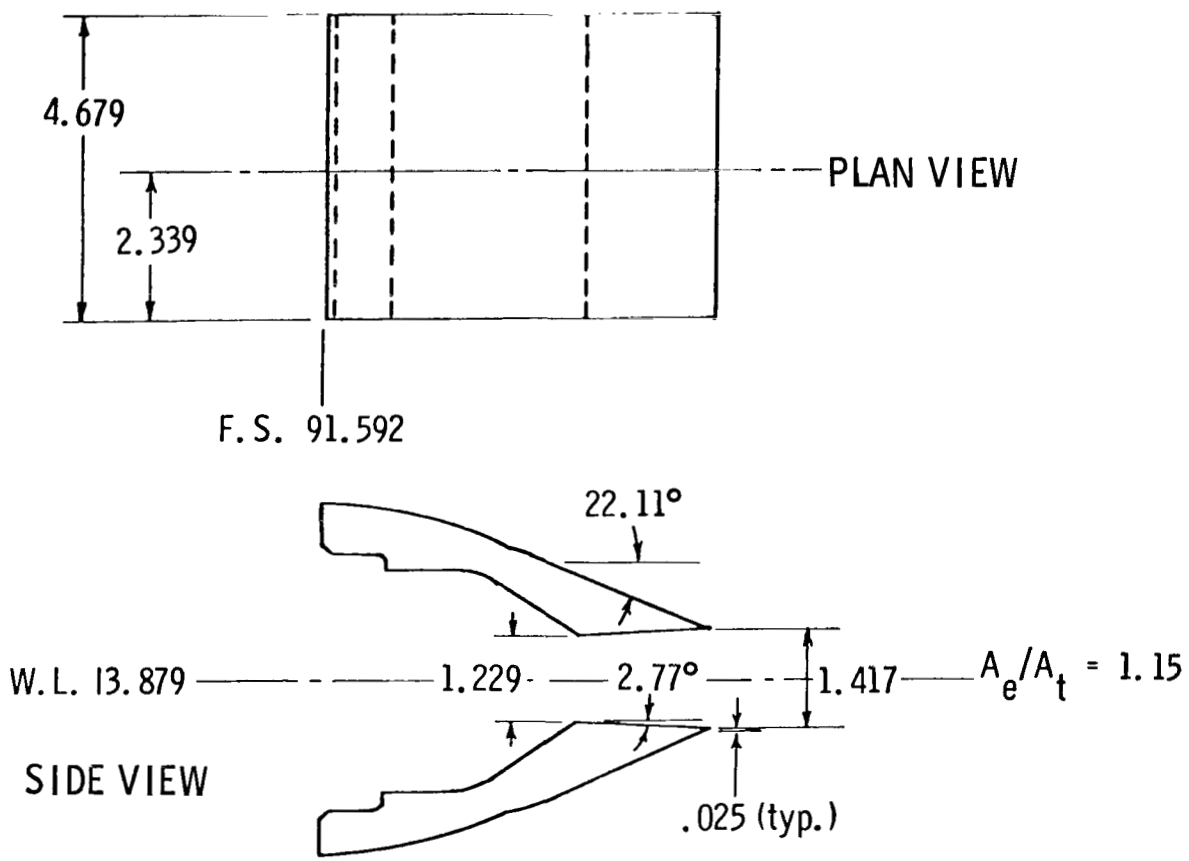

(a) Dry-power 2-D C-D nozzle flaps.

Figure 8.- Sketches of dry-power 2-D C-D nozzle flaps and sidewalls. All dimensions are in centimeters unless otherwise noted.

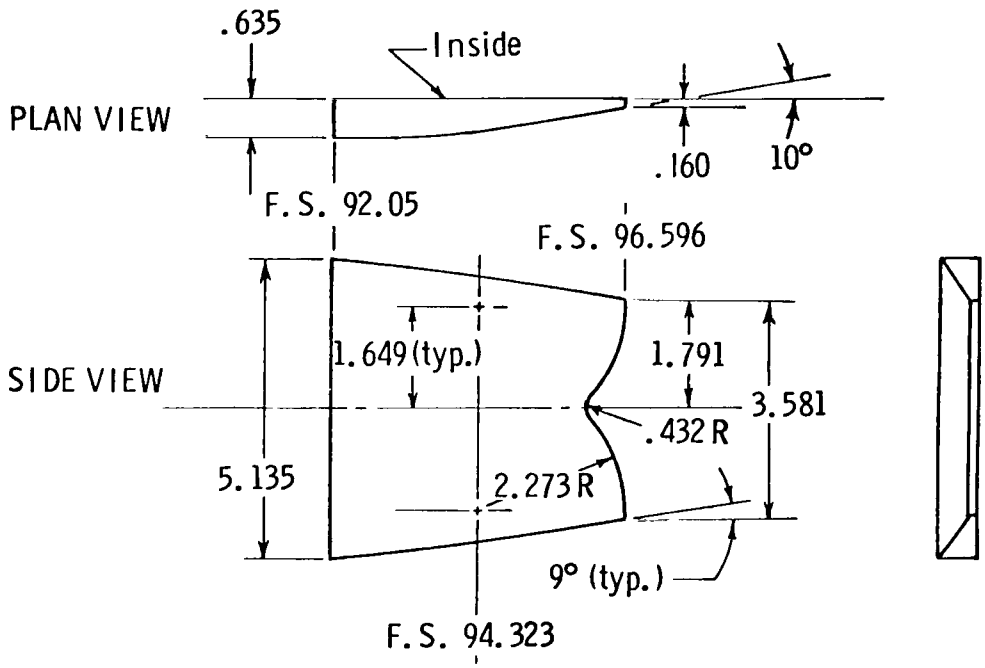

(b) Fixed, straight sidewall (L.H. side).

Figure 8.- Concluded.

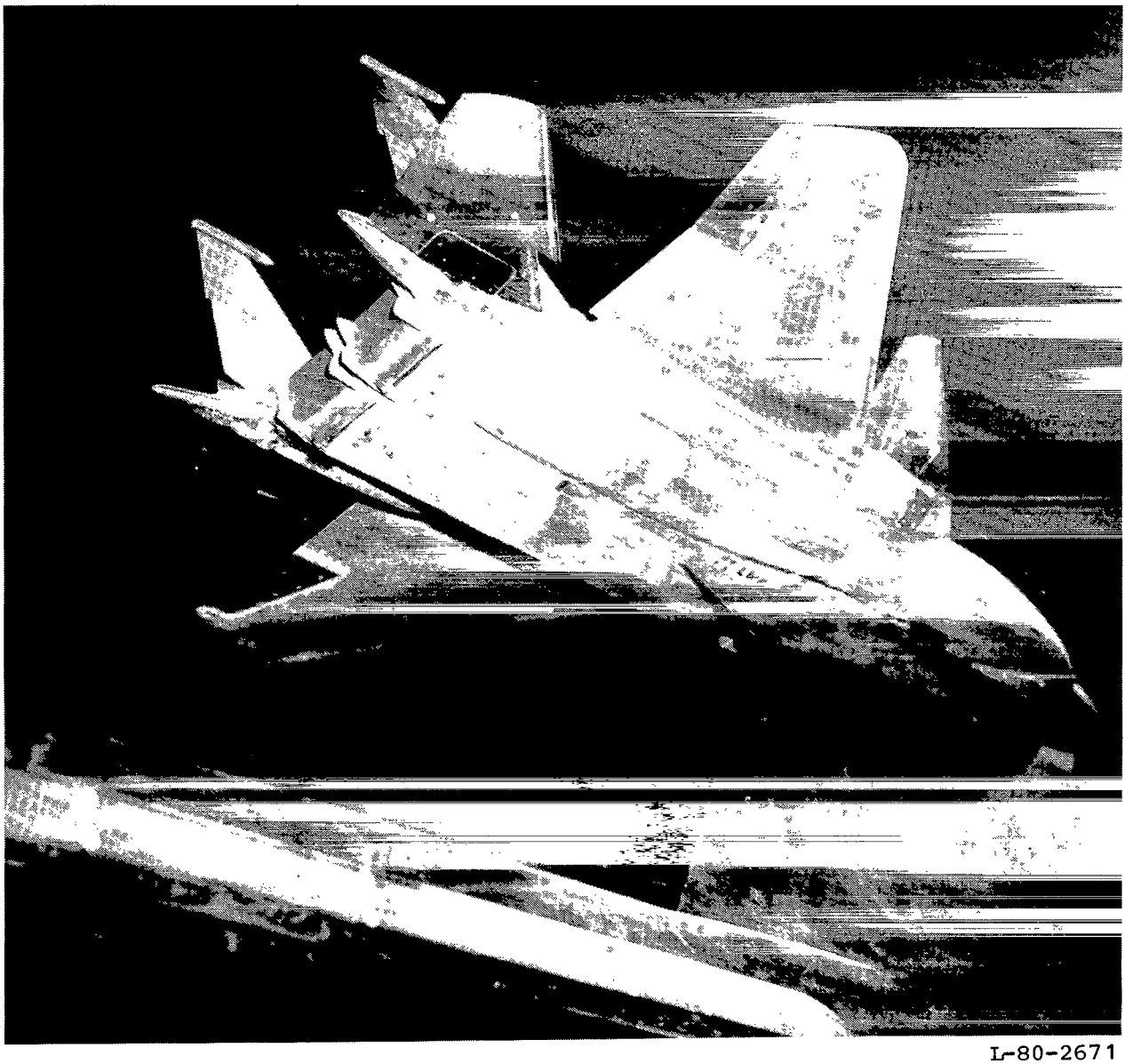

L-80-2671

Figure 9.- Photograph of the model with simulated, fully deployed thrust reversers.

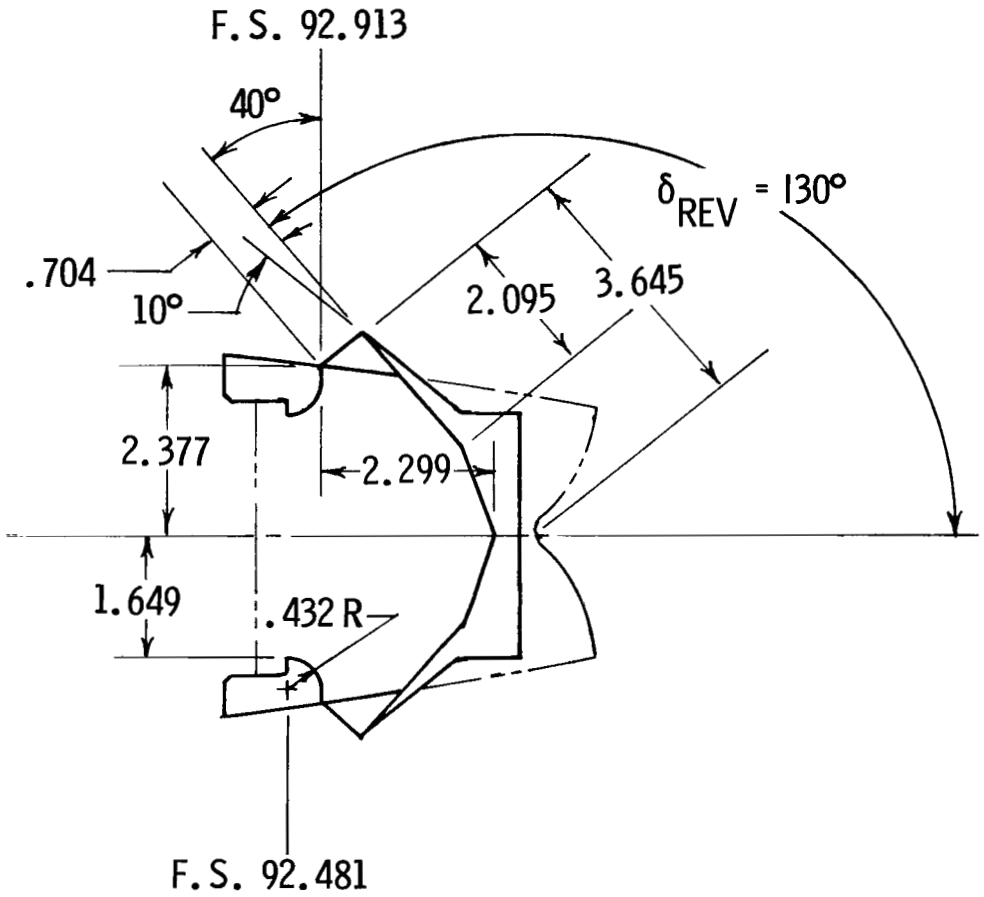

(a) Fully deployed reverser (130°).

Figure 10.- Side-view sketches of 2-D C-D nozzle thrust-reverser flaps. All dimensions are in centimeters unless otherwise noted.

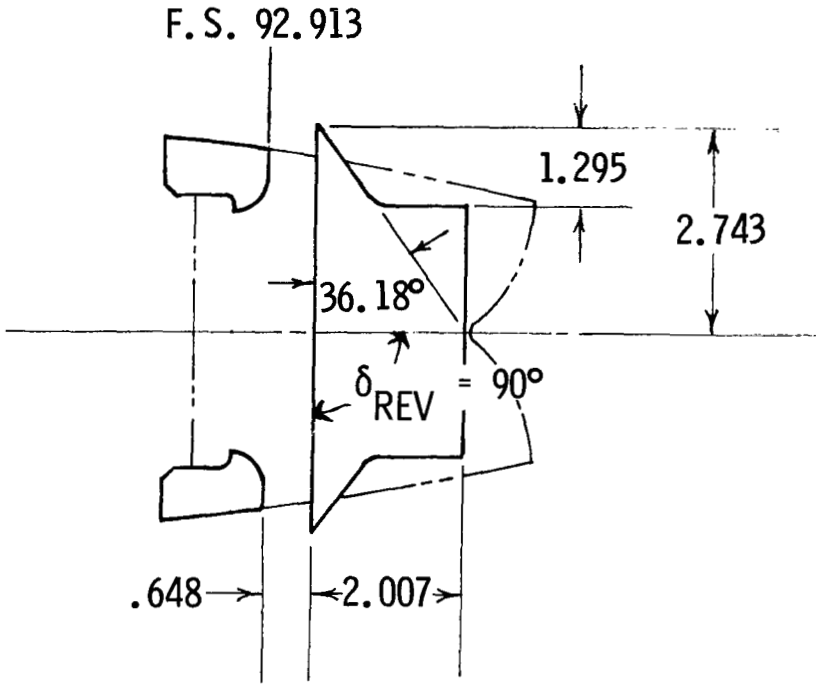

(b) Partially deployed reverser (90°).

Figure 10.- Concluded.

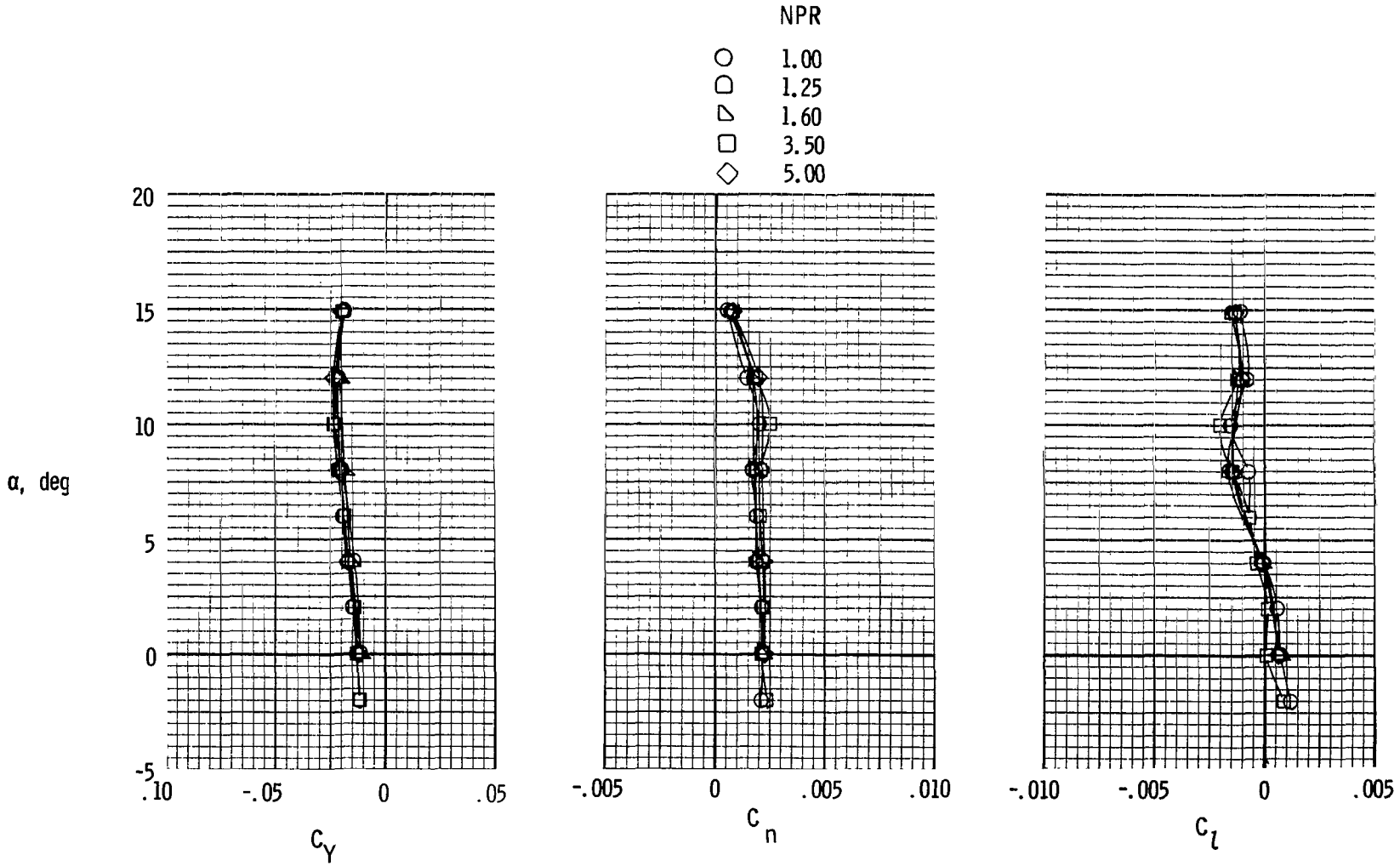

(a) M = 0.60.

Figure 11.- Lateral-directional characteristics of configuration with axisymmetric nozzles, $\beta = 0°$, and $\delta_R = 0°$.

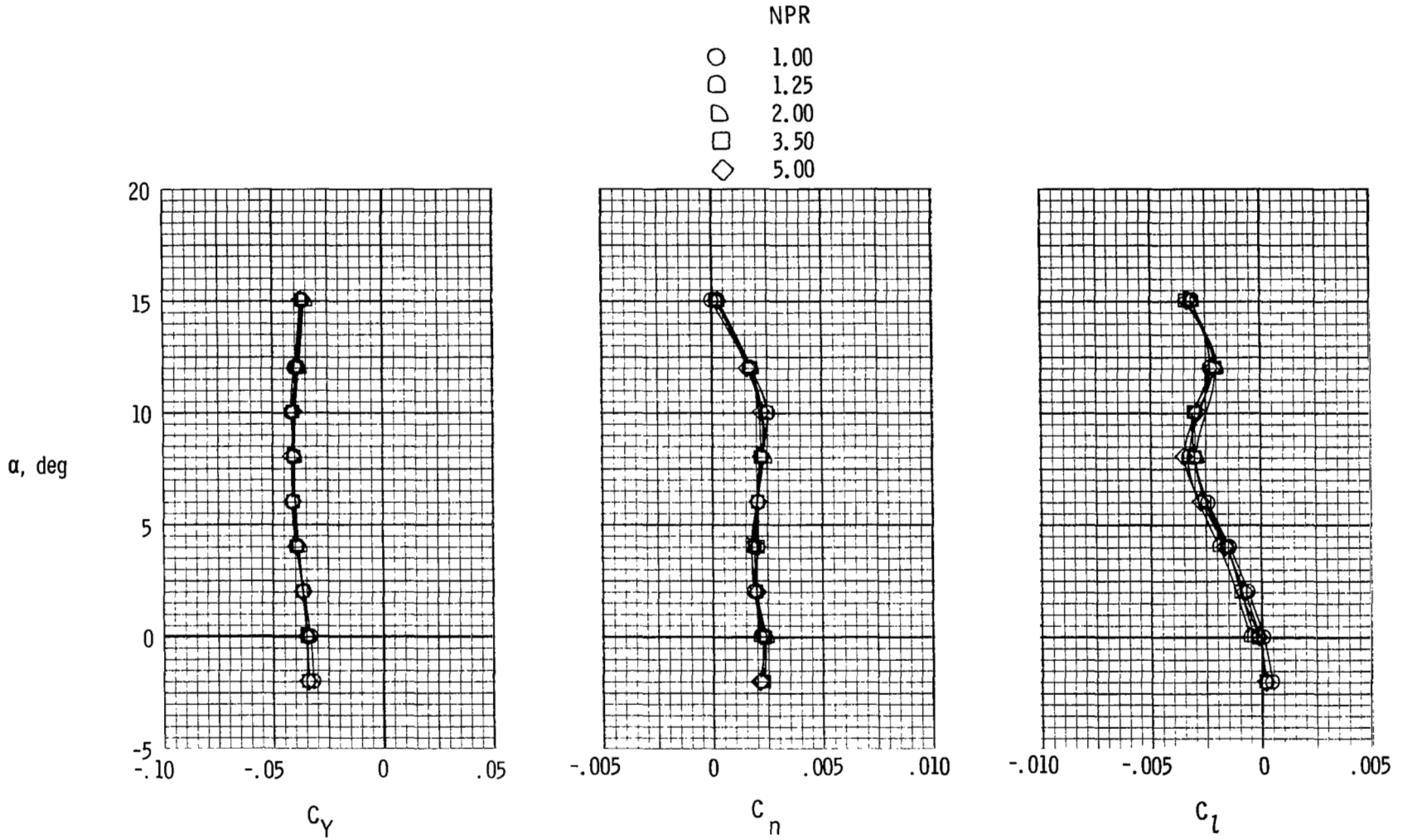

(b) M = 0.90.

Figure 11.- Continued.

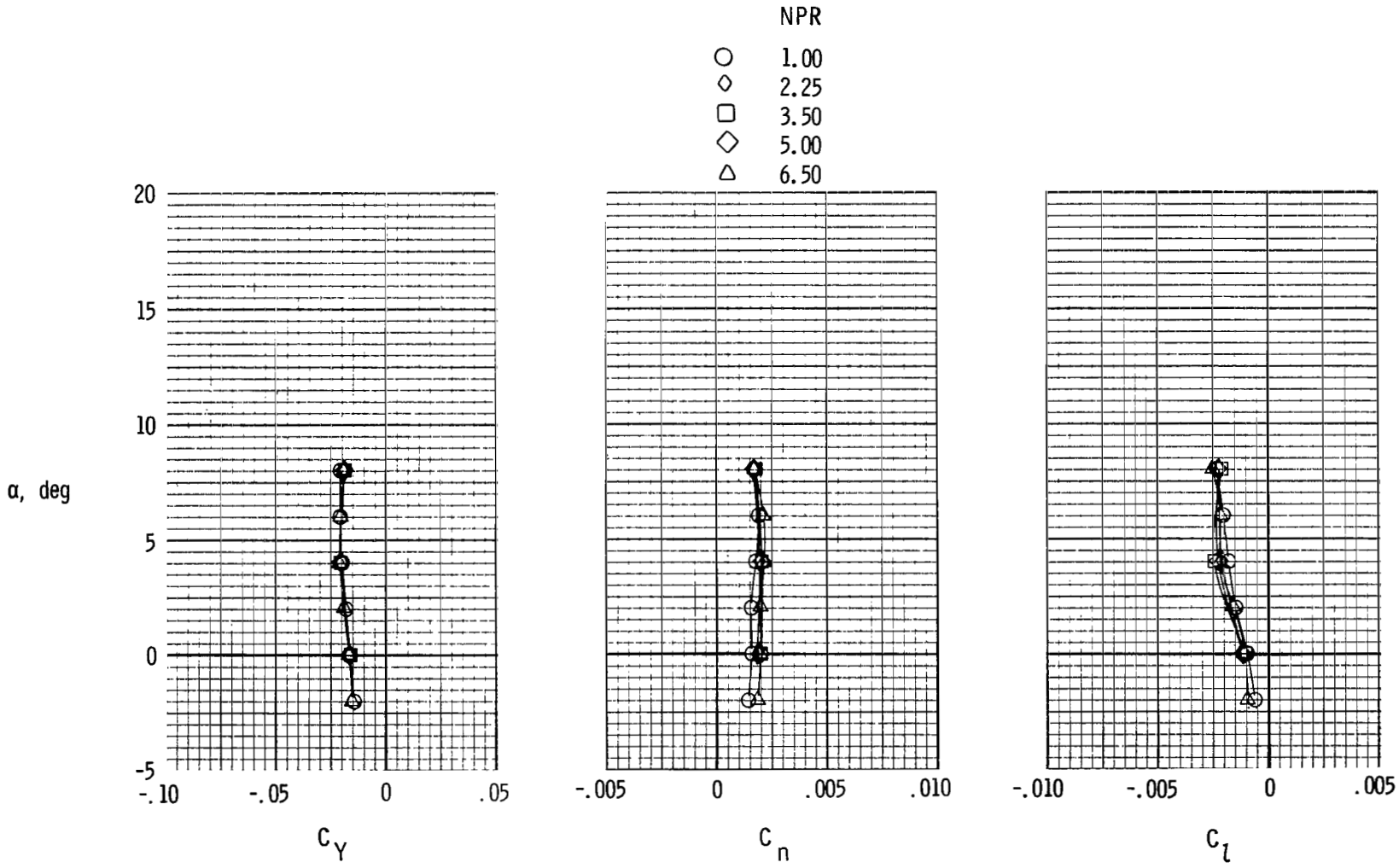

(c) M = 1.20.

Figure 11.- Concluded.

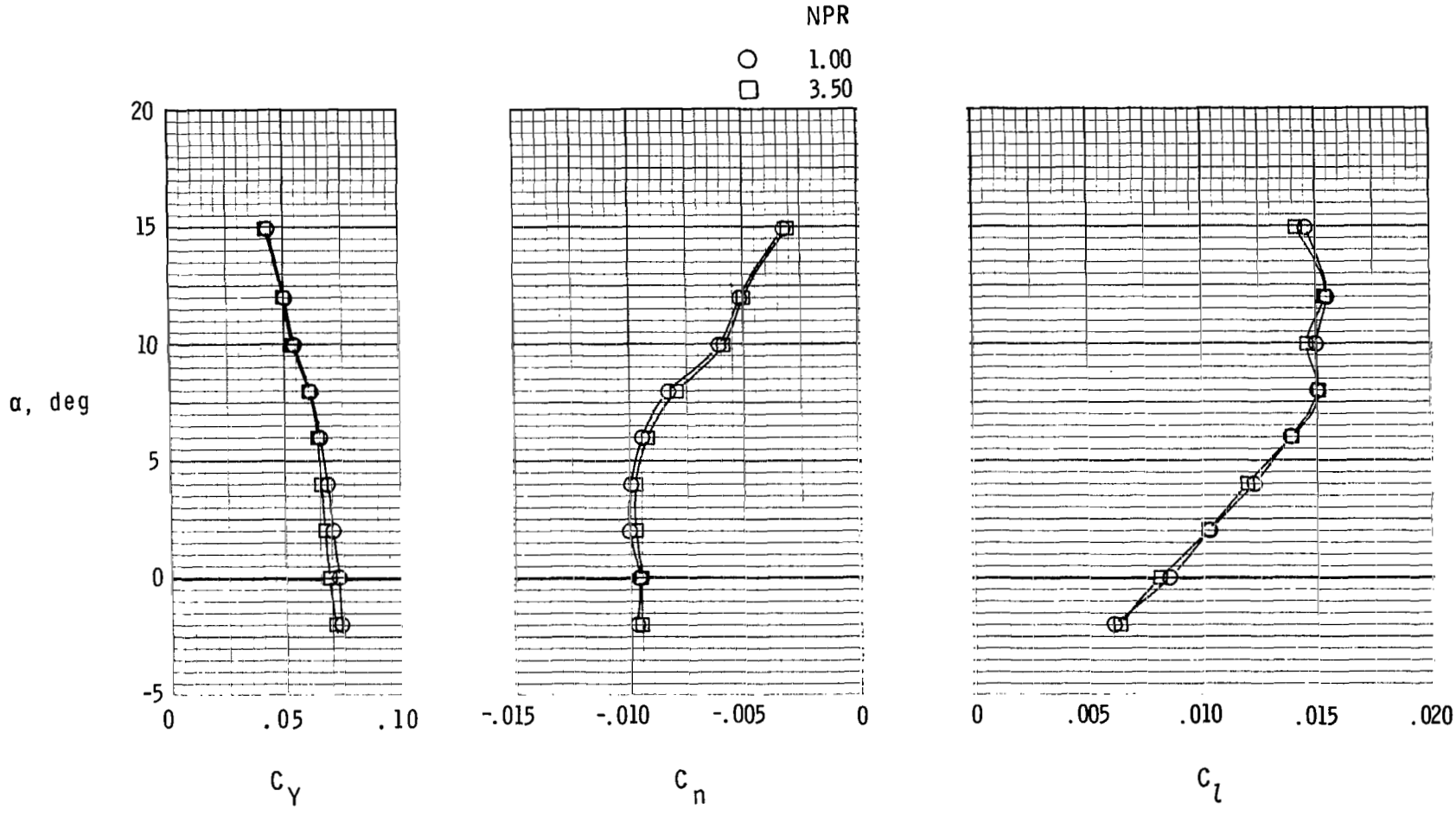

(a) M = 0.60.

Figure 12.- Lateral-directional characteristics of configuration with axisymmetric nozzles, $\beta = -5°$, and $\delta_R = 0°$.

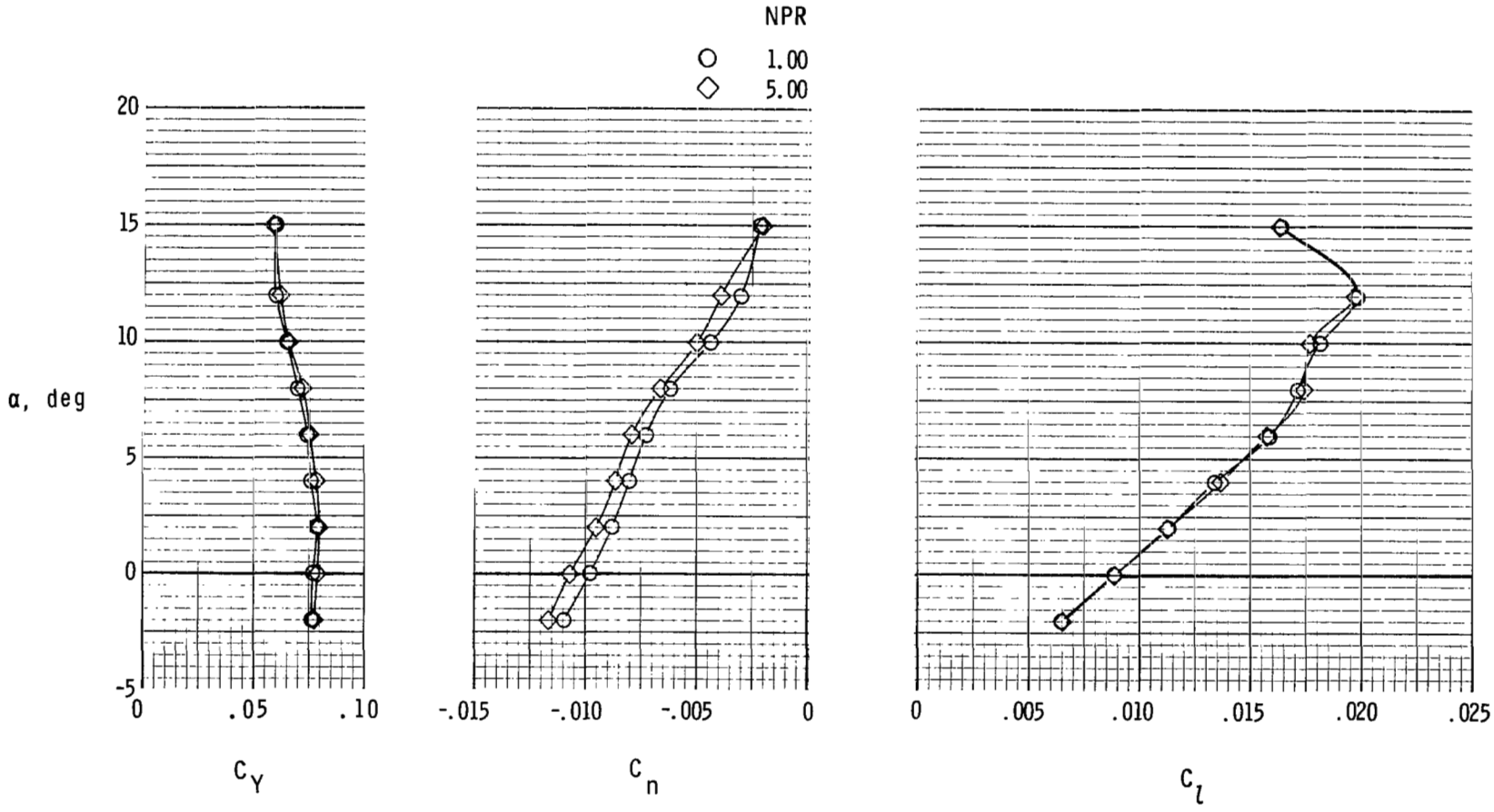

(b) M = 0.90.

Figure 12.- Concluded.

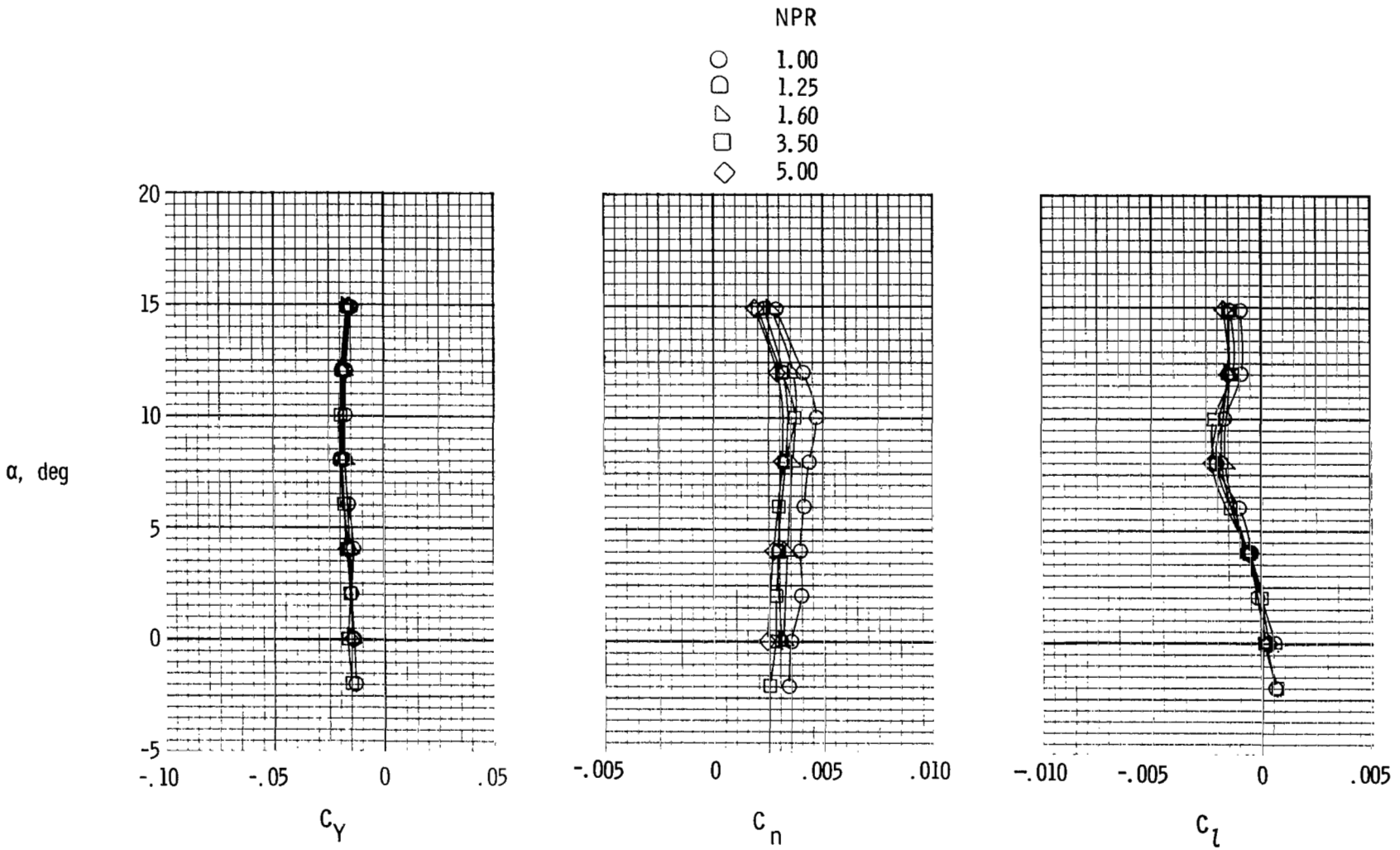

(a) M = 0.60.

Figure 13.- Lateral-directional characteristics of configuration with 2-D C-D nozzles, $\beta = 0°$, and $\delta_R = 0°$.

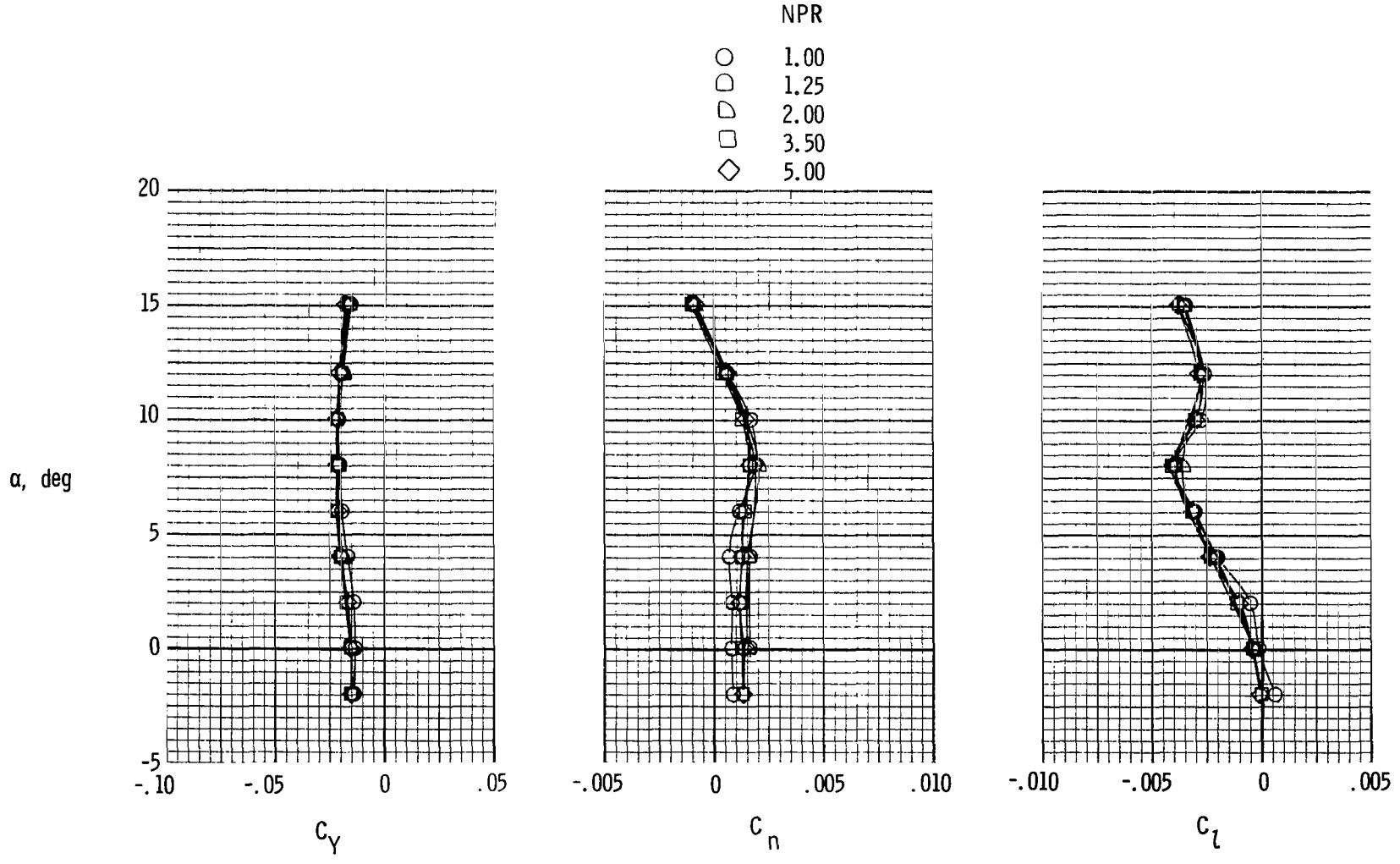

(b) M = 0.90.

Figure 13.- Continued.

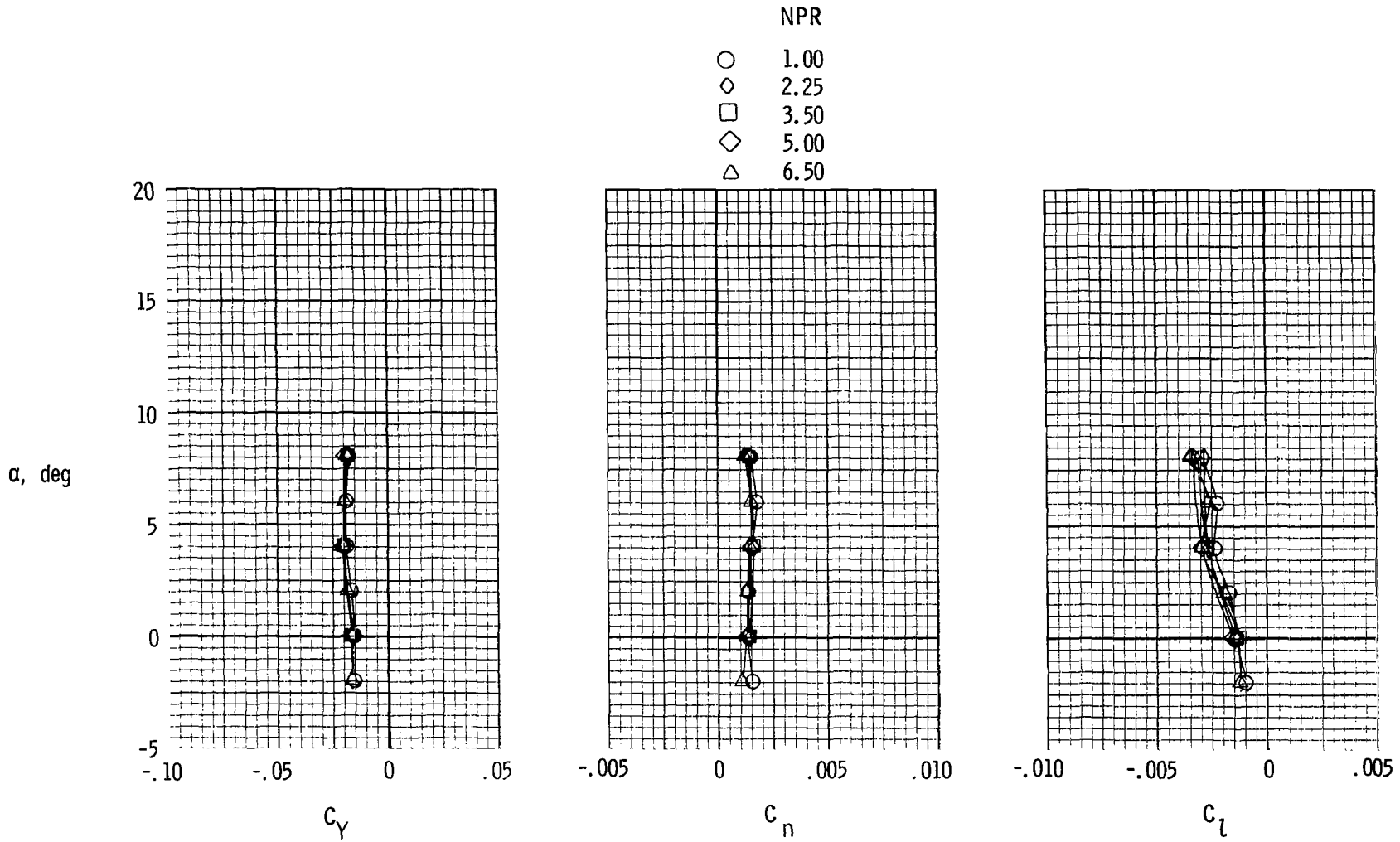

(c) M = 1.20.

Figure 13.- Concluded.

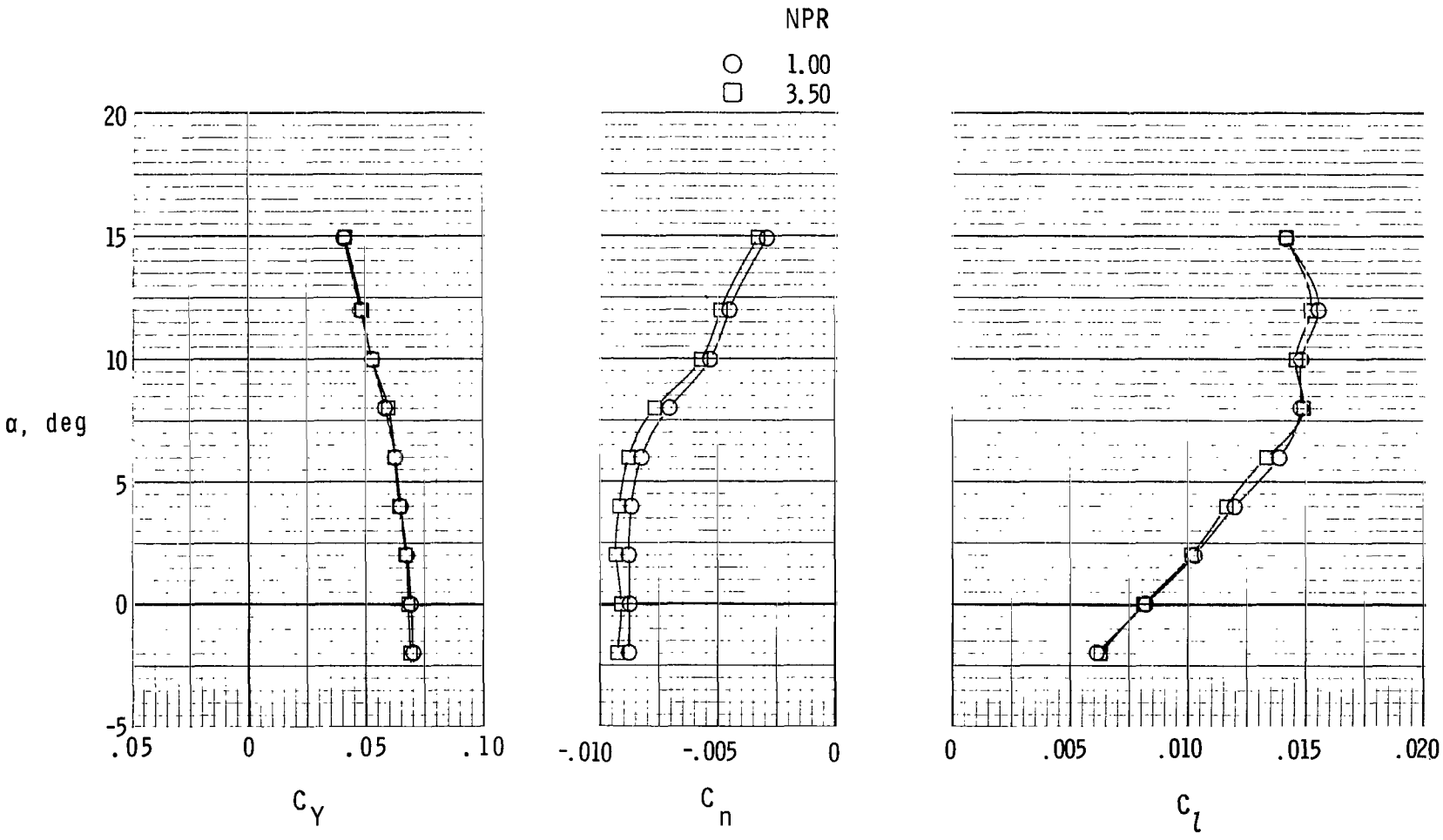

(a) M = 0.60.

Figure 14.- Lateral-directional characteristics of configuration with 2-D C-D nozzles, $\beta = -5°$, and $\delta_R = 0°$.

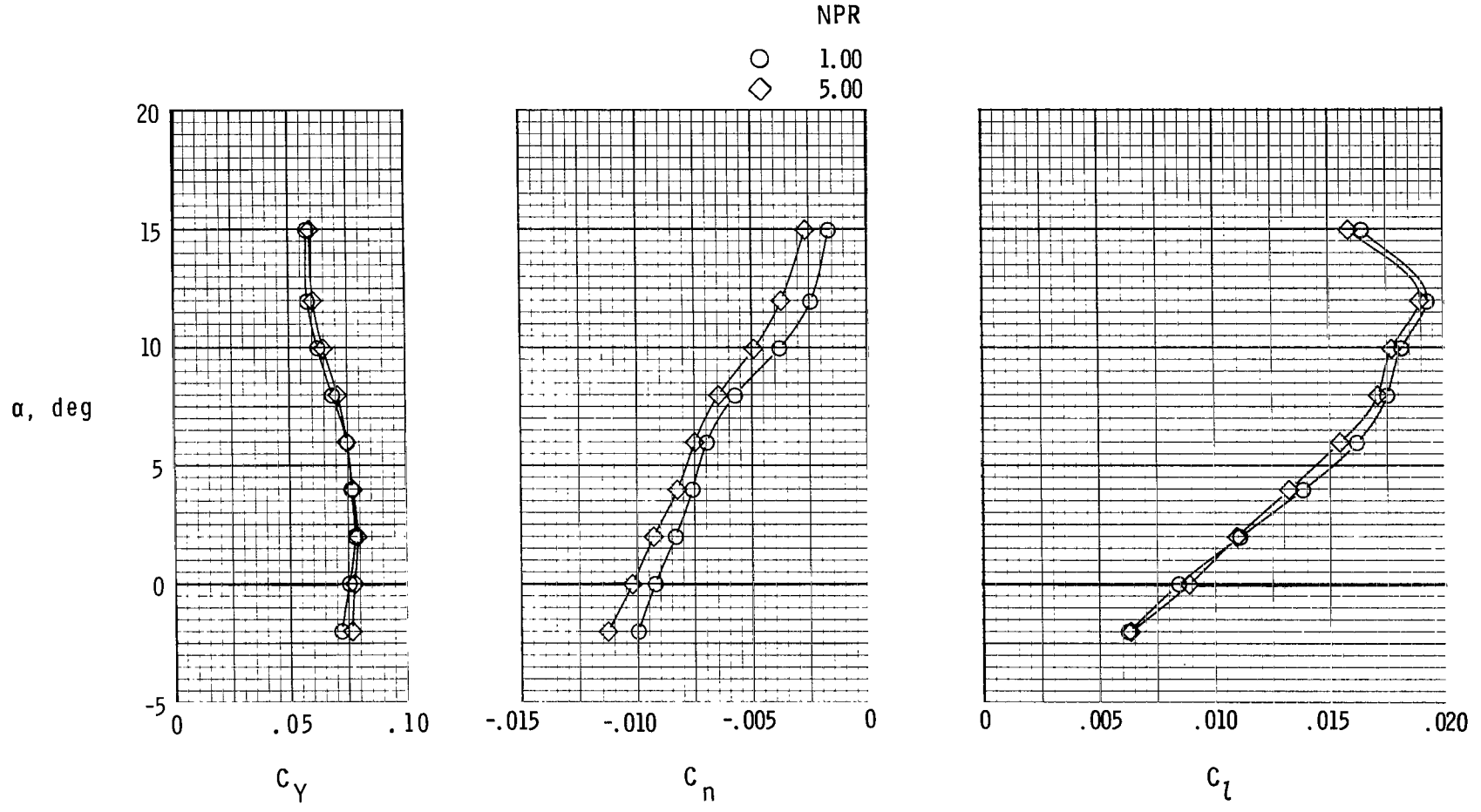

(b) M = 0.90.

Figure 14.- Concluded.

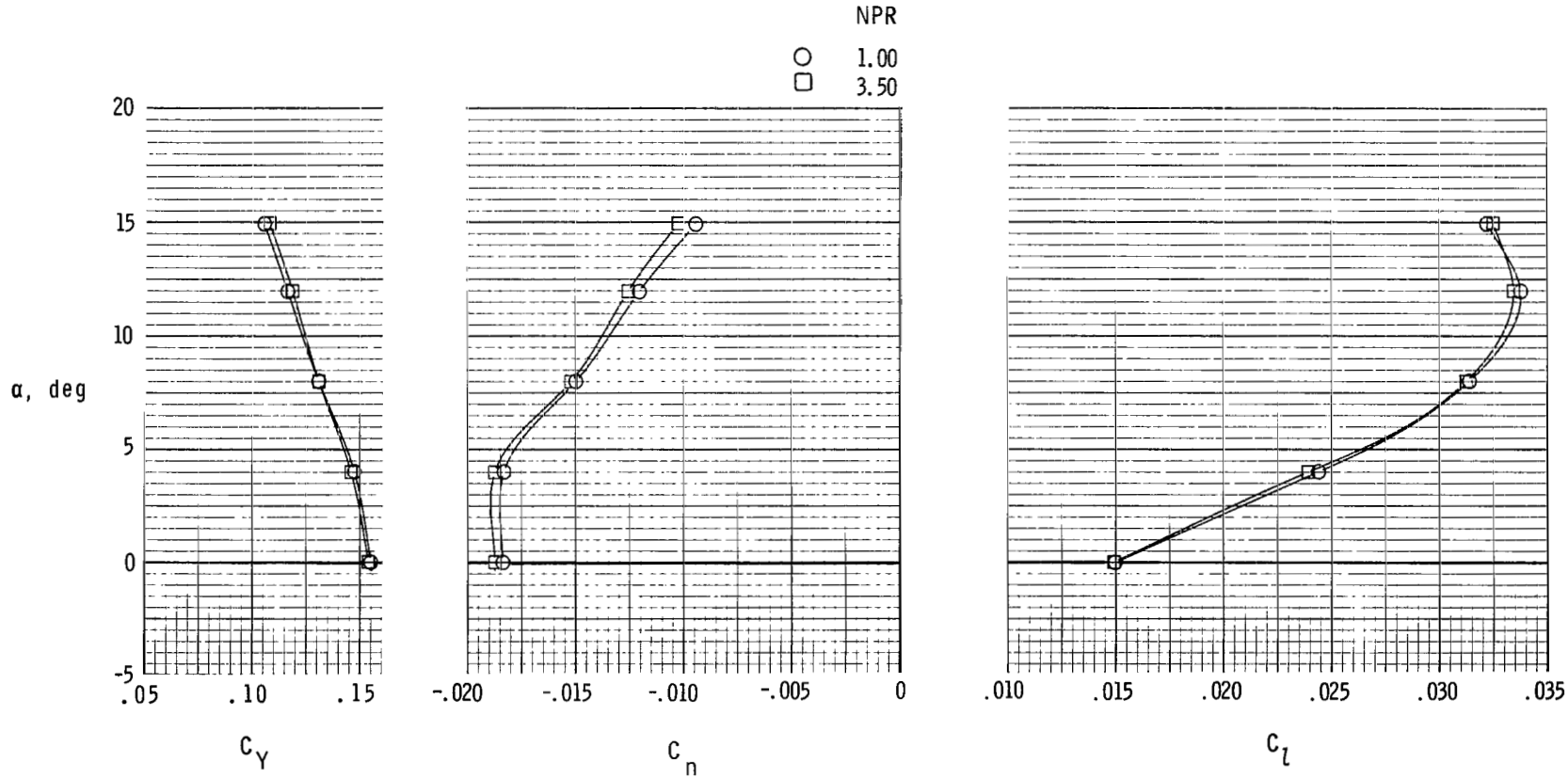

(a) M = 0.60.

Figure 15.- Lateral-directional characteristics of configuration with 2-D C-D nozzles, $\beta = -10°$, and $\delta_R = 0°$.

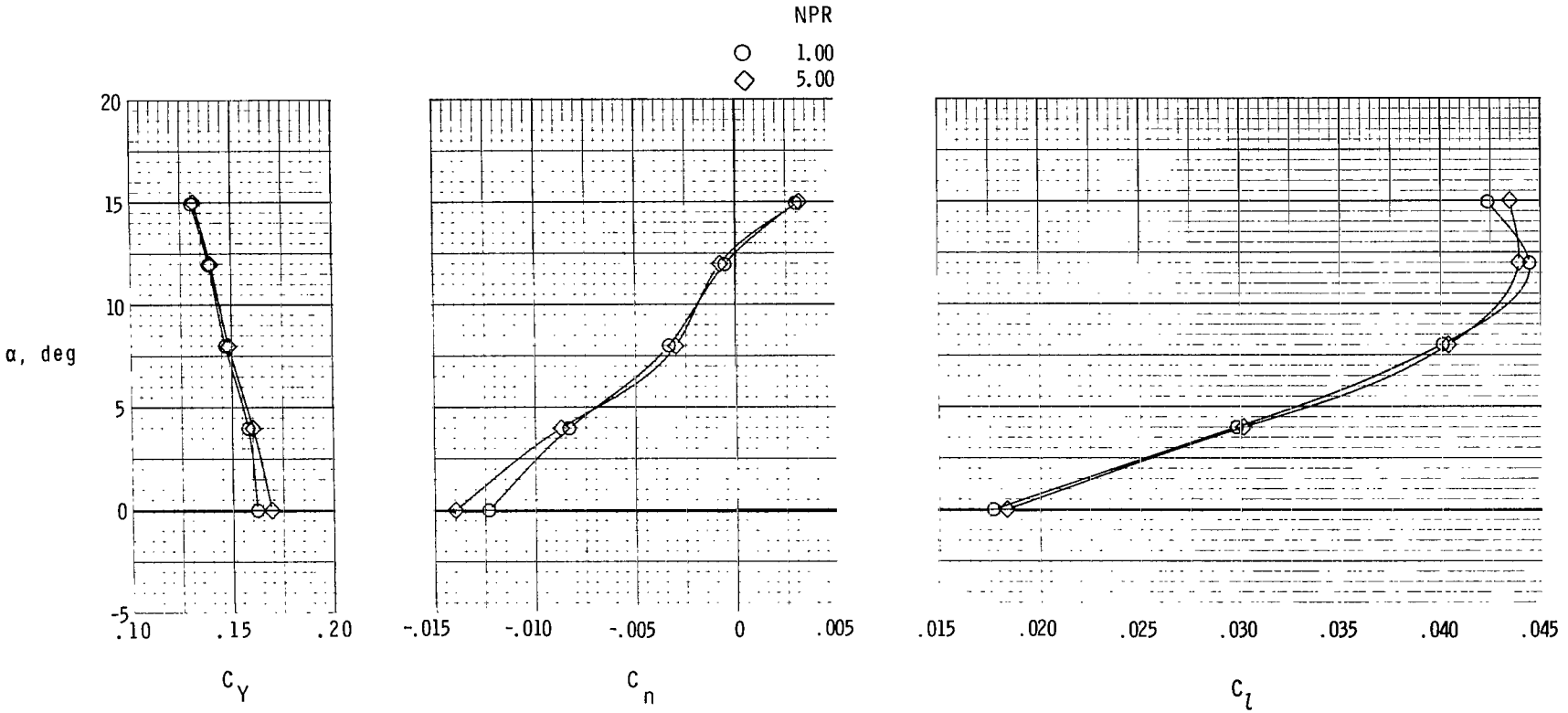

(b) M = 0.90.

Figure 15.- Concluded.

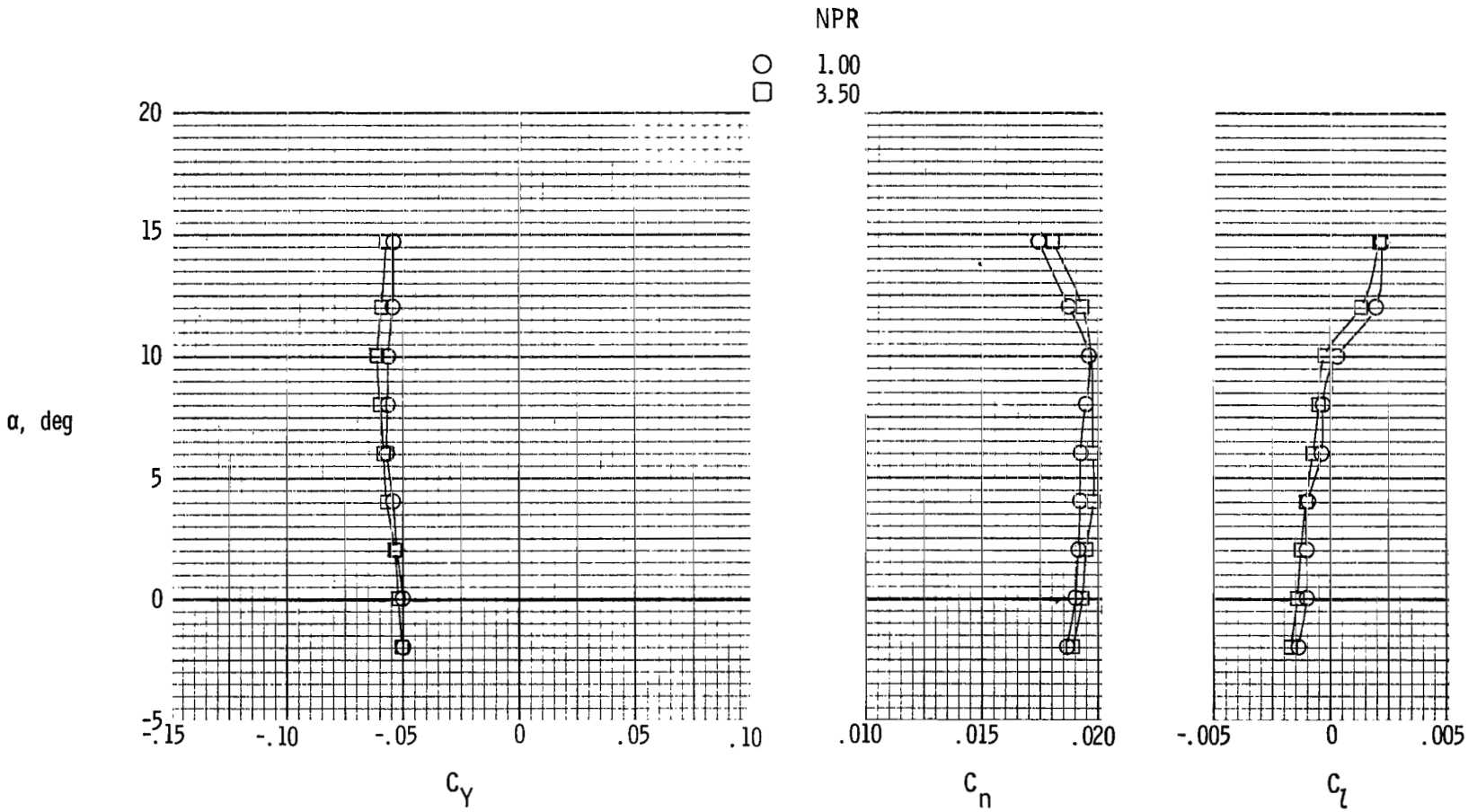

(a) M = 0.60.

Figure 16.- Lateral-directional characteristics of configuration with 2-D C-D nozzles, $\beta = 0°$, and $\delta_R = -10°$.

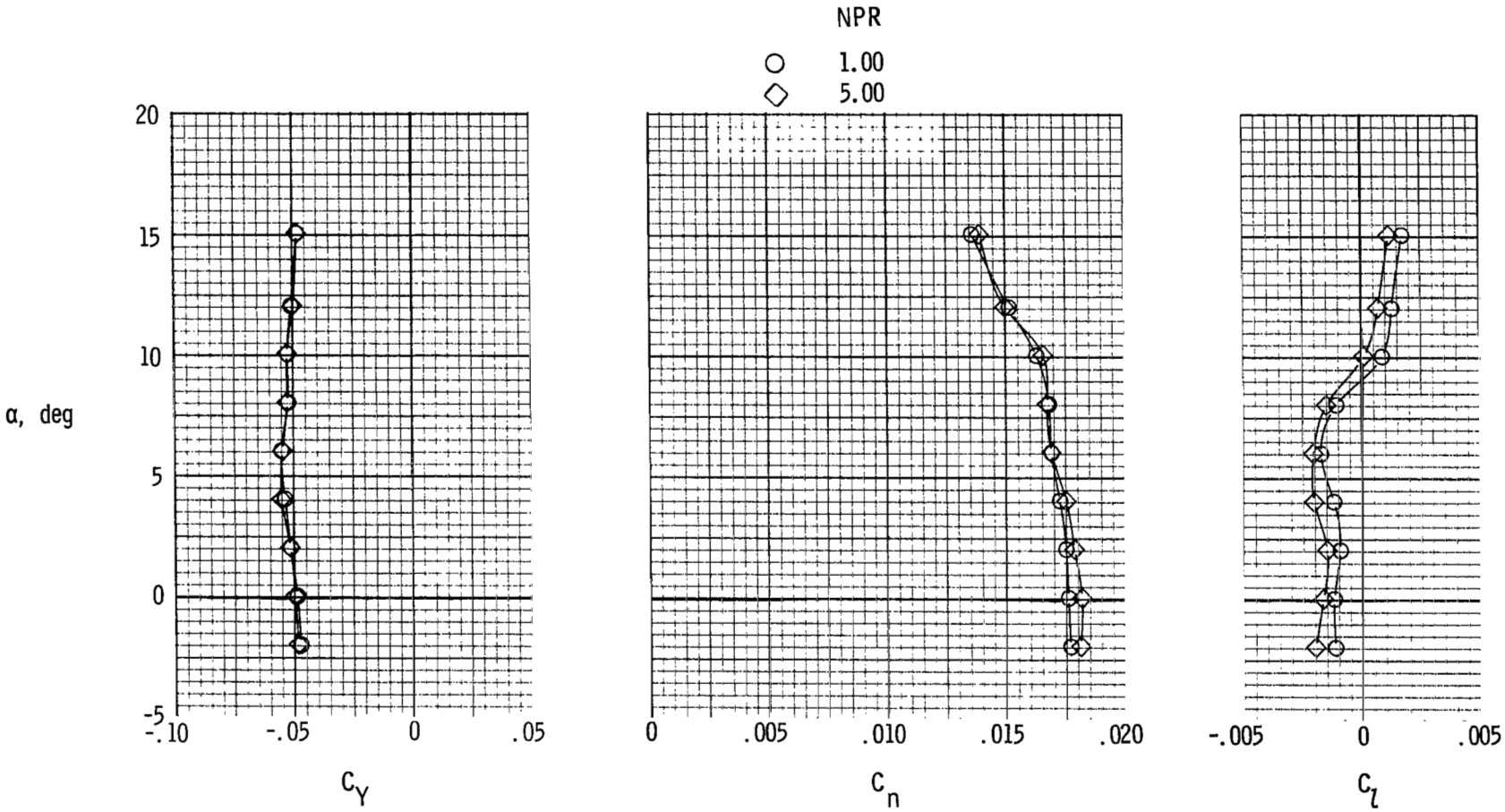

(b) M = 0.90.

Figure 16.- Continued.

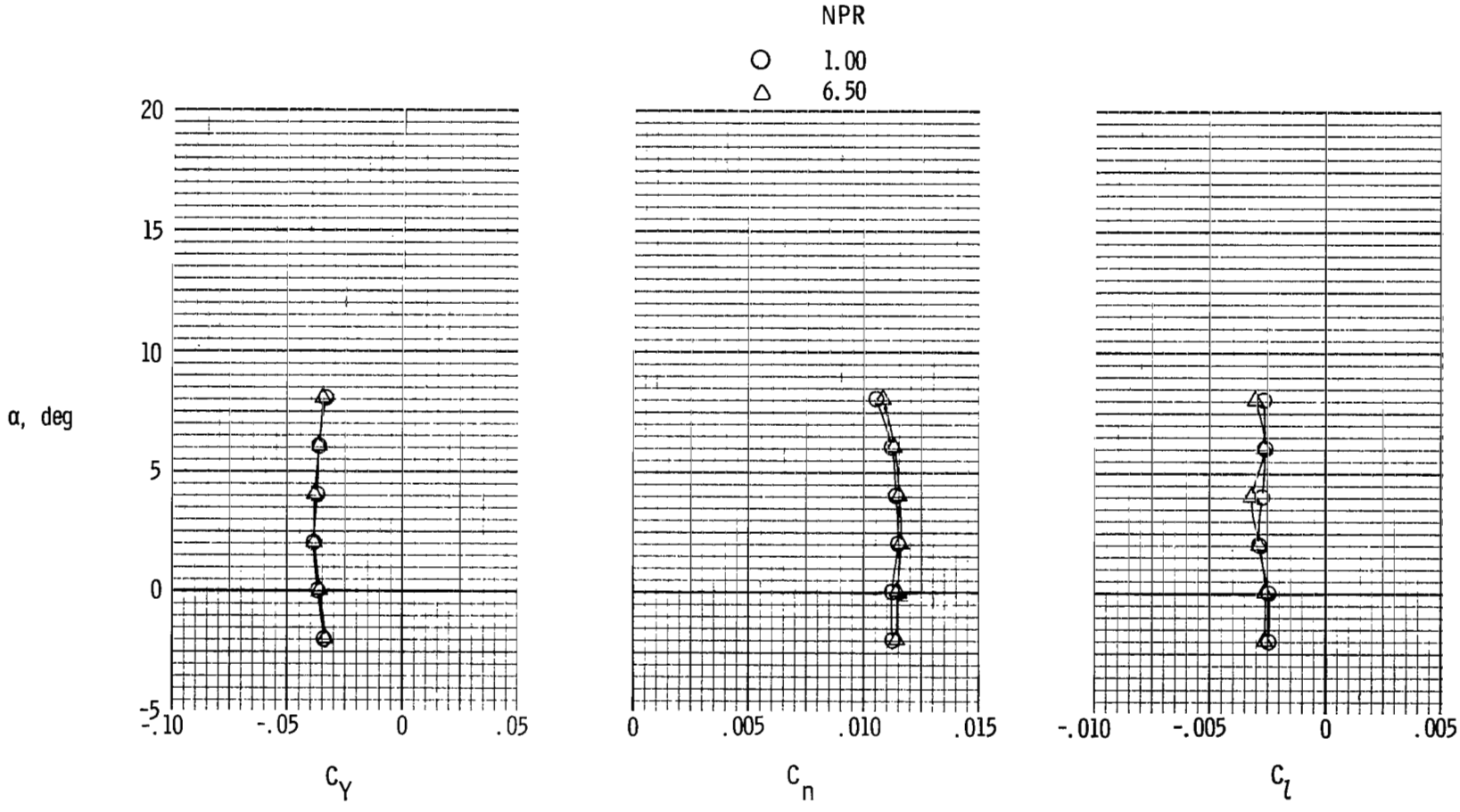

(c) M = 1.20.

Figure 16.- Concluded.

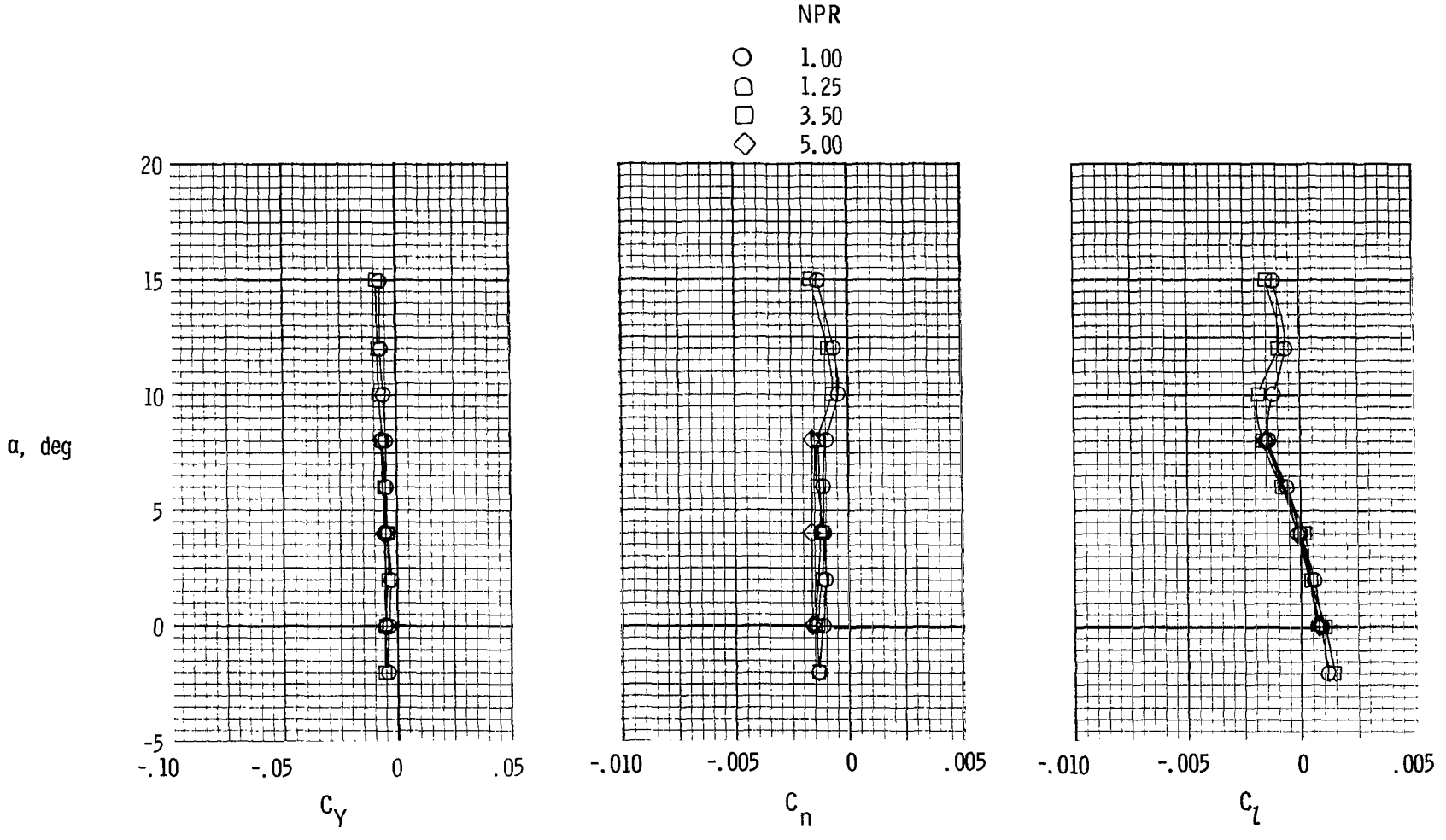

(a) M = 0.60.

Figure 17.- Lateral-directional characteristics of configuration with 2-D C-D nozzles, vertical tails removed, and $\beta = 0°$.

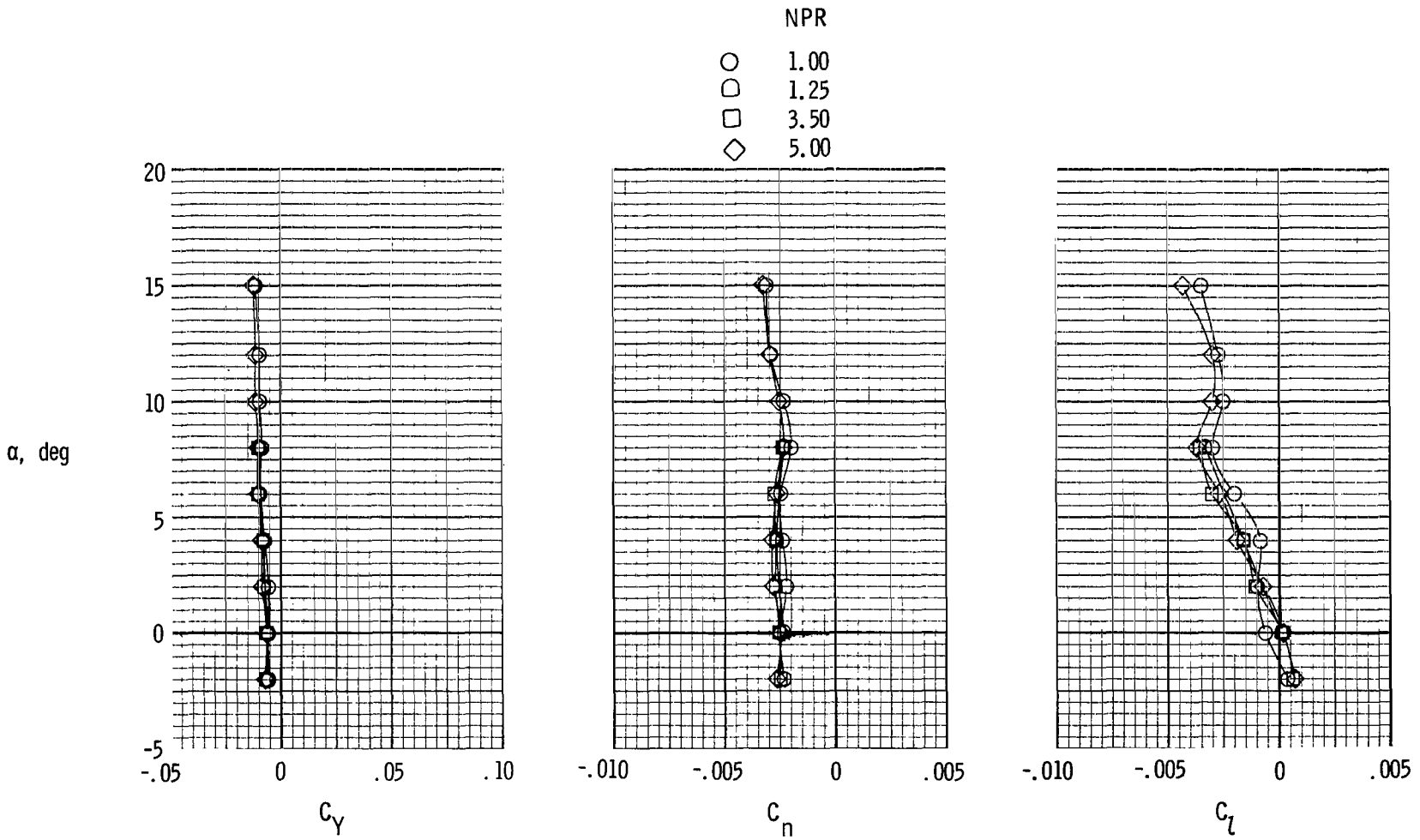

(b) M = 0.90.

Figure 17.- Continued.

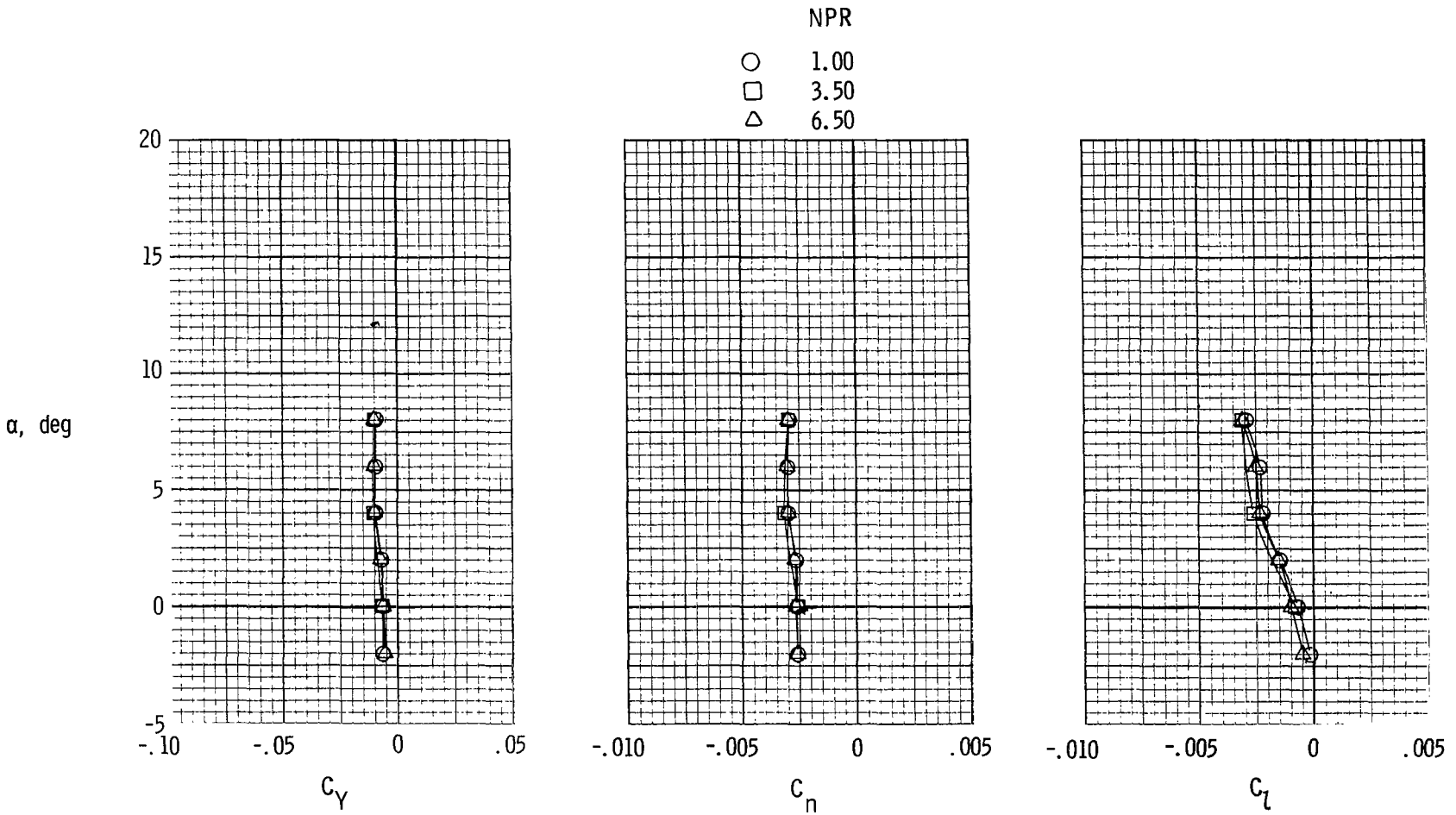

(c) M = 1.20.

Figure 17.- Concluded.

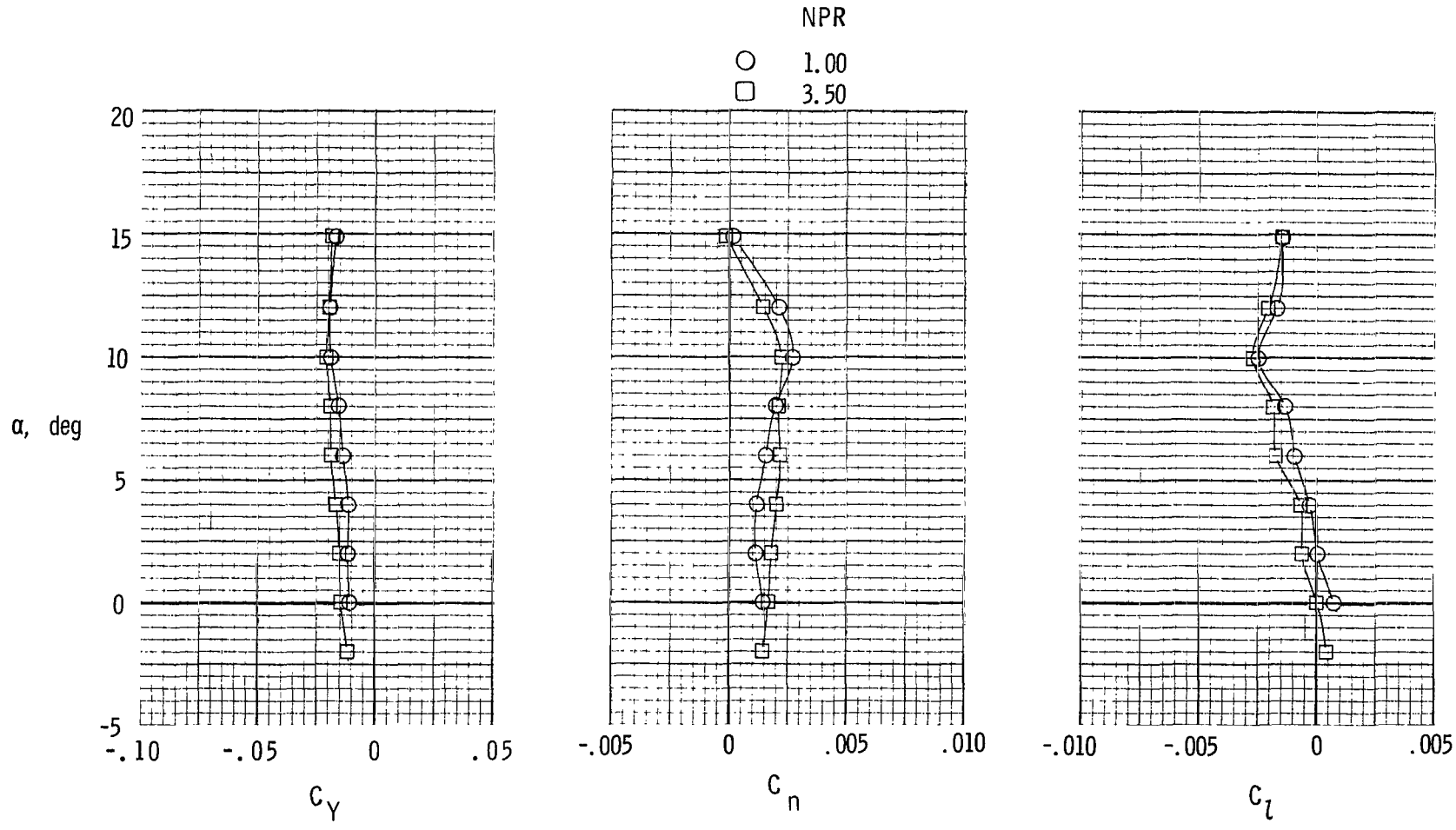

(a) M = 0.60.

Figure 18.- Lateral-directional characteristics of configuration with reversers partially deployed (δ_{REV} = 90°), β = 0°, and δ_R = 0°.

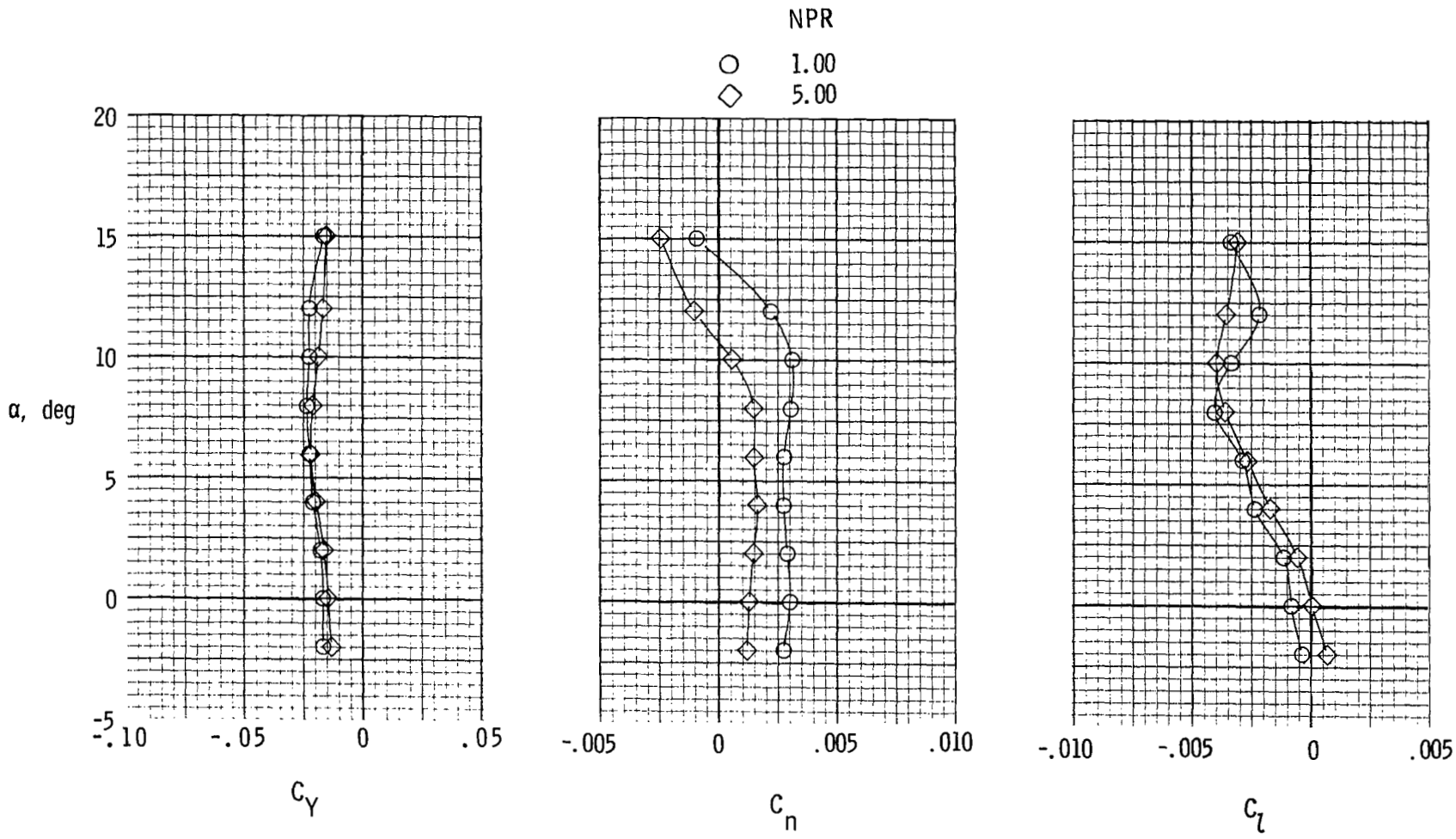

(b) M = 0.90.

Figure 18.- Continued.

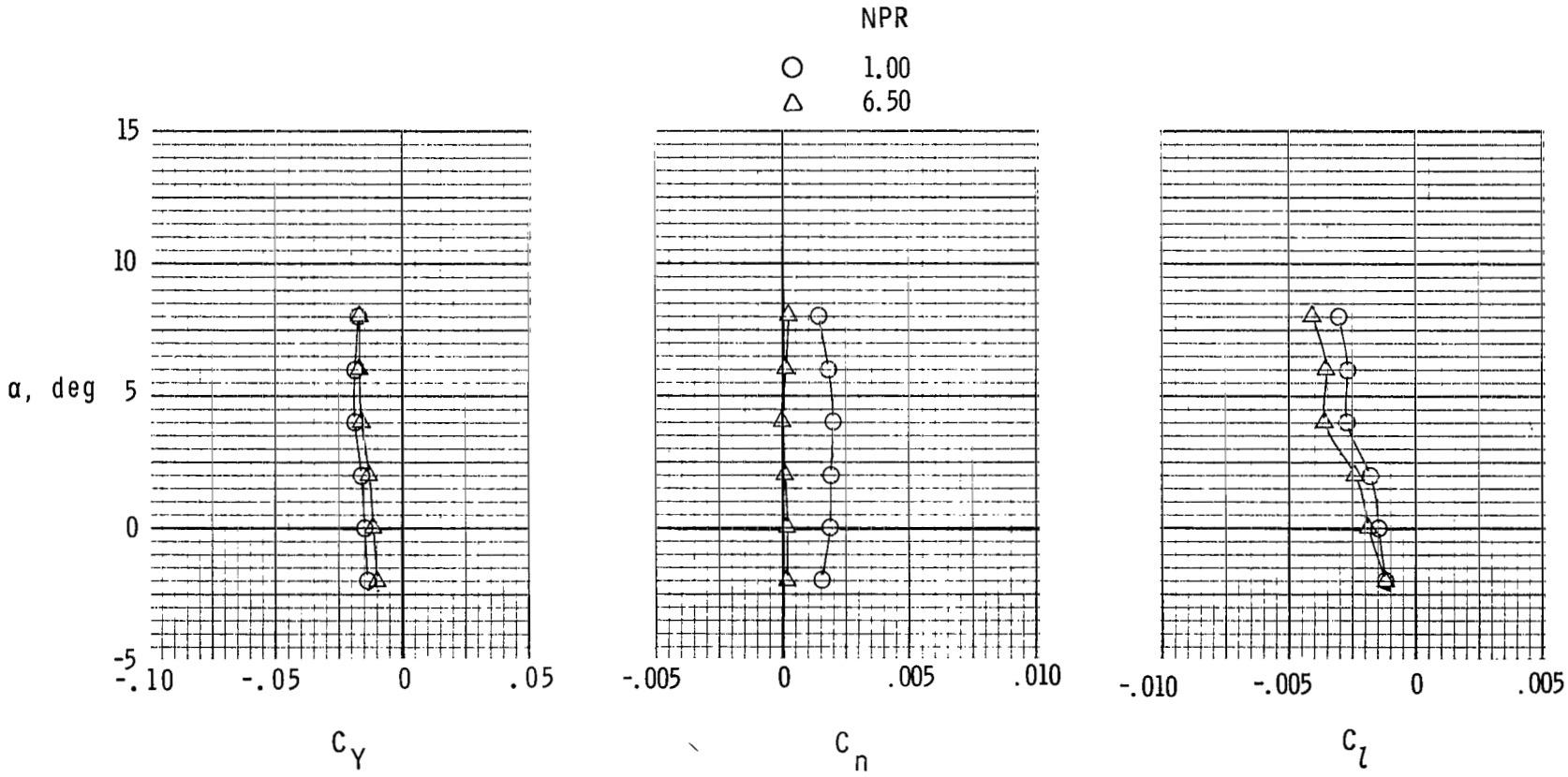

(c) M = 1.20.

Figure 18.- Concluded.

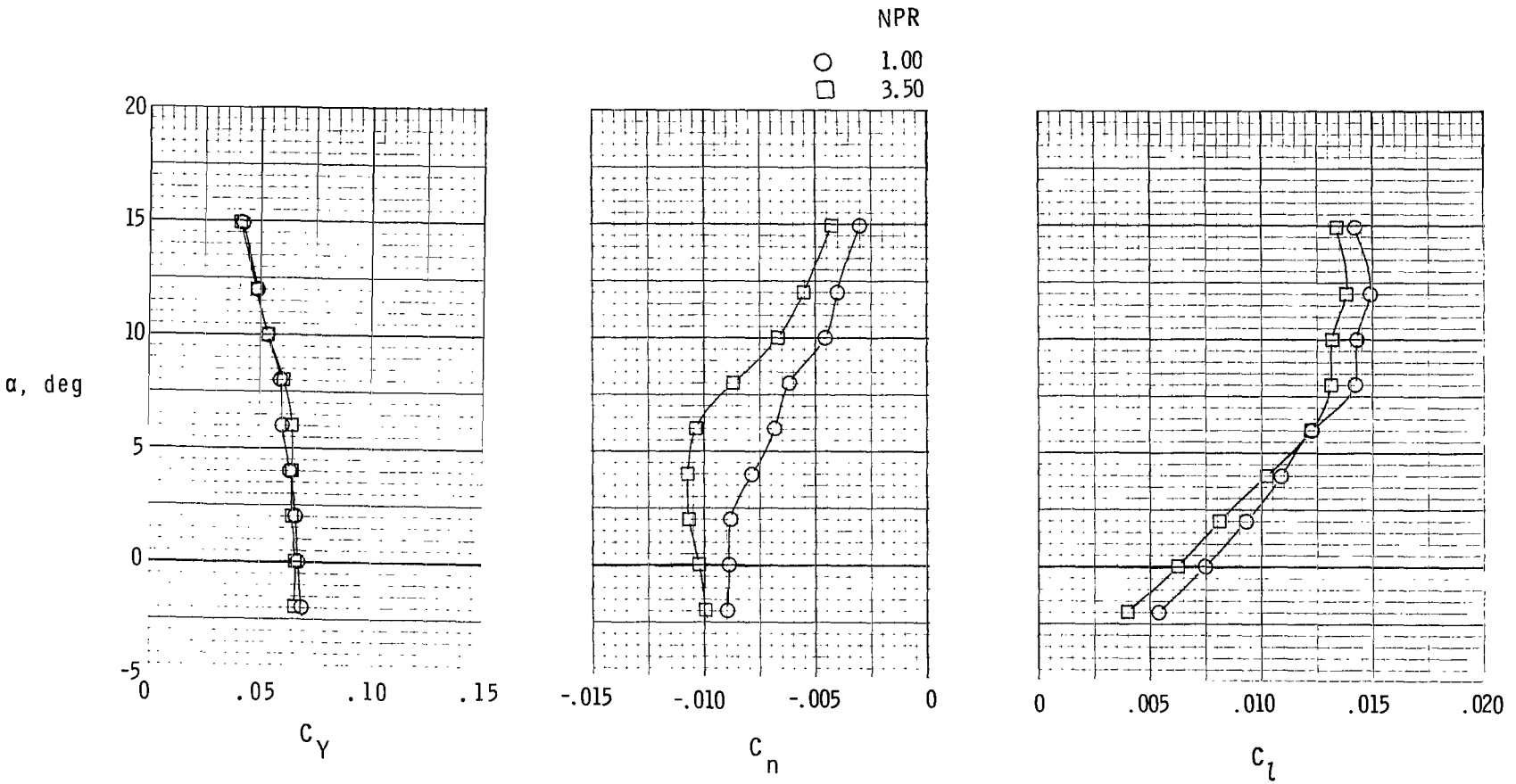

(a) M = 0.60.

Figure 19.- Lateral-directional characteristics of configuration with reversers partially deployed (δ_{REV} = 90°), β = -5°, and δ_R = 0°.

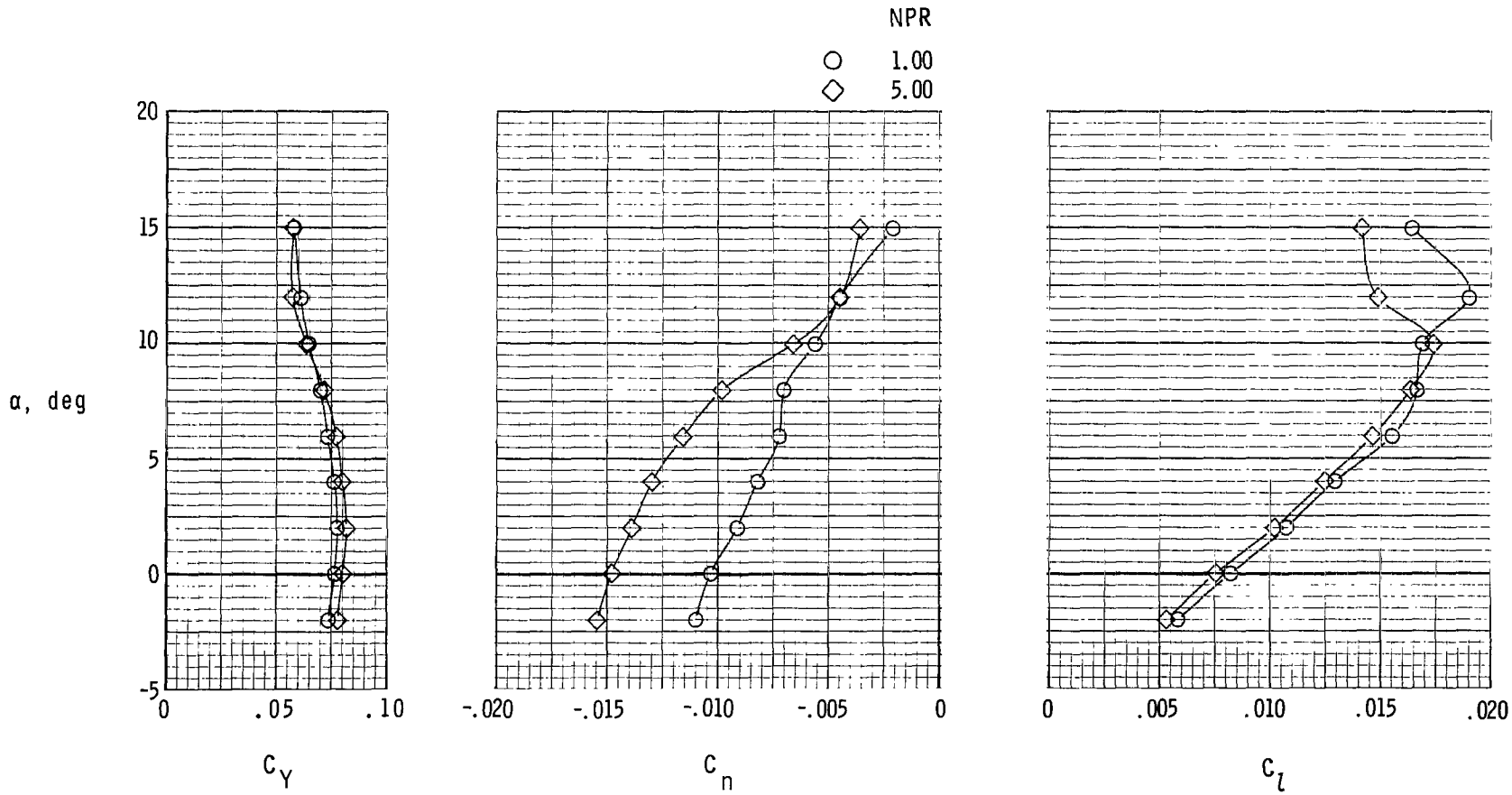

(b) M = 0.90.

Figure 19.- Concluded.

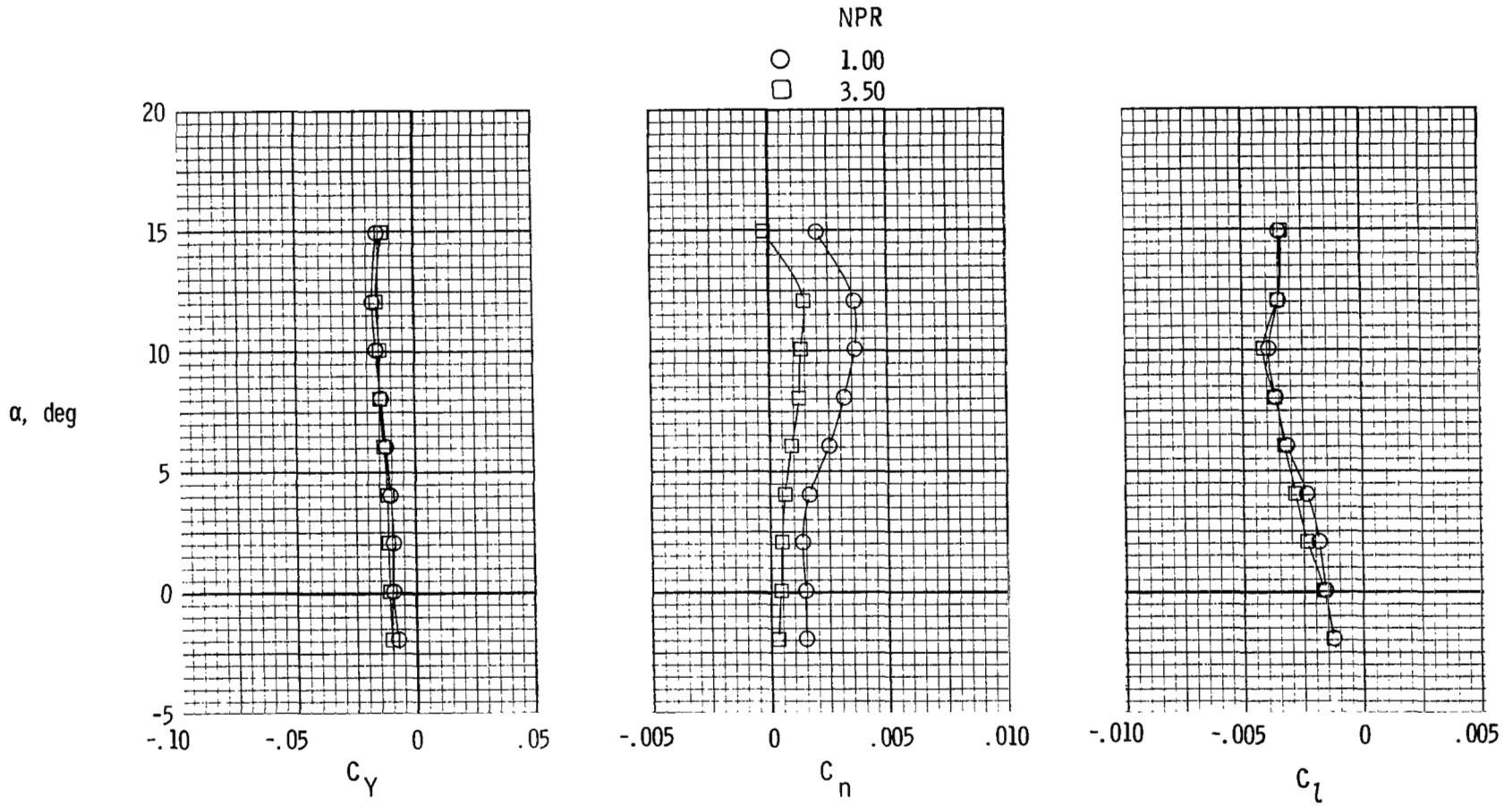

(a) M = 0.60.

Figure 20.- Lateral-directional characteristics of configuration with reversers fully deployed (δ_{REV} = 130°), β = 0°, and δ_R = 0°.

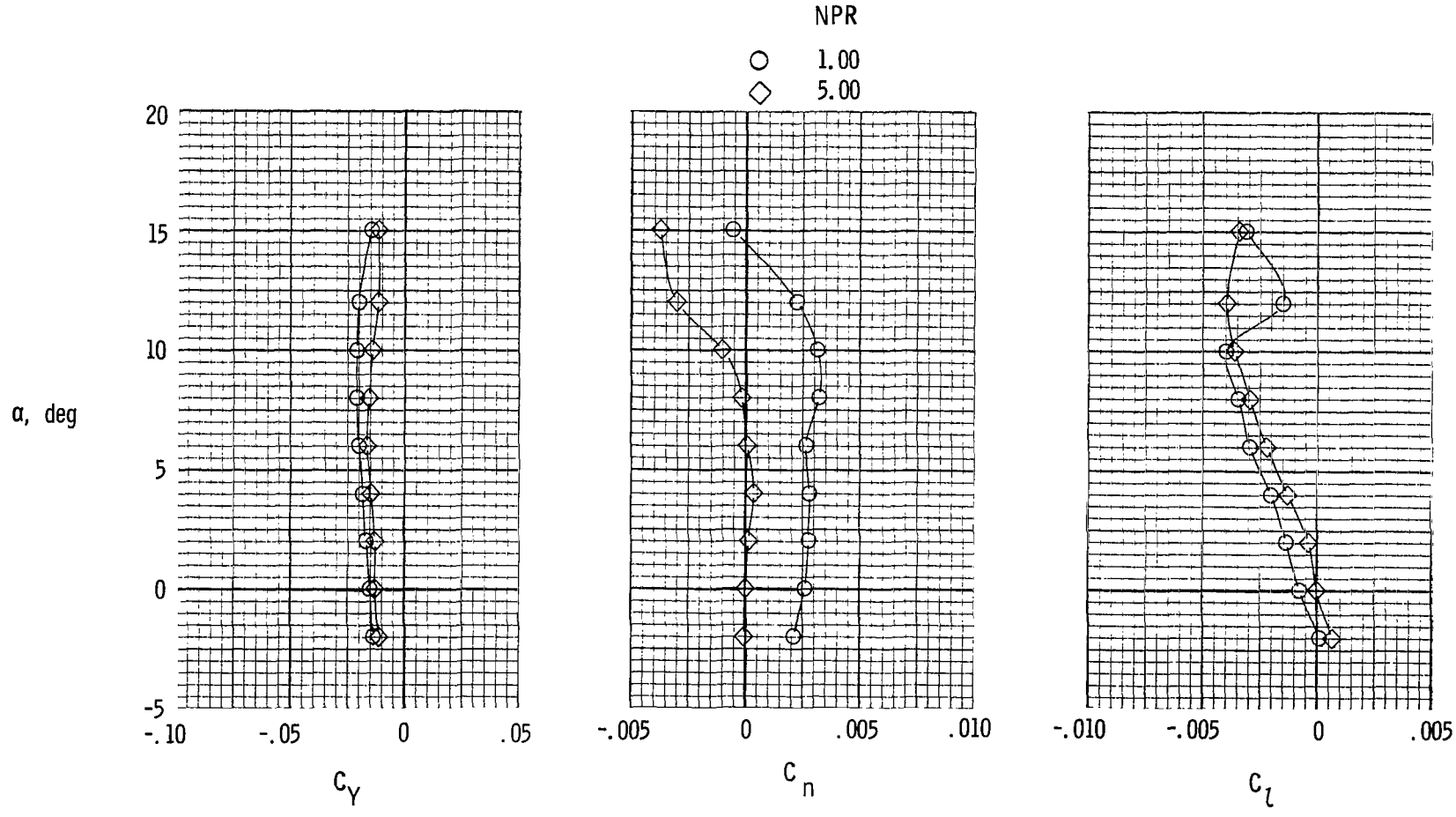

(b) M = 0.90.

Figure 20.- Continued.

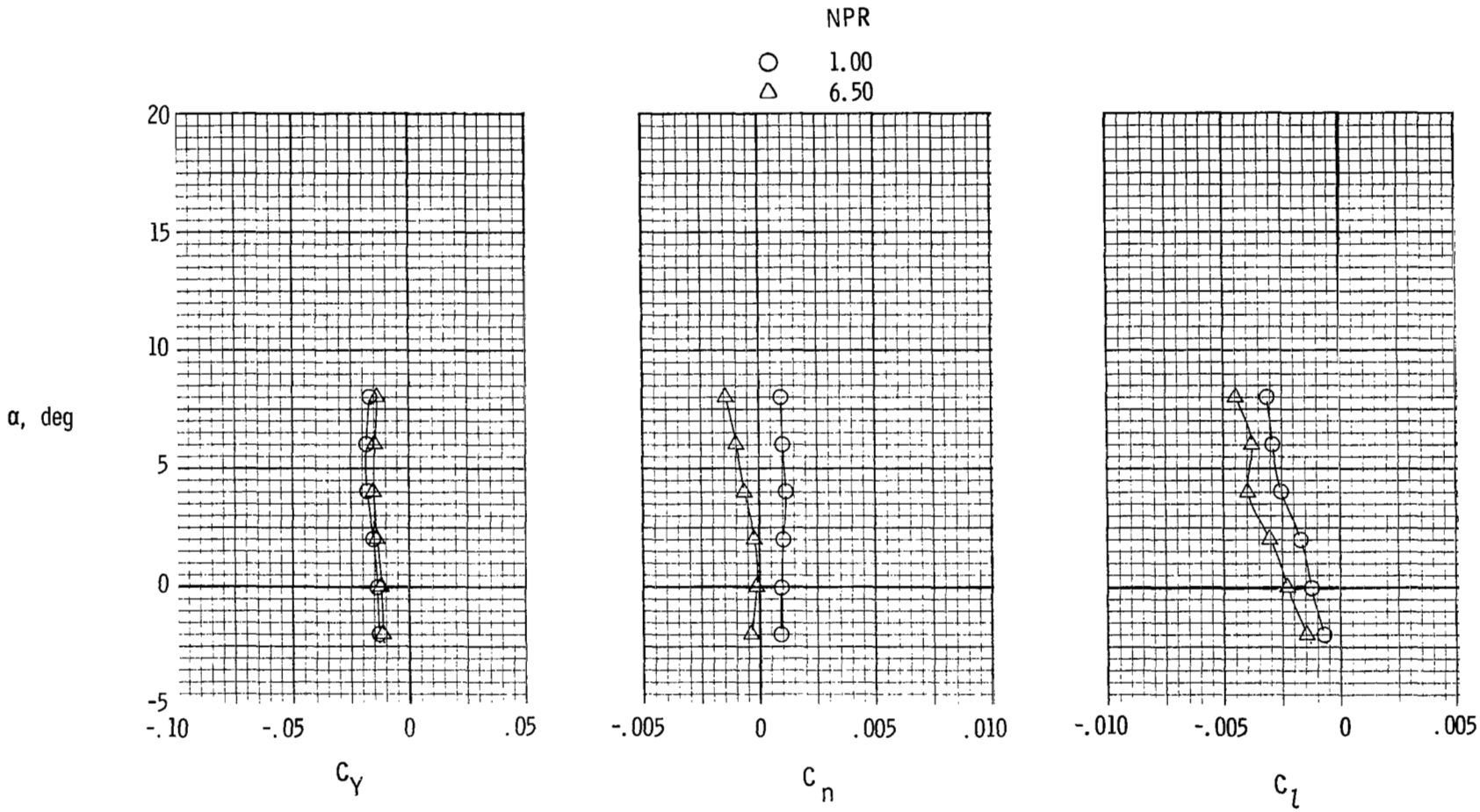

(c) M = 1.20.

Figure 20.- Concluded.

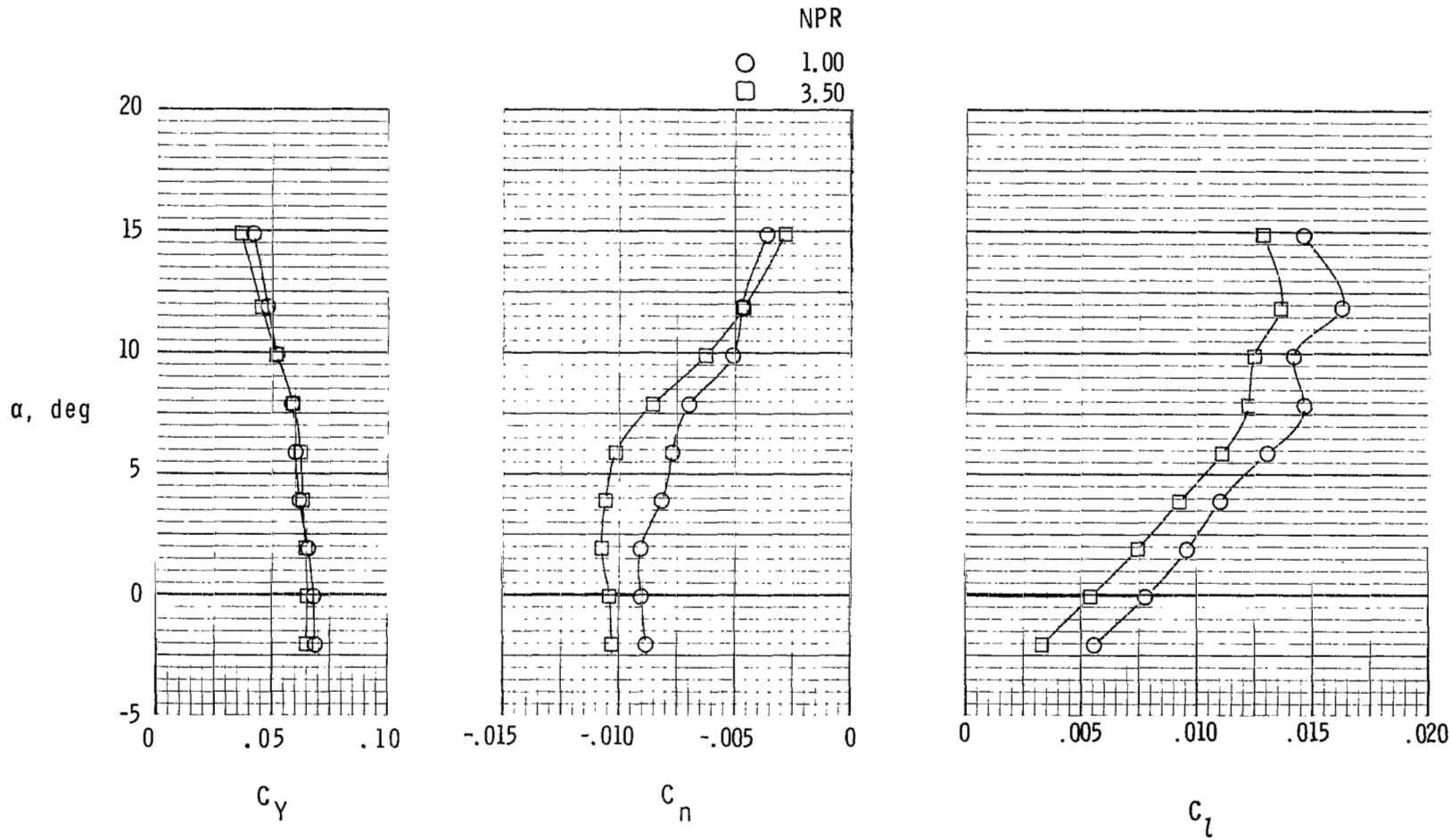

(a) M = 0.60.

Figure 21.- Lateral-directional characteristics of configuration with reversers fully deployed (δ_{REV} = 130°), β = -5°, and δ_R = 0°.

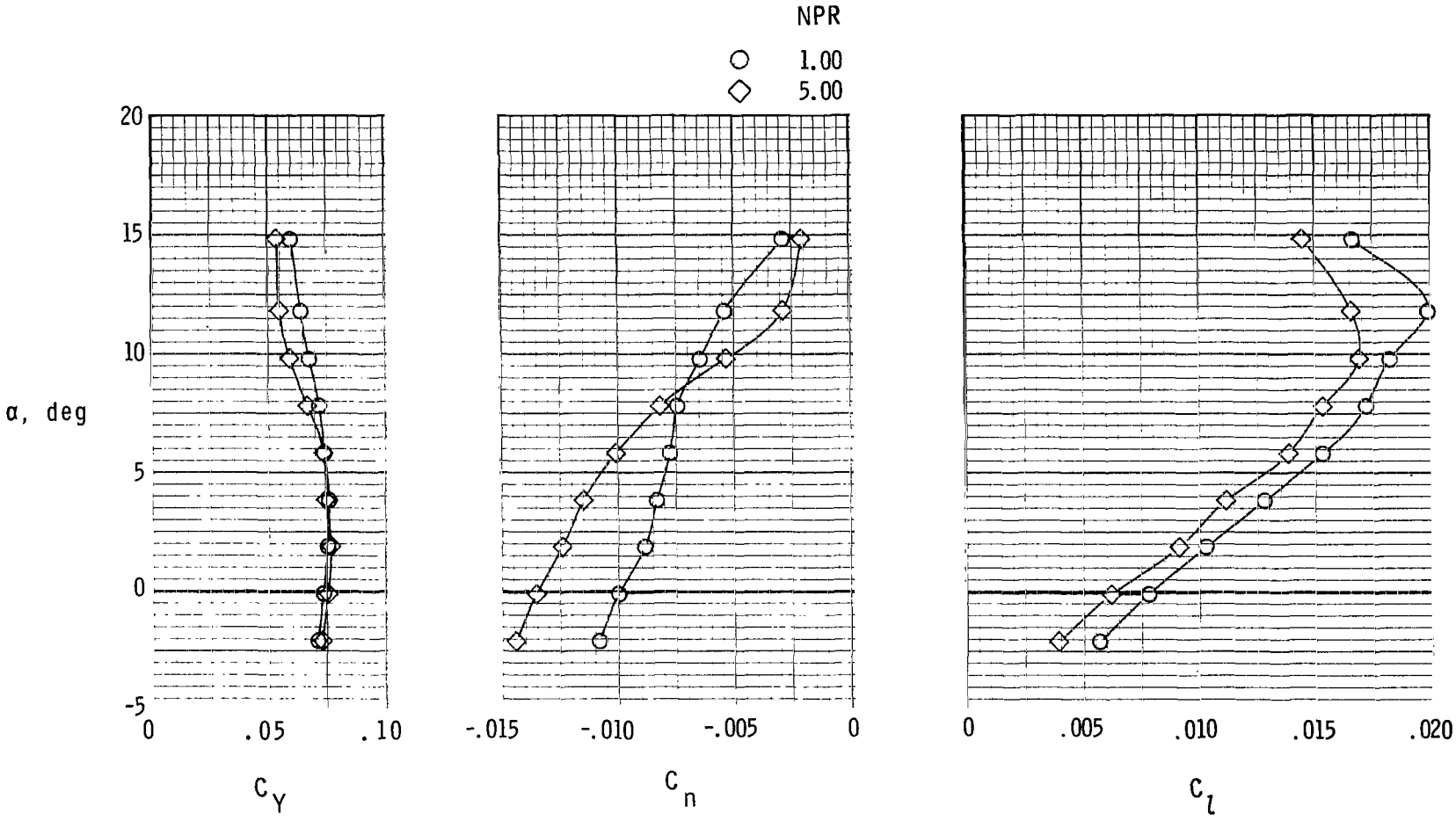

(b) M = 0.90.

Figure 21.- Concluded.

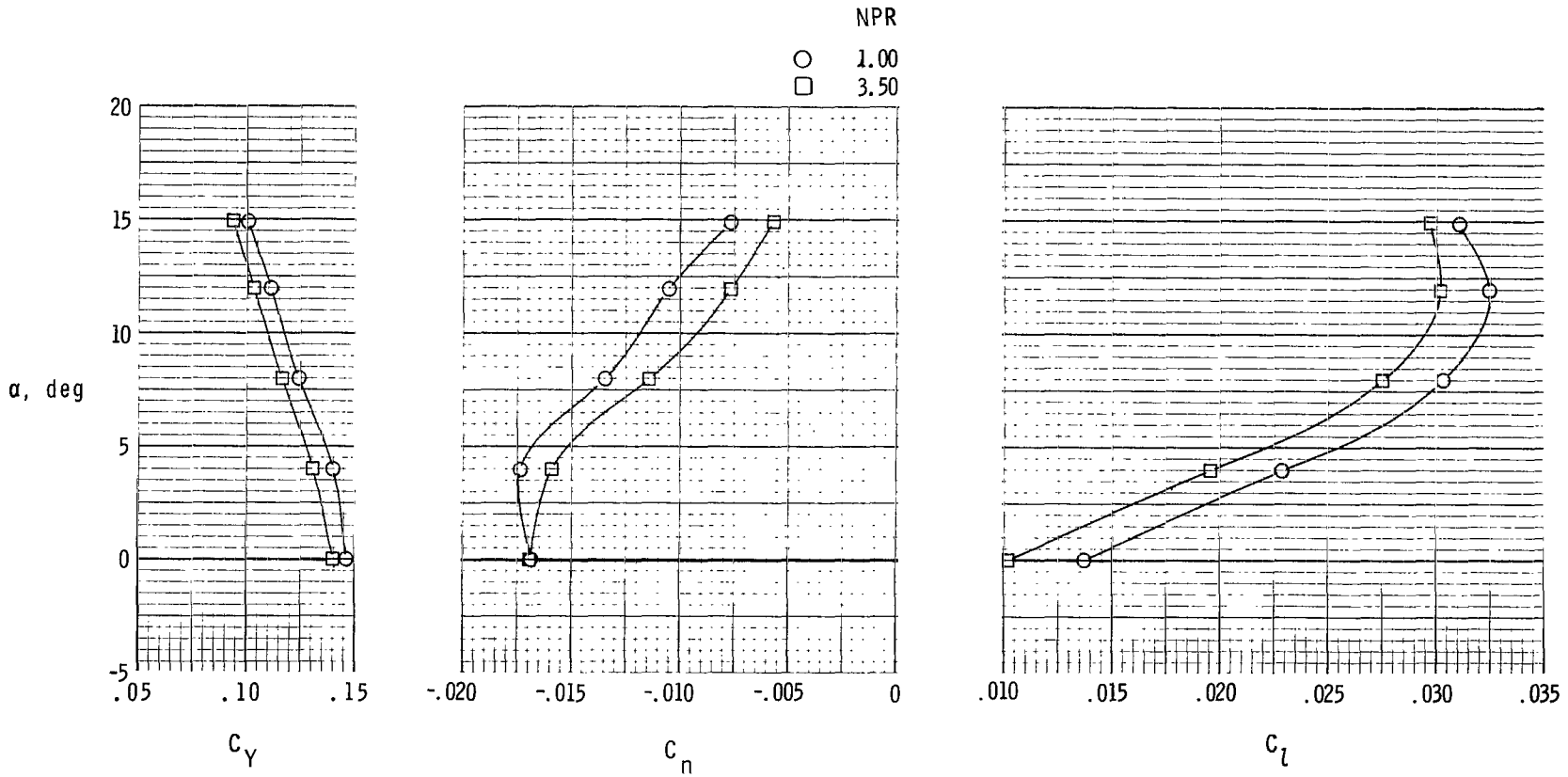

(a) M = 0.60.

Figure 22.- Lateral-directional characteristics of configuration with reversers fully deployed (δ_{REV} = 130°), β = -10°, and δ_R = 0°.

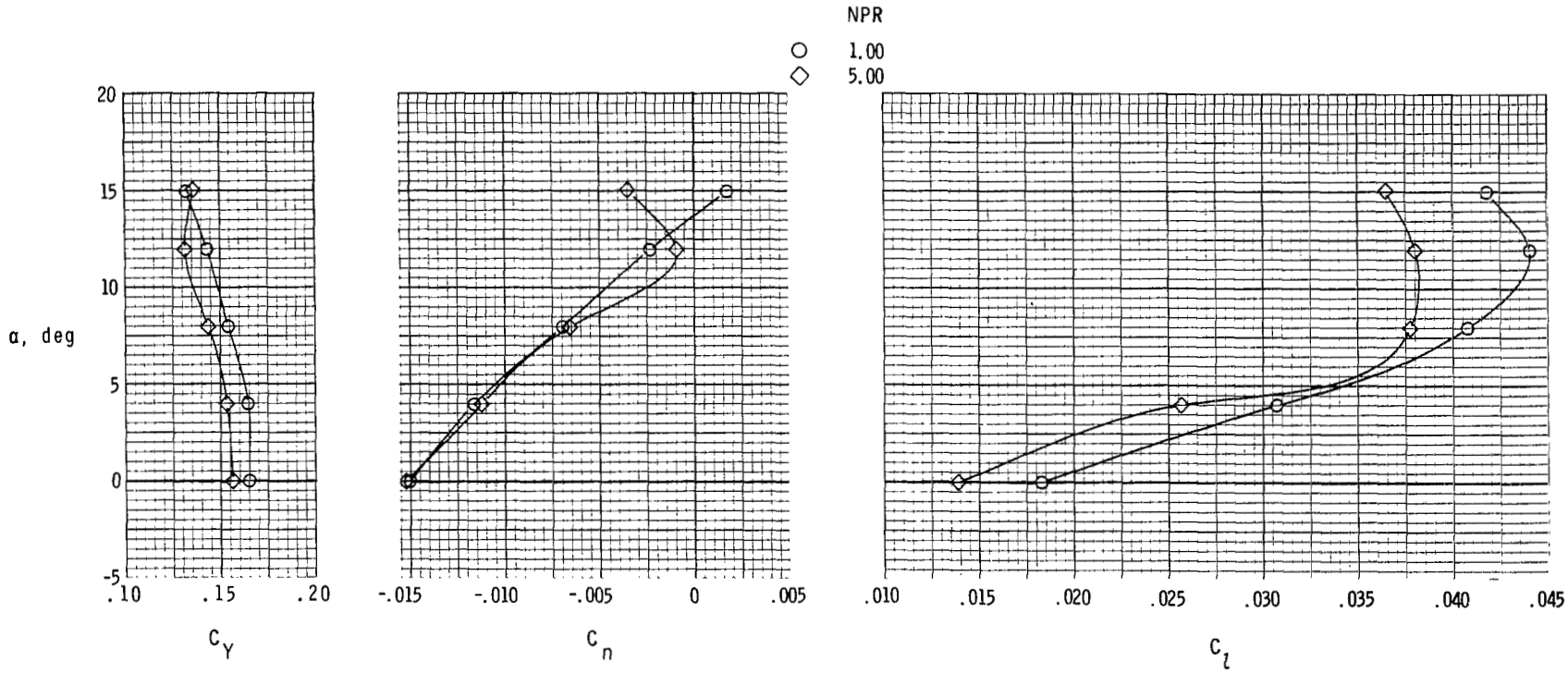

(b) M = 0.90.

Figure 22.- Concluded.

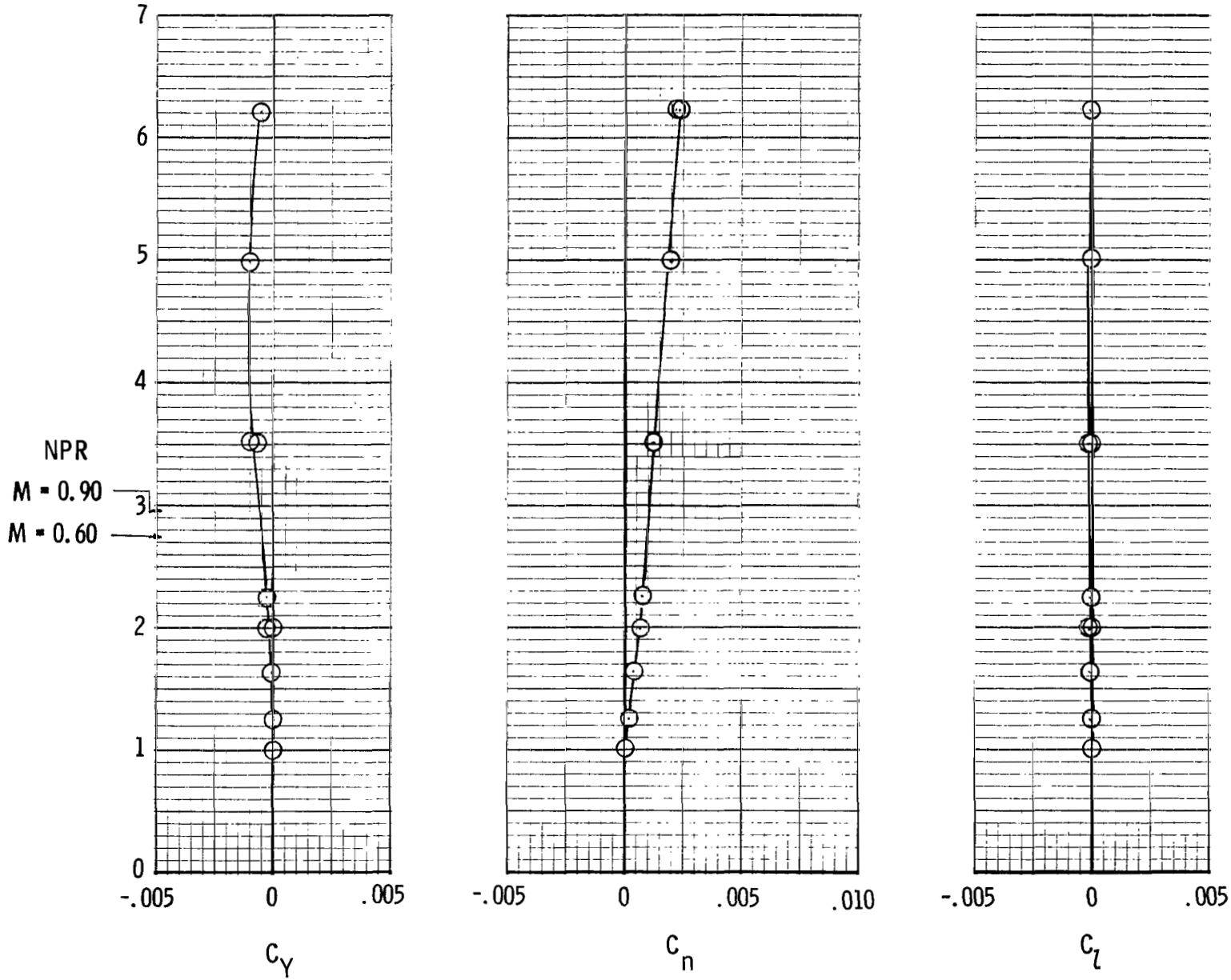

(a) M = 0, α = 0°. Indicated points are jet total-pressure values equivalent to operating NPR at Mach numbers shown.

Figure 23.- Lateral-directional characteristics of configuration with differential reversing (δ_{REV} = 0° for L.H. nozzle and δ_{REV} = 130° for R.H. nozzle), β = 0°, and δ_R = 0°.

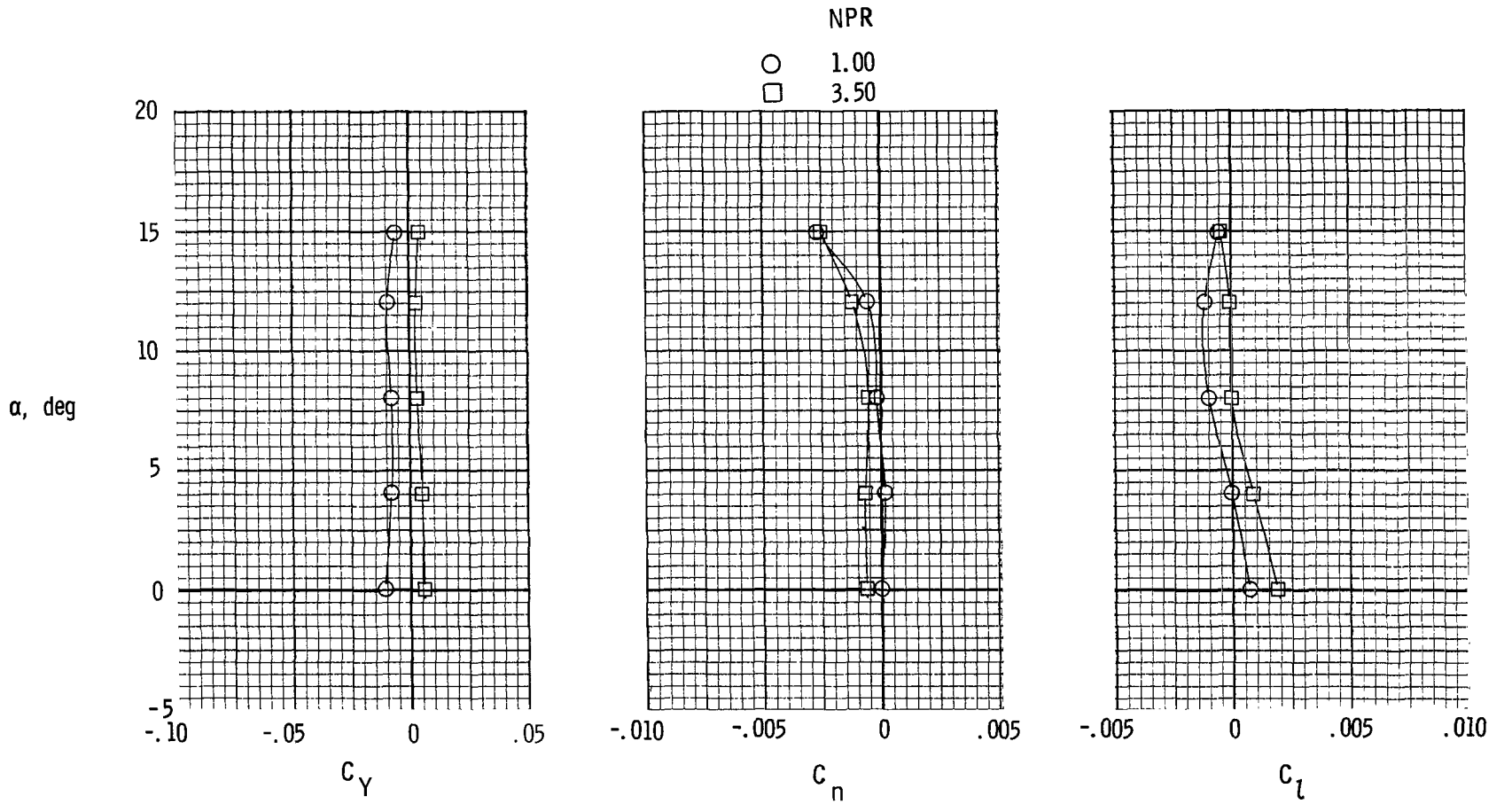

(b) M = 0.60.

Figure 23.- Continued.

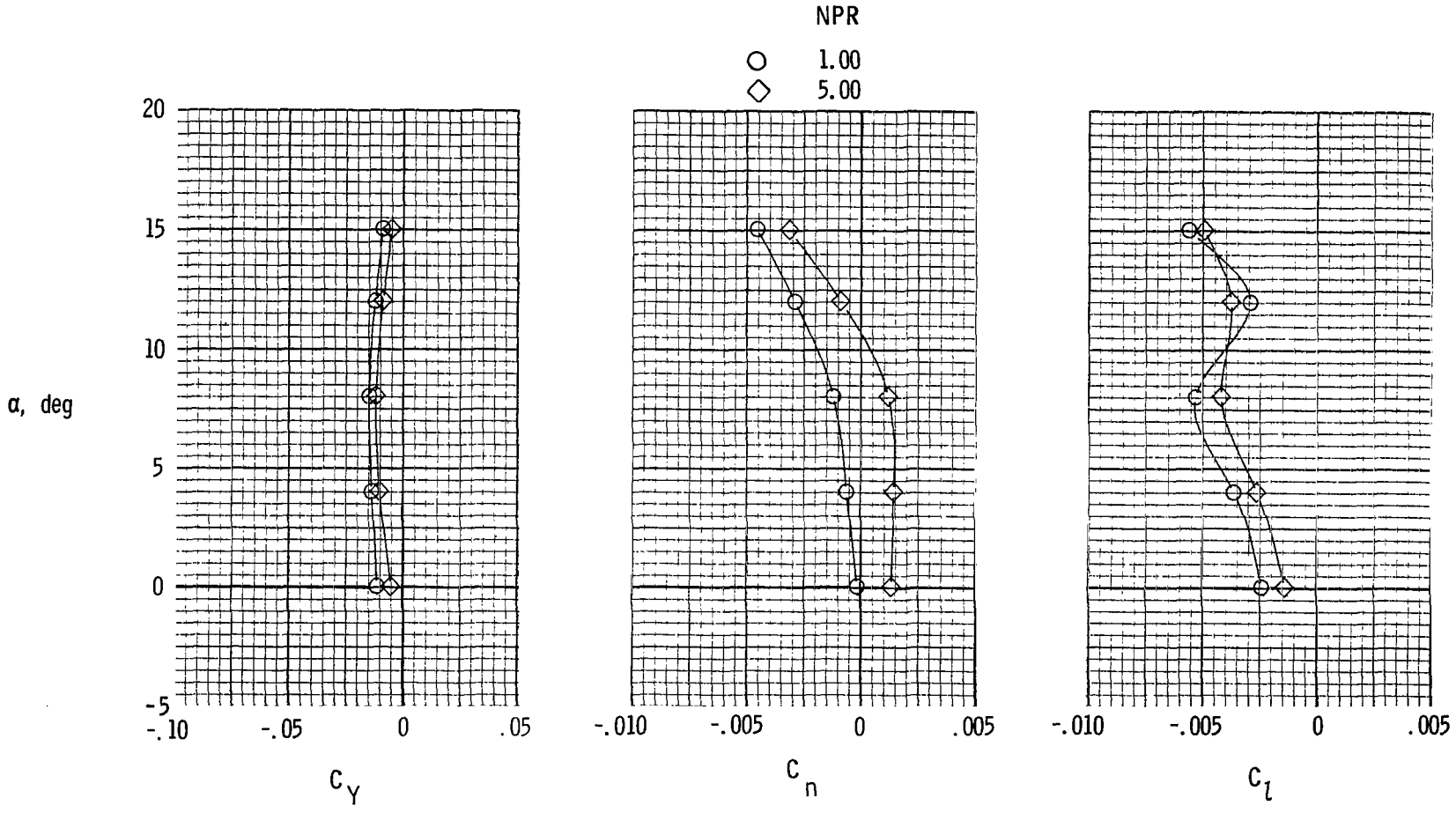

(c) M = 0.90.

Figure 23.- Concluded.

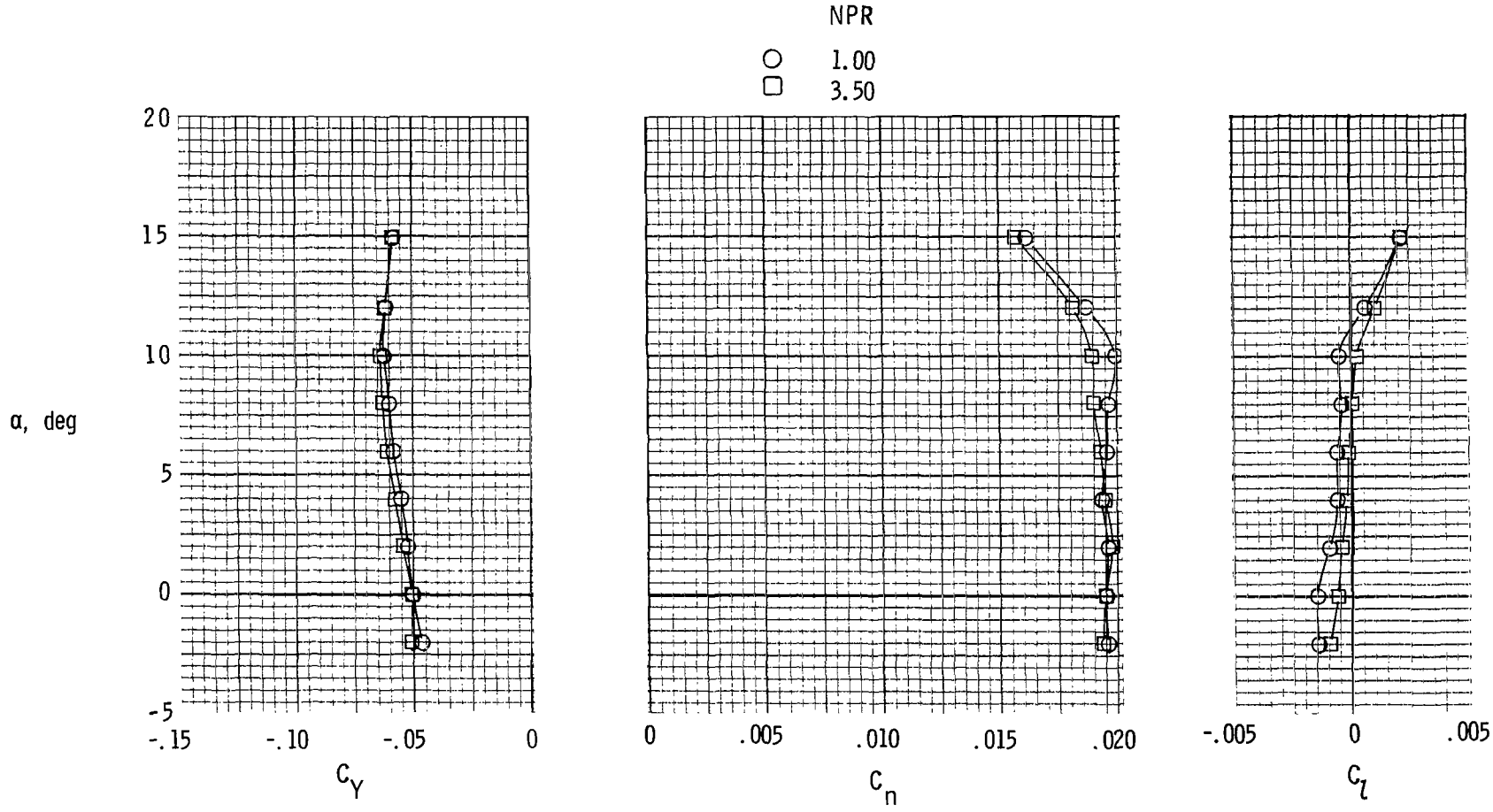

(a) M = 0.60.

Figure 24.- Lateral-directional characteristics of configuration with reversers partially deployed (δ_{REV} = 90°), β = 0°, and δ_R = -10°.

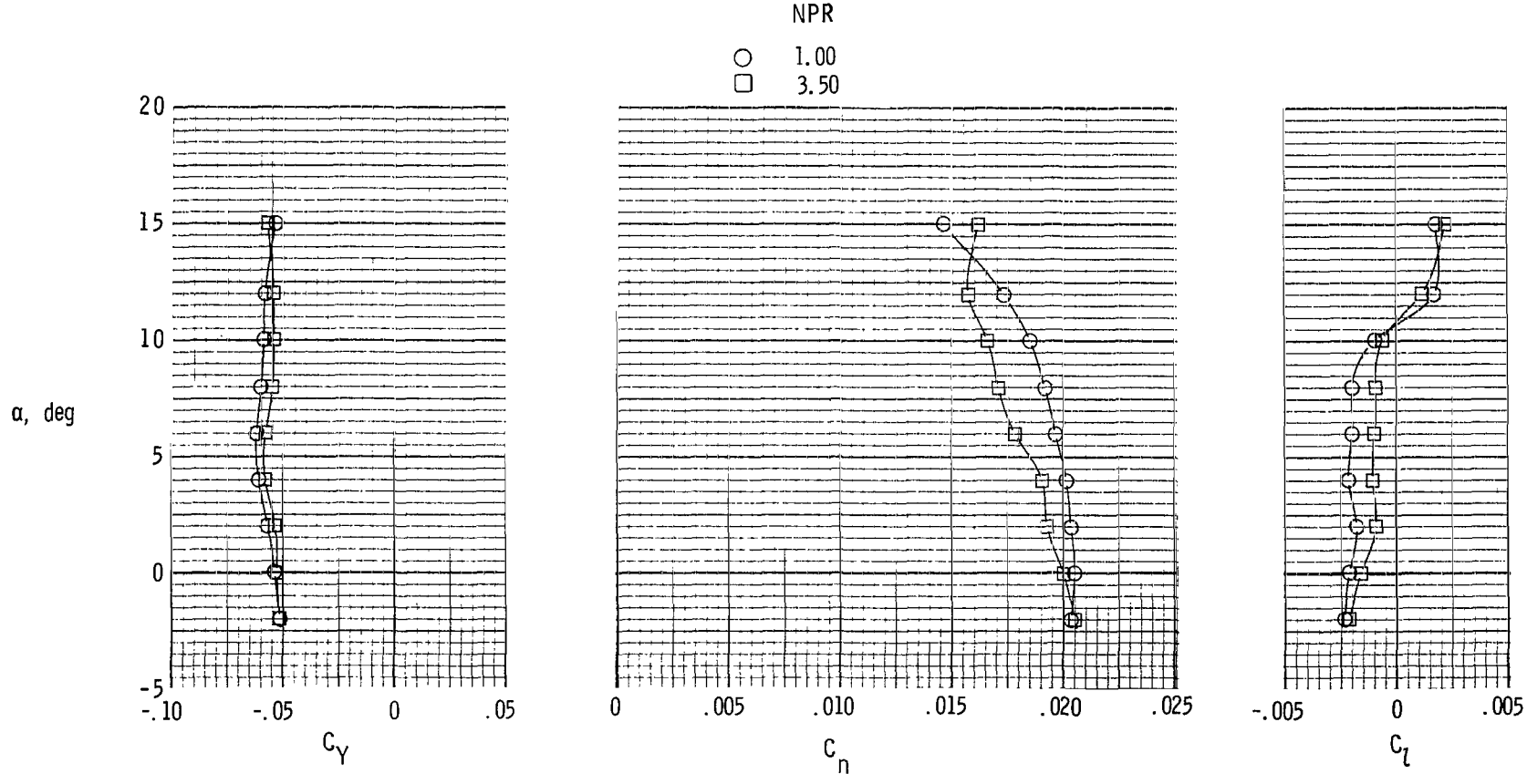

(b) M = 0.90.

Figure 24.- Continued.

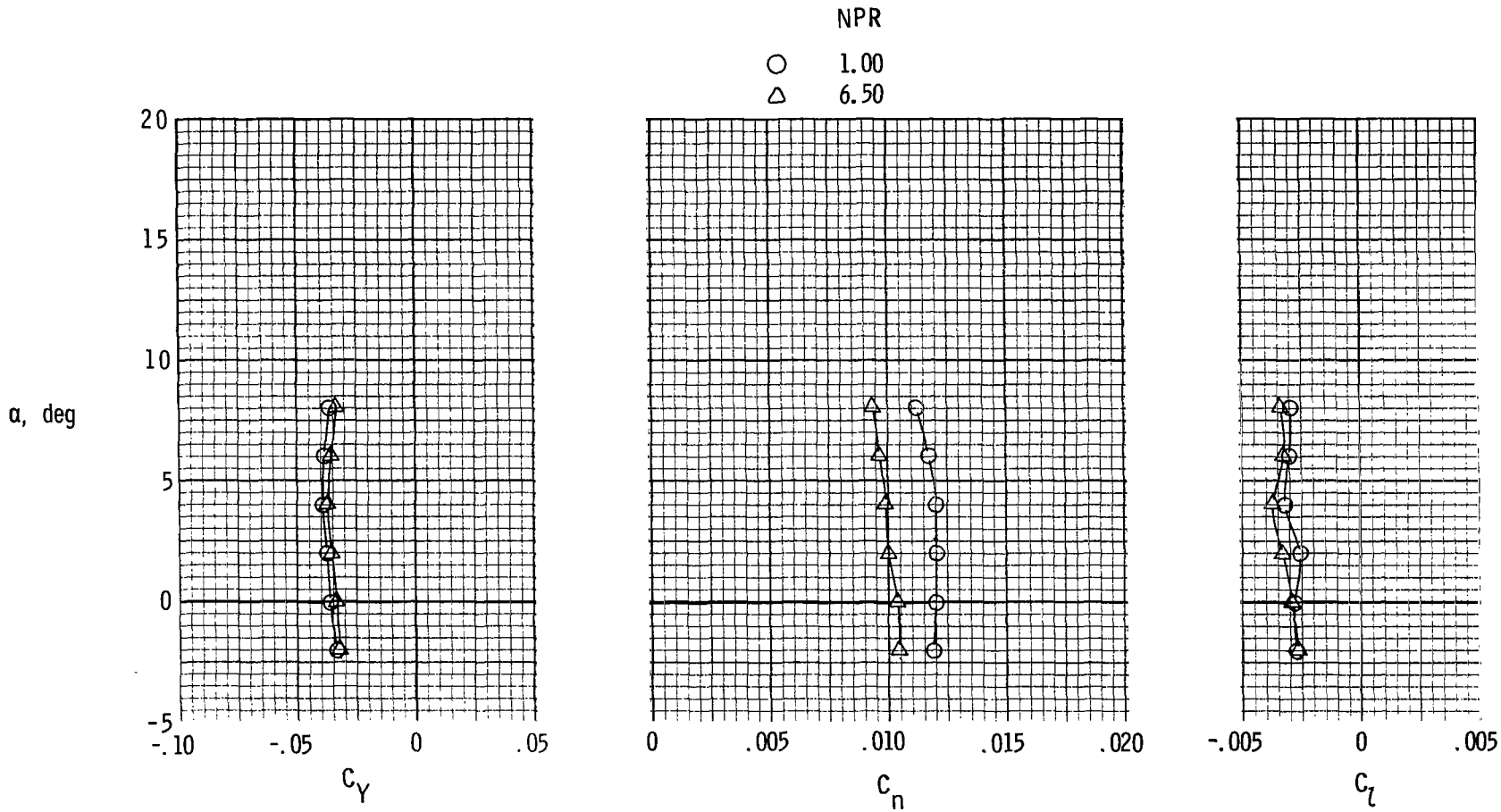

(c) M = 1.20.

Figure 24.- Concluded.

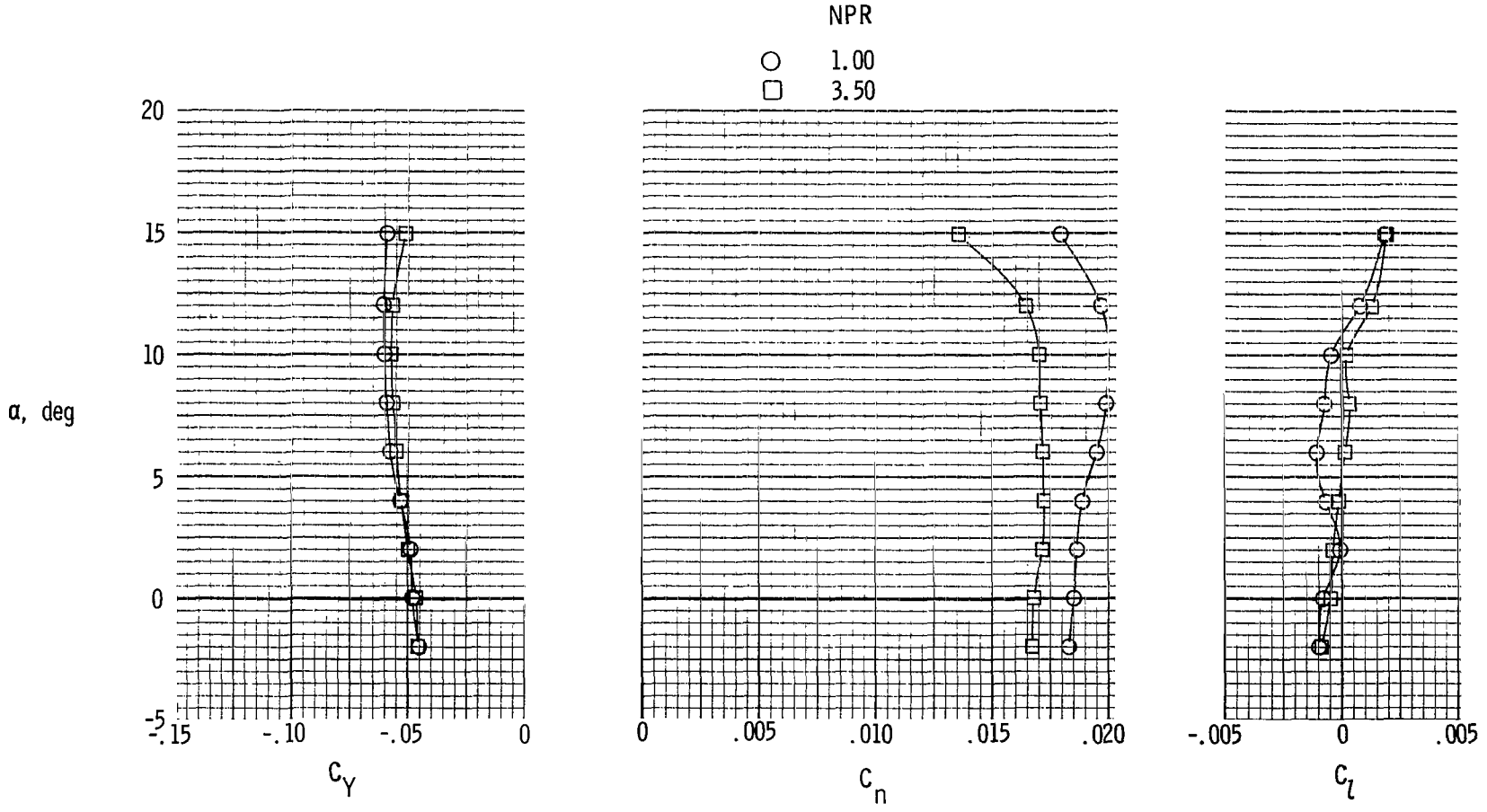

(a) M = 0.60.

Figure 25.- Lateral-directional characteristics of configuration with reversers fully deployed (δ_{REV} = 130°), β = 0°, and δ_R = -10°.

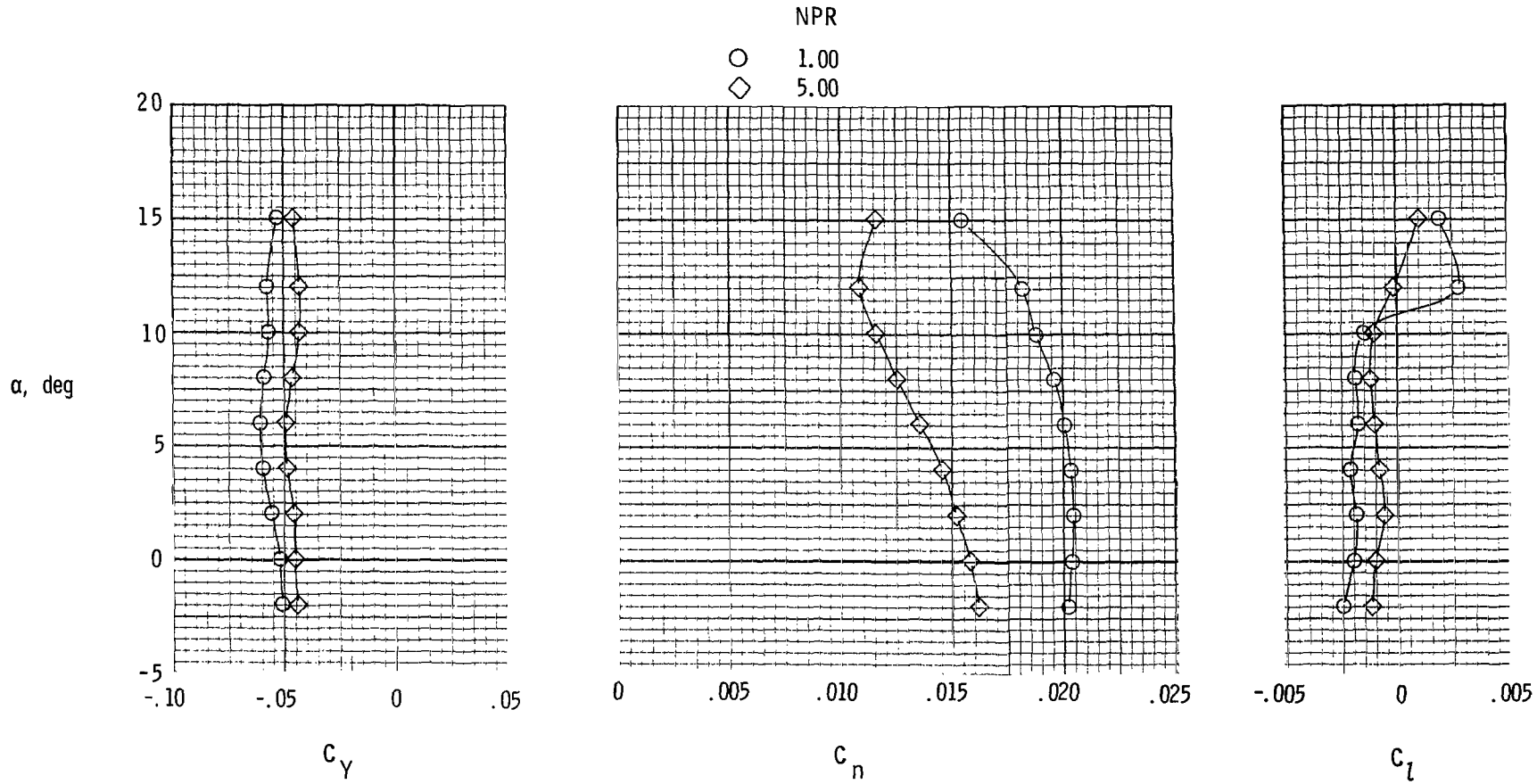

(b) M = 0.90.

Figure 25.- Continued.

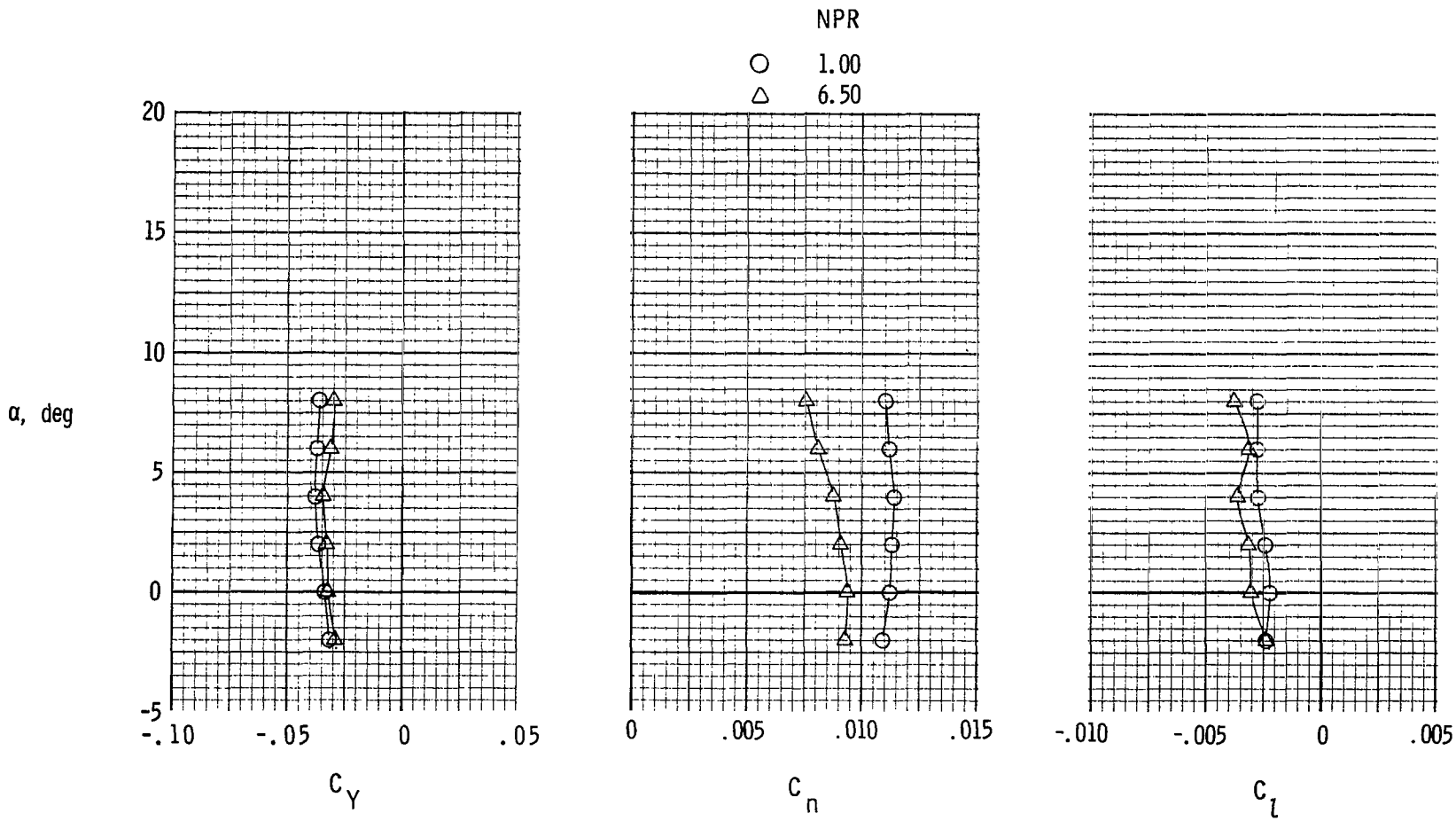

(c) M = 1.20.

Figure 25.- Concluded.

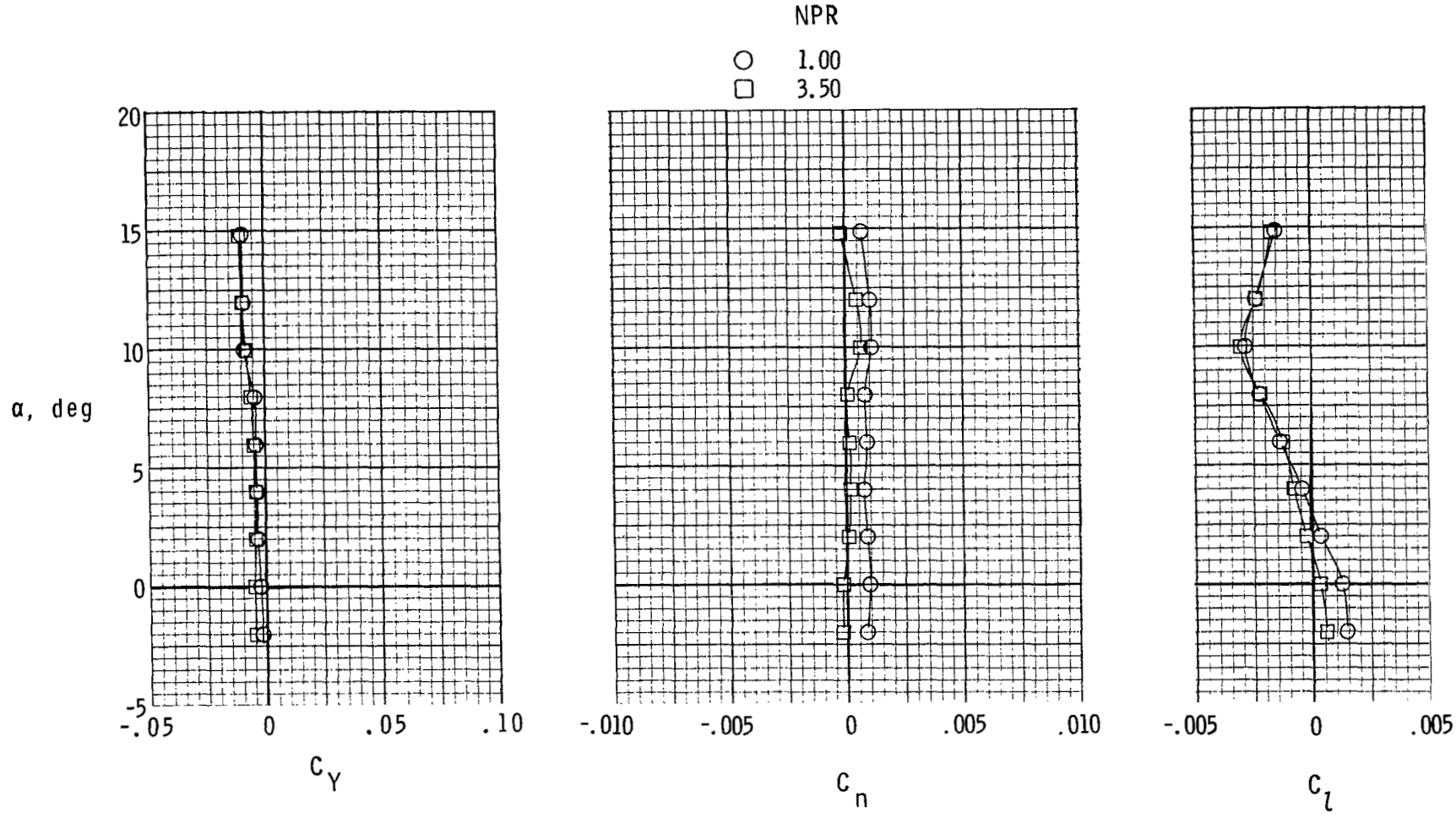

(a) M = 0.60.

Figure 26.- Lateral-directional characteristics of configuration with reversers fully deployed (δ_{REV} = 130°), vertical tails removed, and β = 0°.

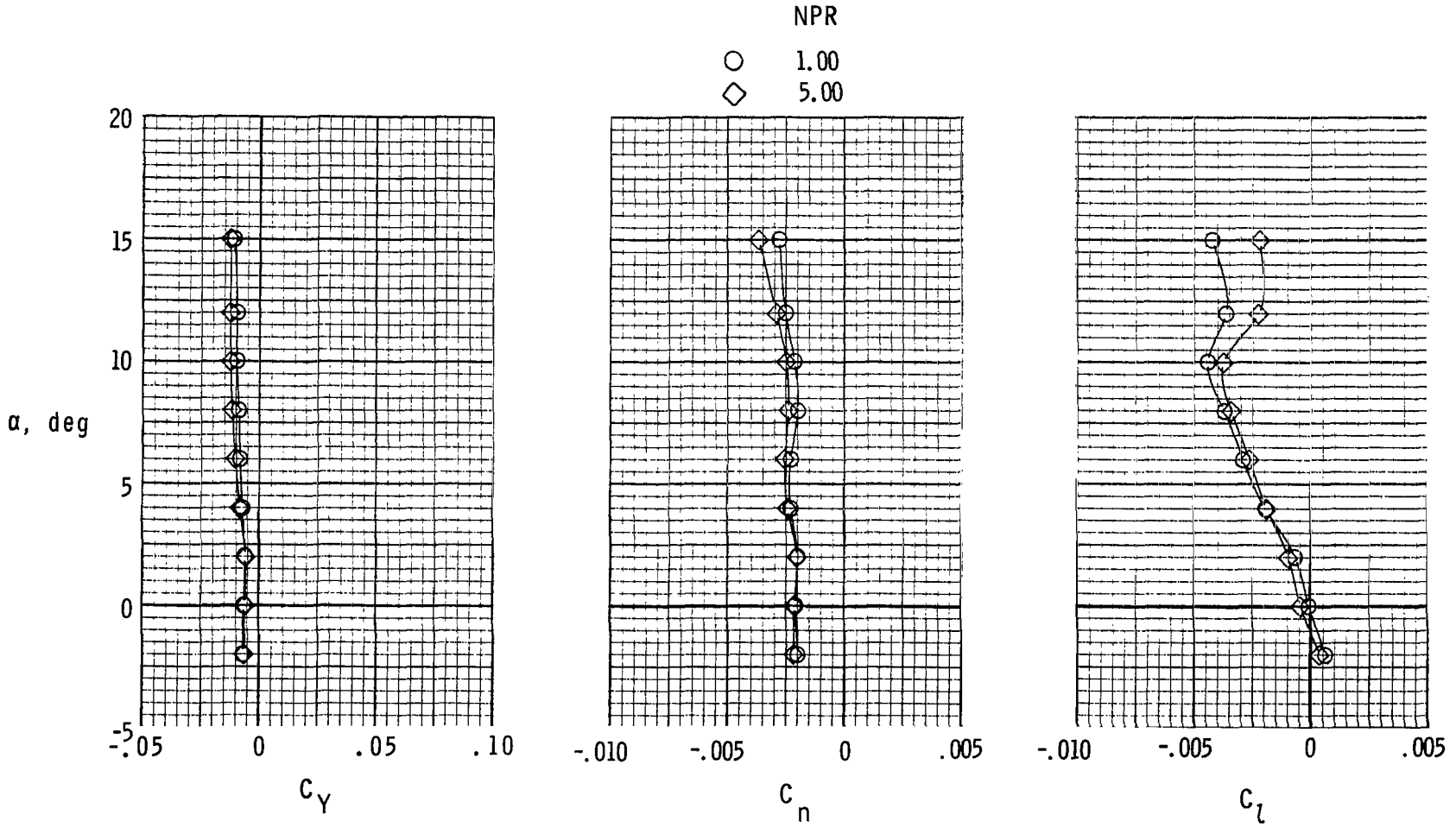

(b) M = 0.90.

Figure 26.- Concluded.

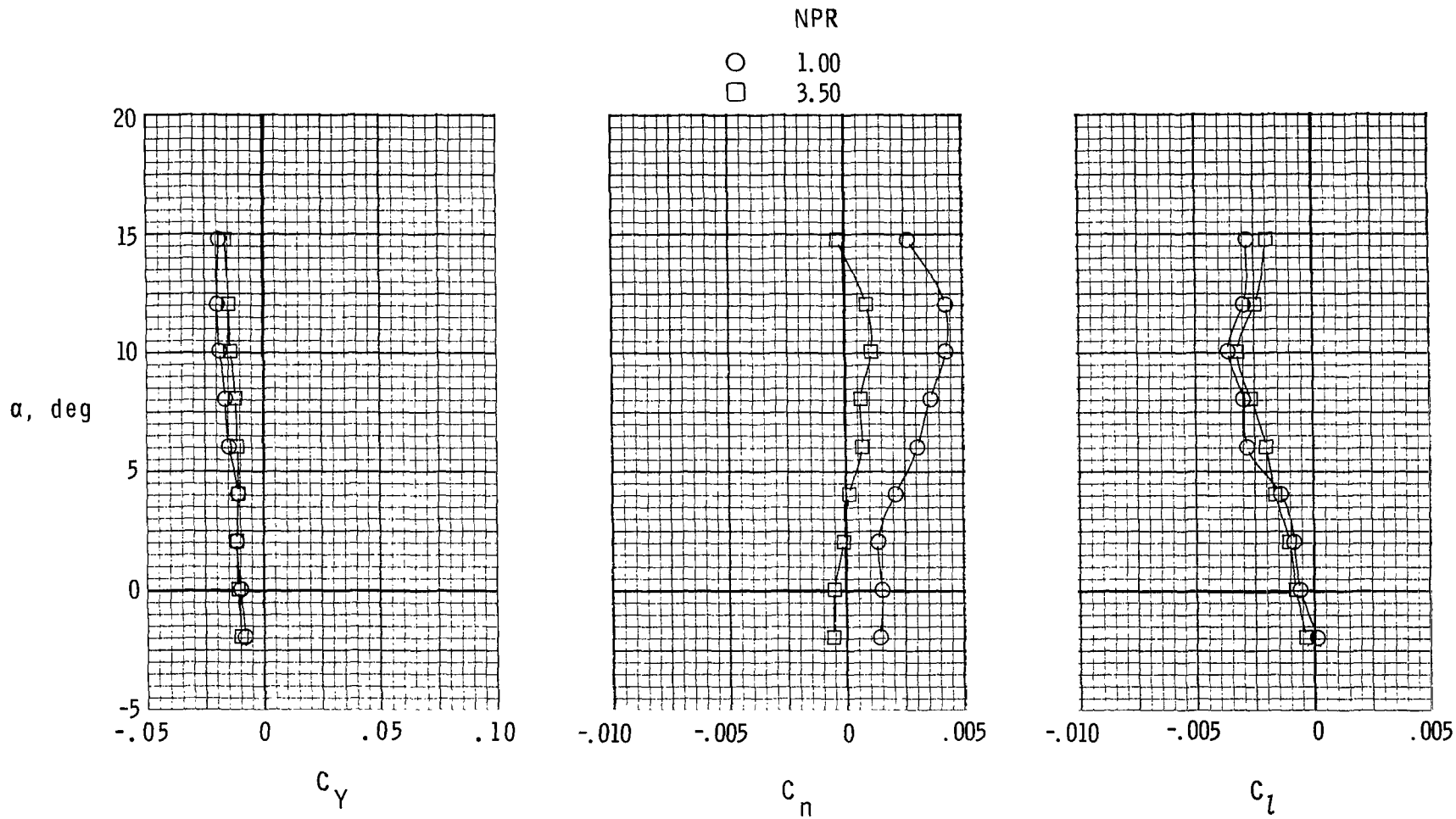

(a) M = 0.60.

Figure 27.- Lateral-directional characteristics of configuration with reversers fully deployed (δ_{REV} = 130°), horizontal tails removed, β = 0°, and δ_R = 0°.

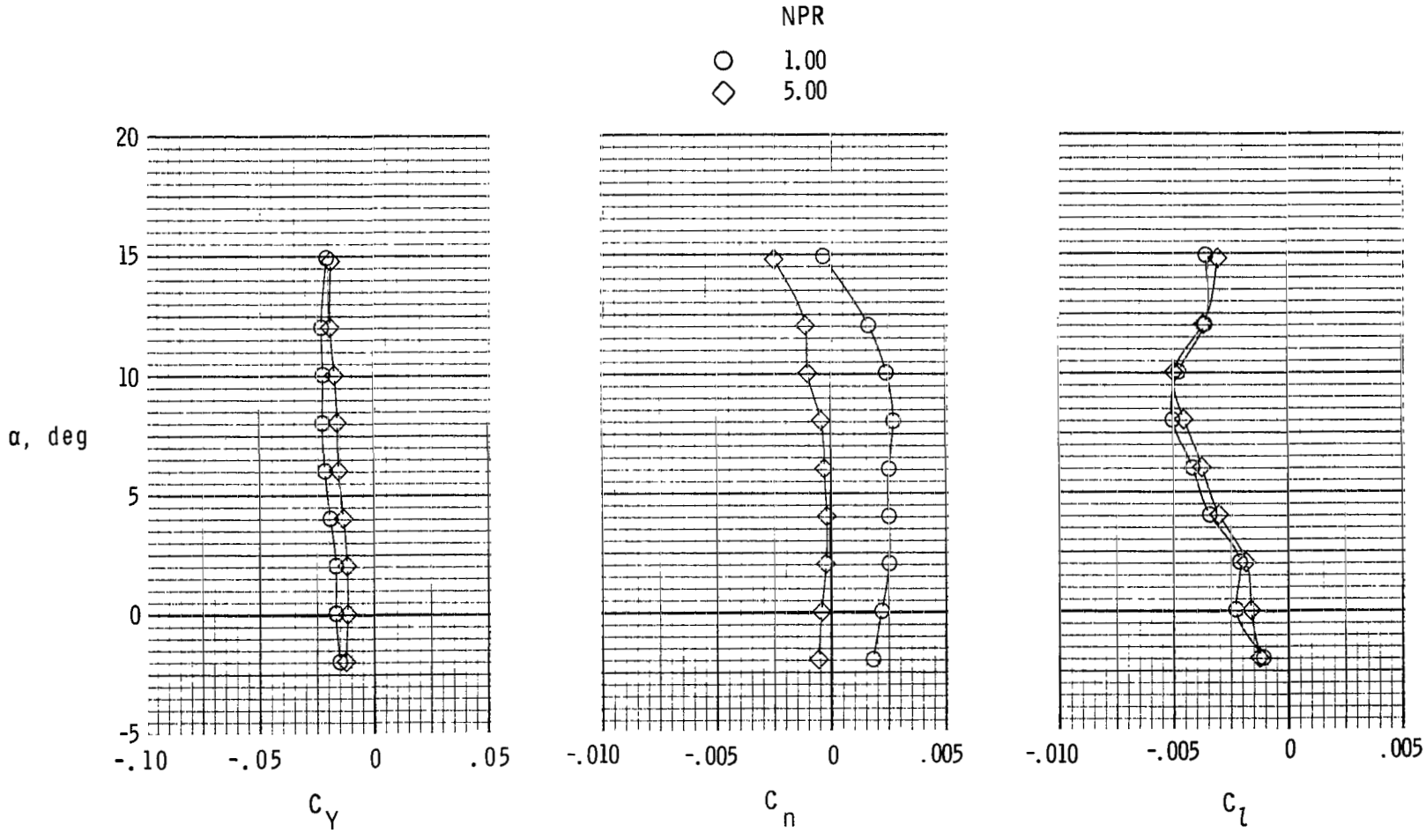

(b) M = 0.90.

Figure 27.- Continued.

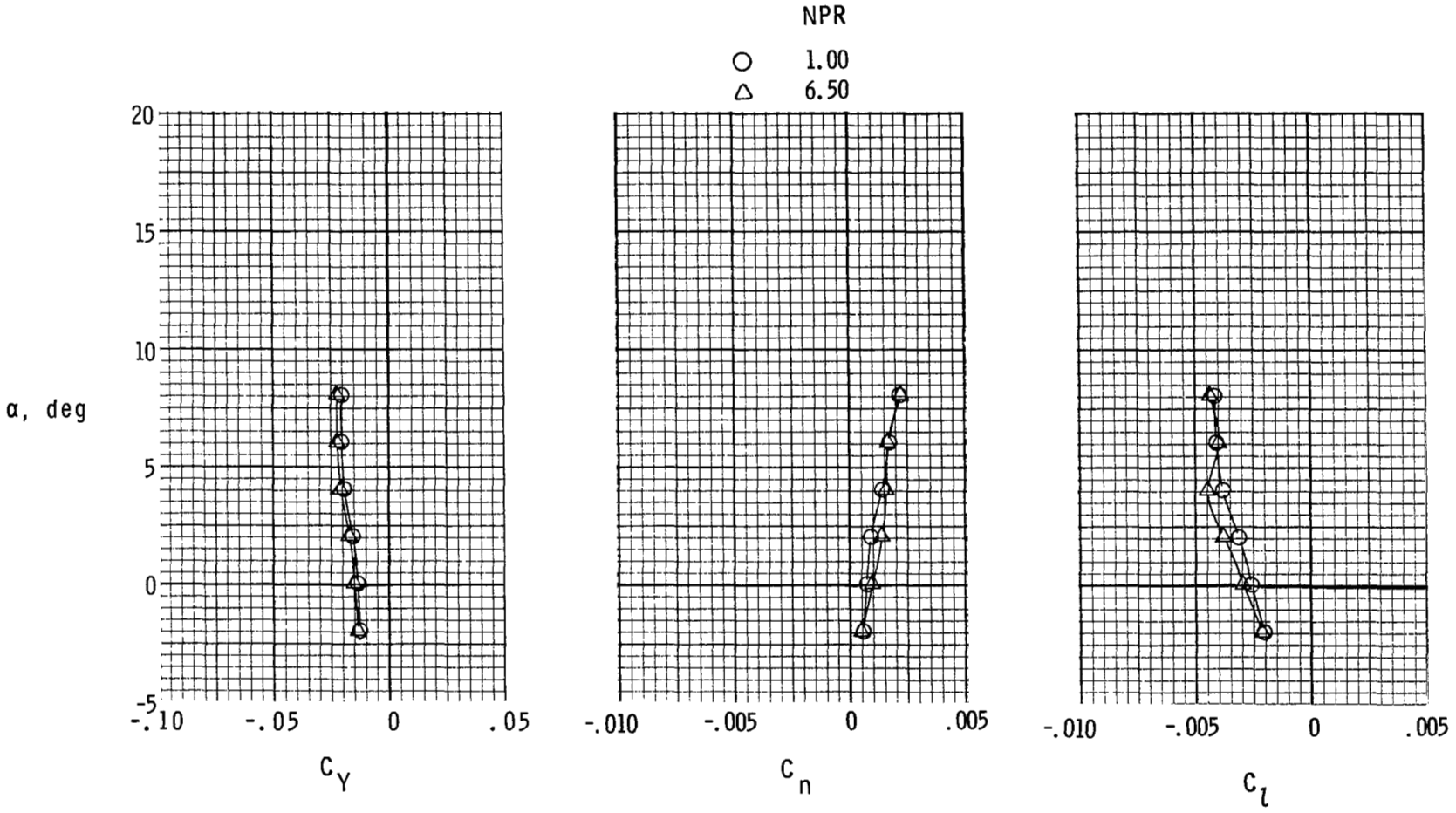

(c) M = 1.20.

Figure 27.- Concluded.

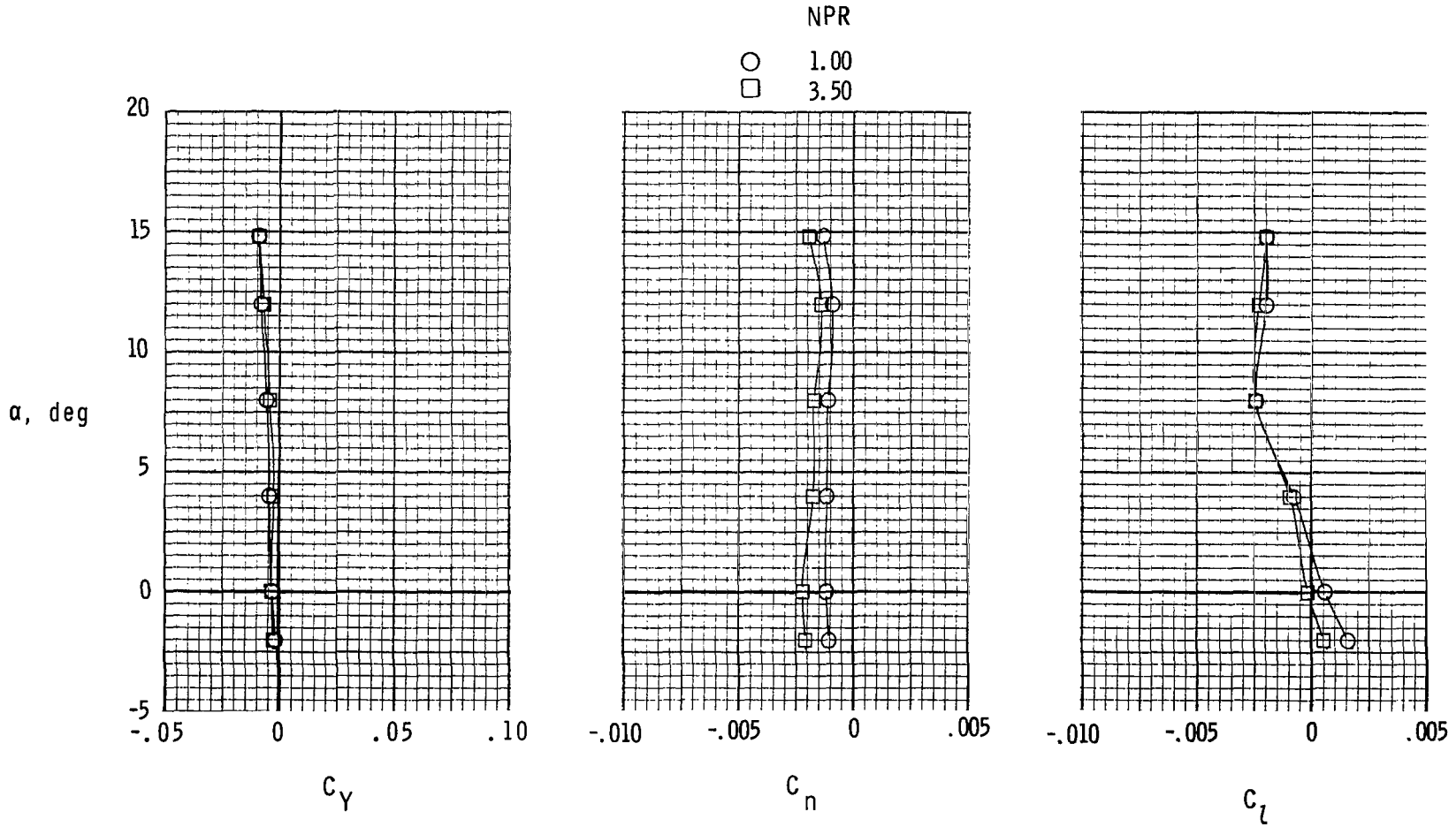

(a) M = 0.60.

Figure 28.- Lateral-directional characteristics of configuration with reversers fully deployed (δ_{REV} = 130°), vertical tails and horizontal tails removed, and β = 0°.

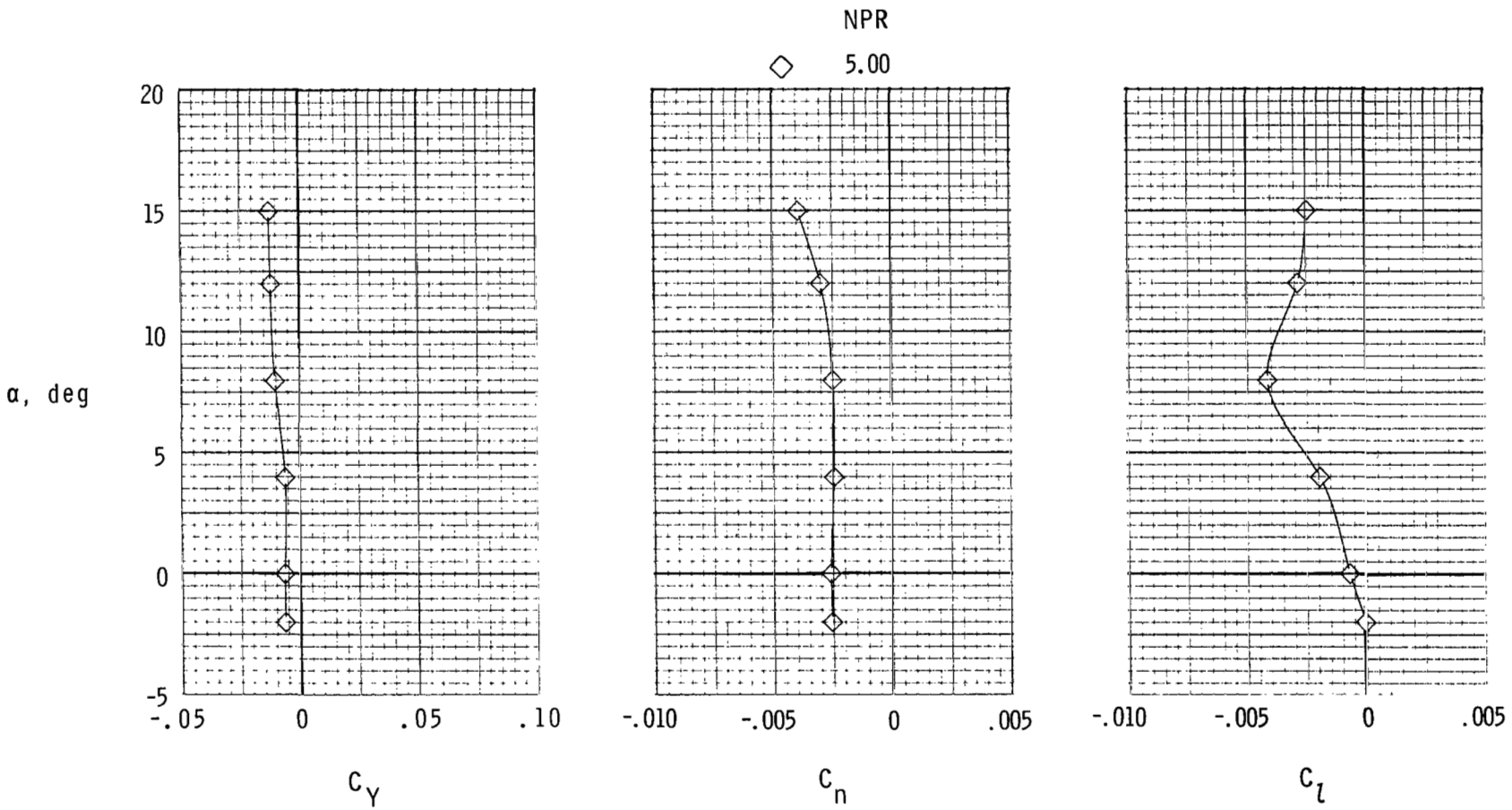

(b) M = 0.90.

Figure 28.- Concluded.

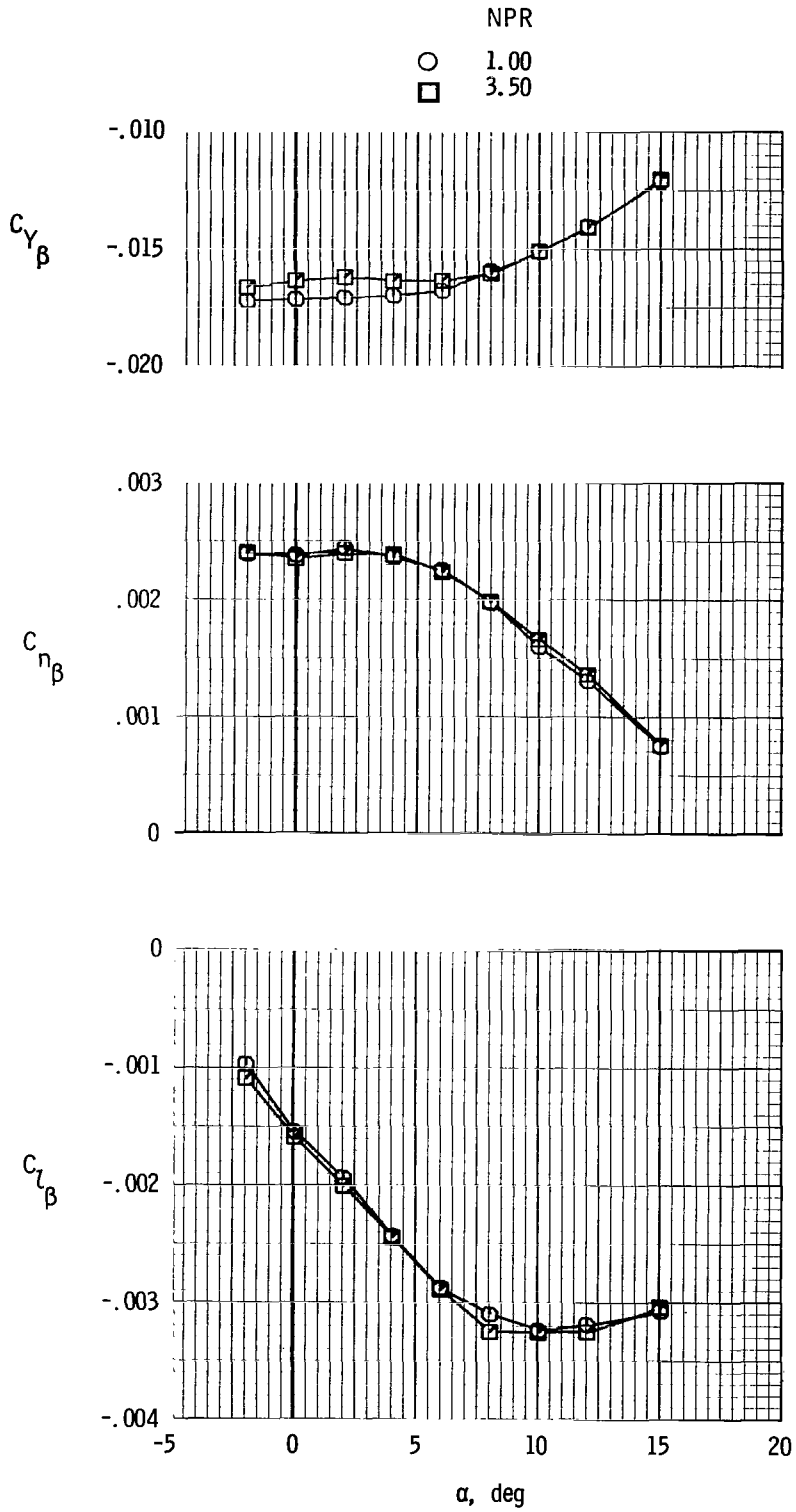

(a) M = 0.60.

Figure 29.- Static stability derivatives of baseline configuration with axisymmetric nozzles and $\delta_R = 0°$.

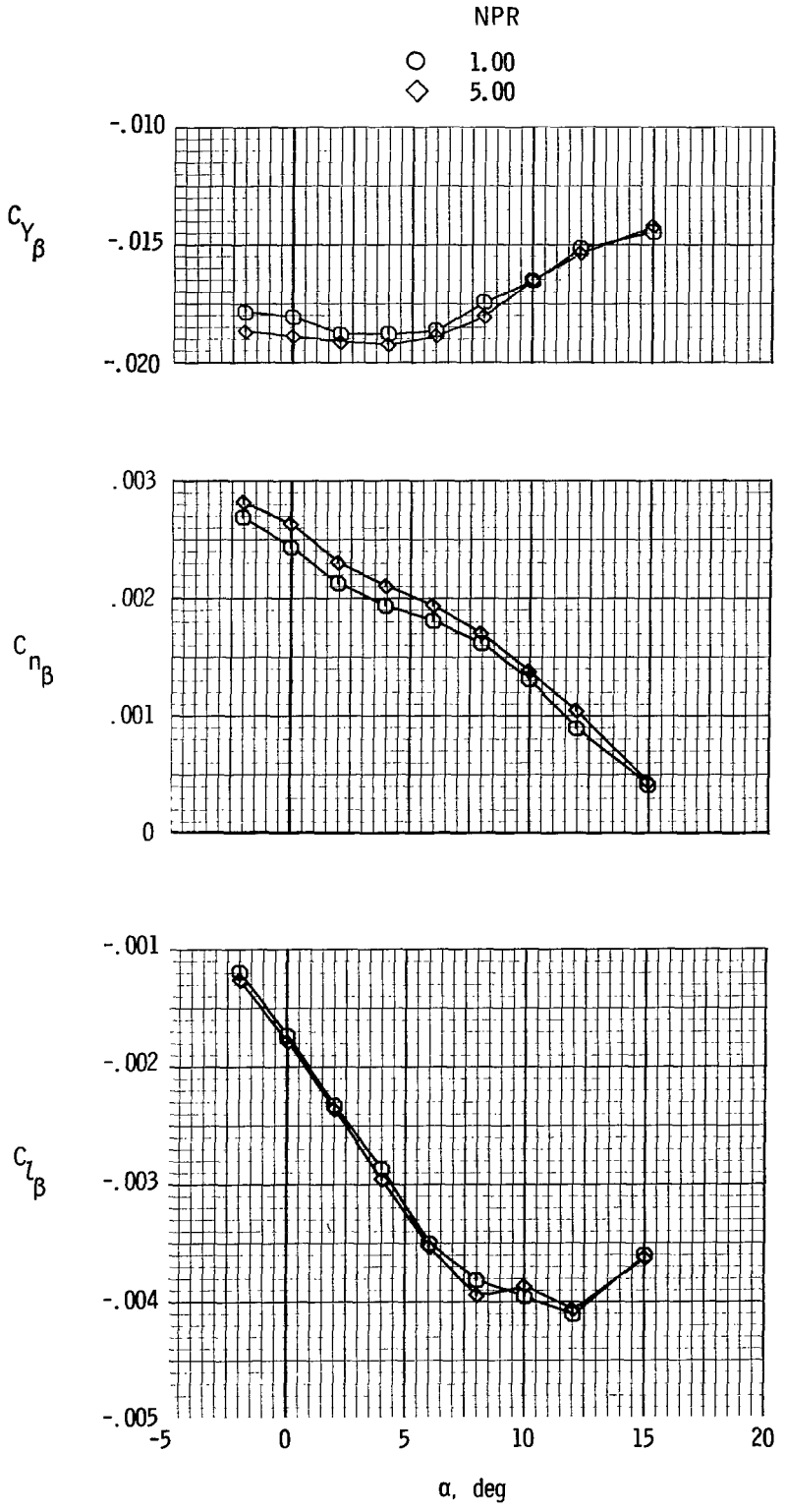

(b) M = 0.90.

Figure 29.- Concluded.

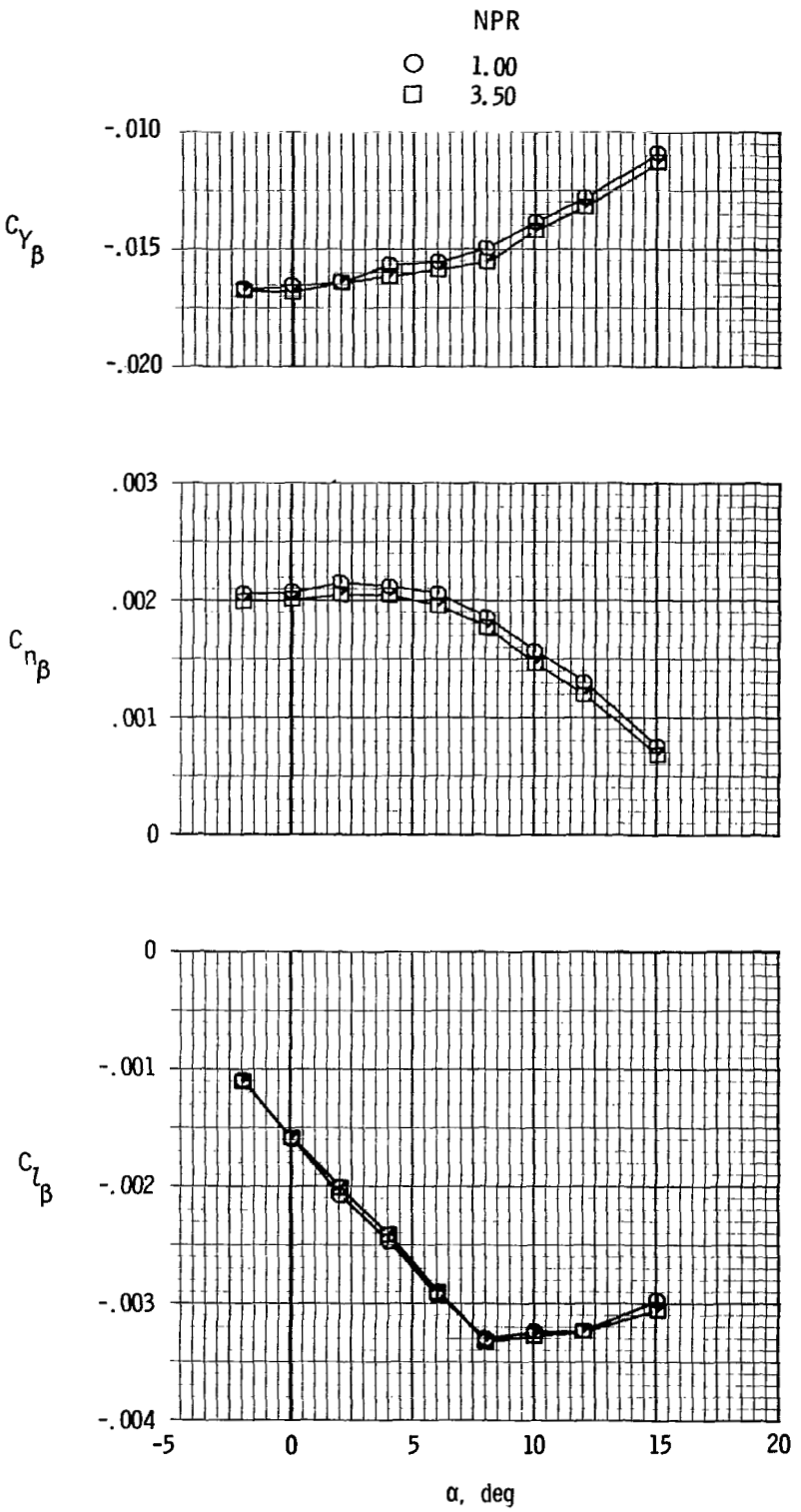

(a) M = 0.60.

Figure 30.- Static stability derivatives of configuration with 2-D C-D nozzles and $\delta_R = 0°$.

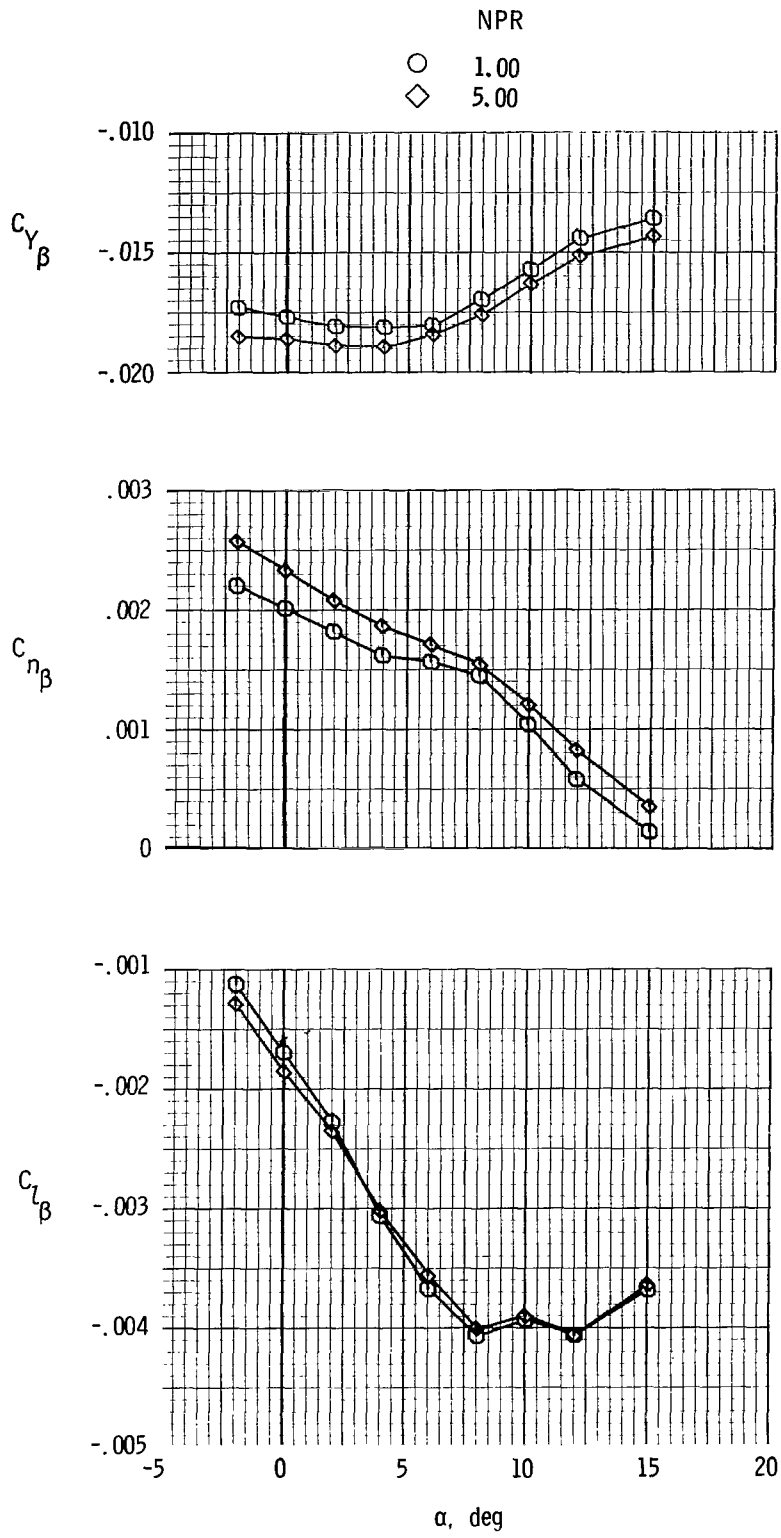

(b) M = 0.90.

Figure 30.- Concluded.

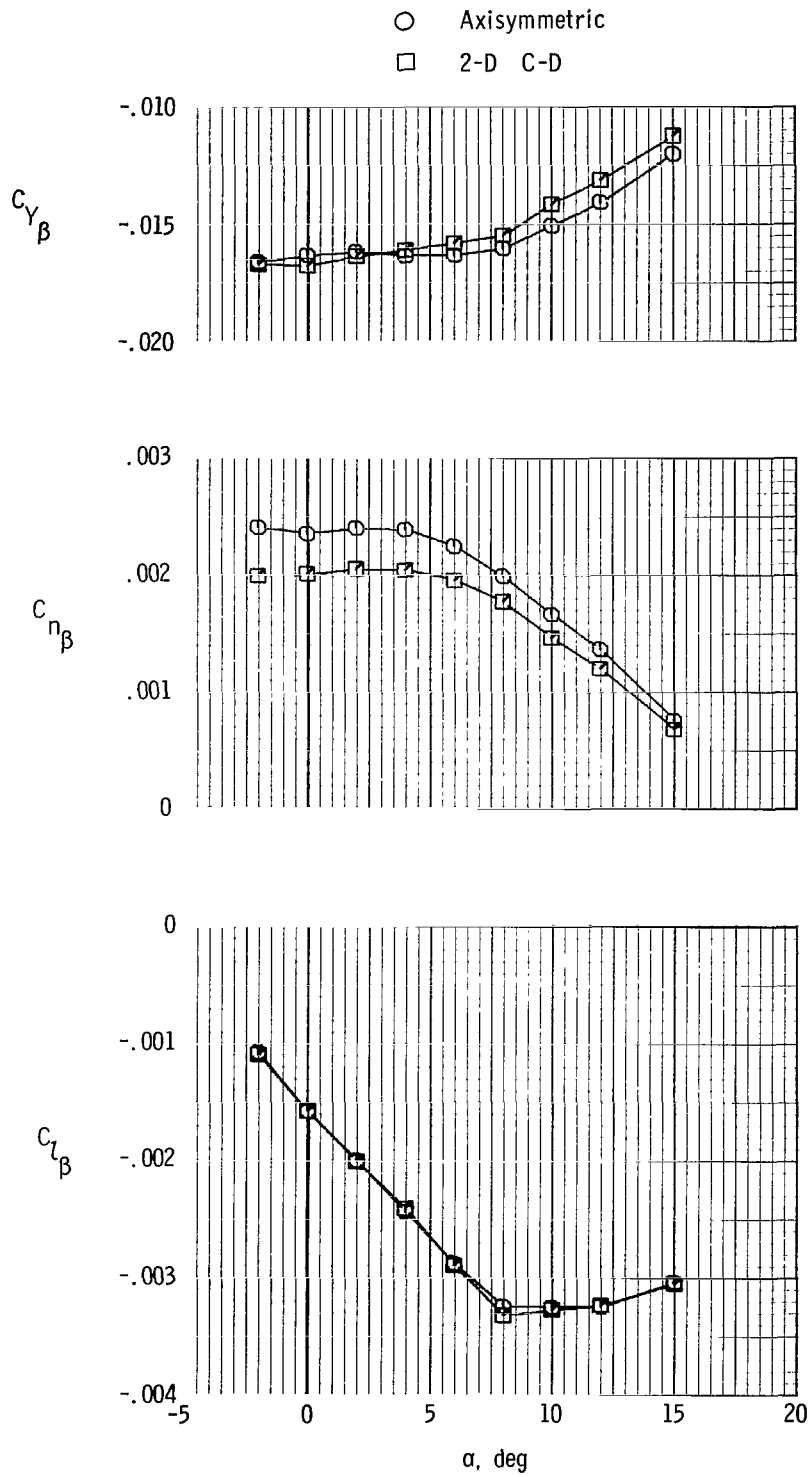

(a) M = 0.60.; NPR = 3.50.

Figure 31.- Effect of axisymmetric and 2-D C-D afterbody/nozzle shapes on static stability derivatives with $\delta_R = 0°$ and $\delta_{REV} = 0°$.

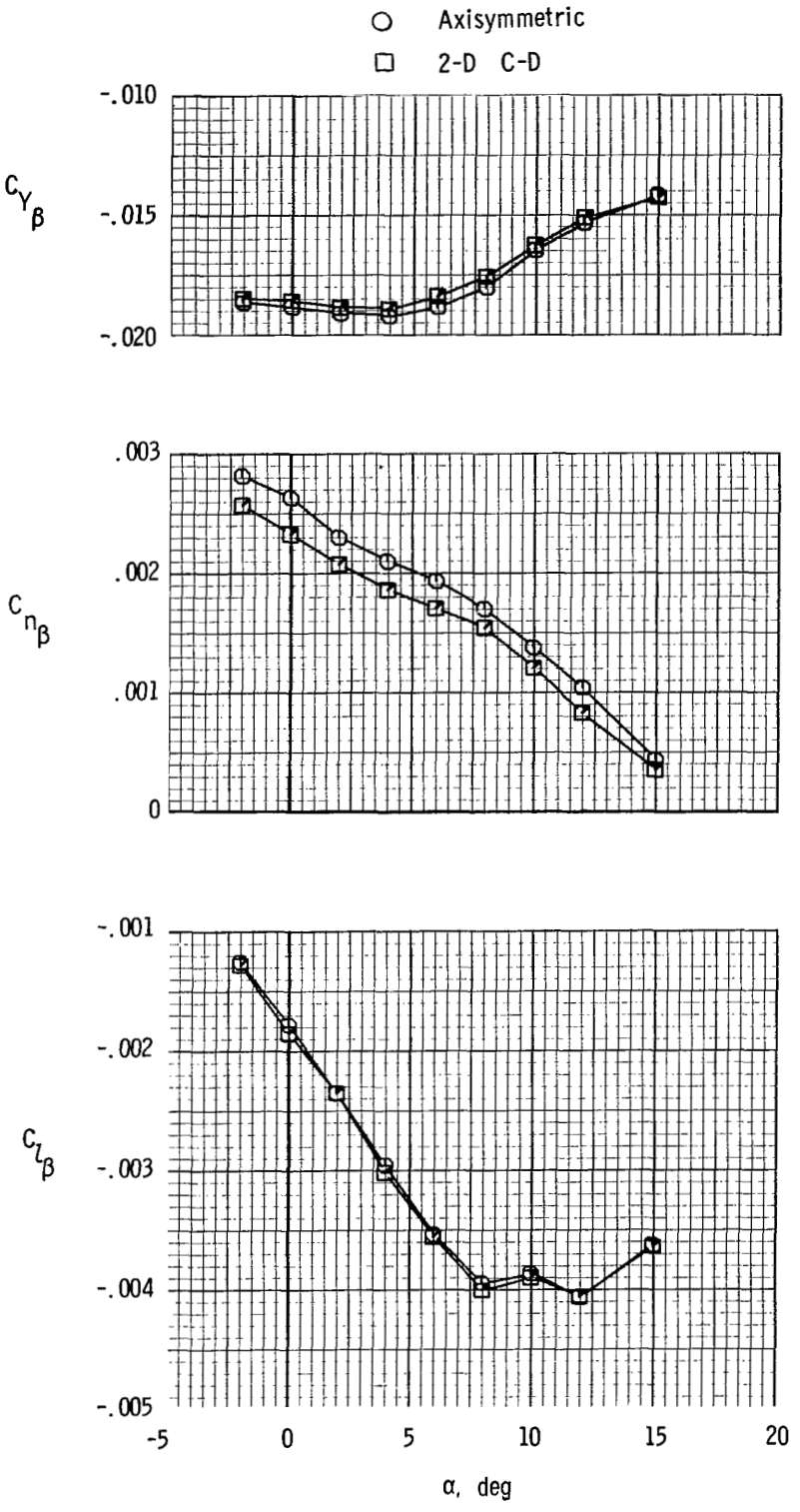

(b) M = 0.90; NPR = 5.00.

Figure 31.- Concluded.

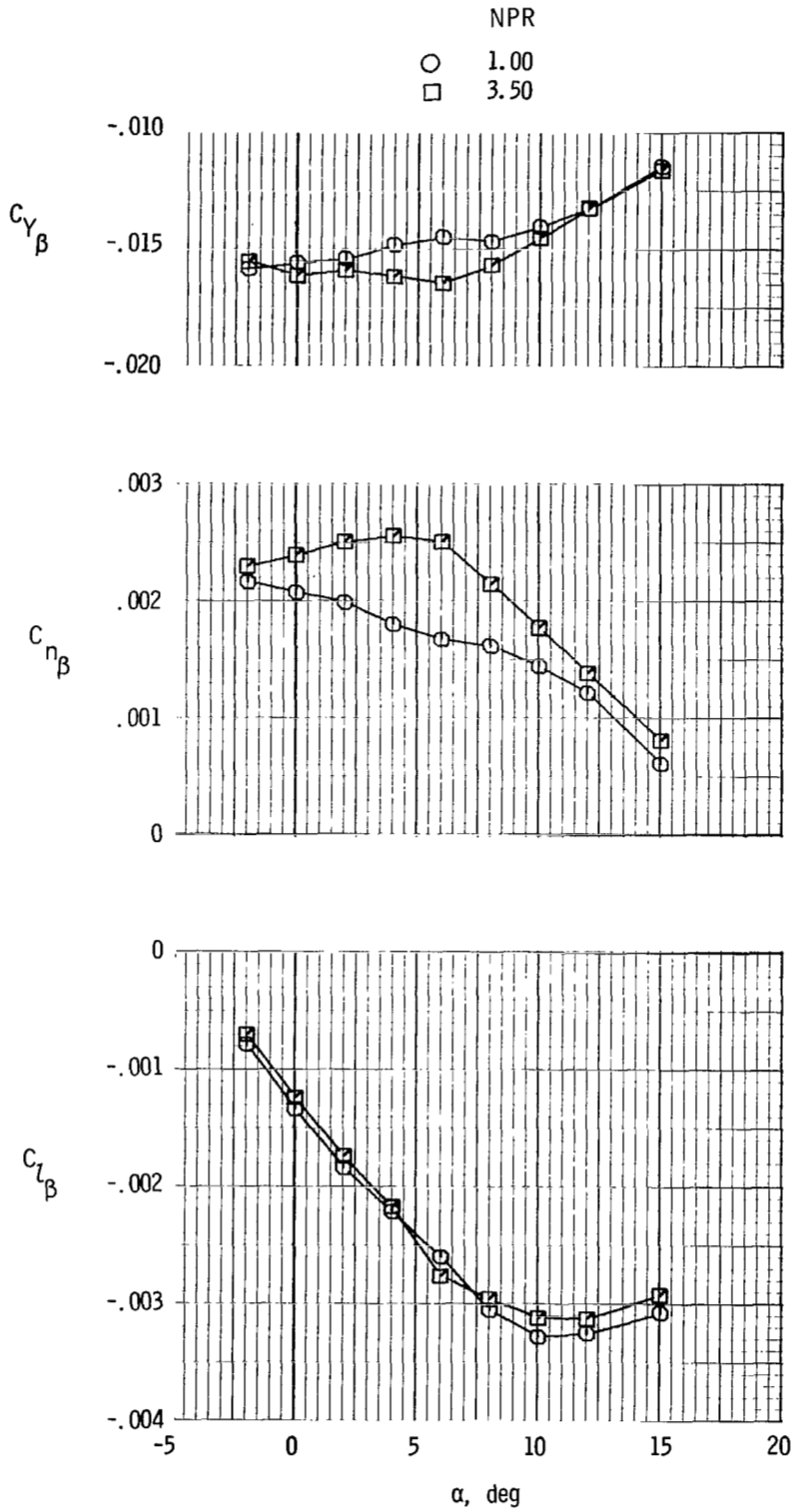

(a) M = 0.60.

Figure 32.- Static stability derivatives of configuration with 2-D C-D nozzles, reversers partially deployed (δ_{REV} = 90°), and δ_R = 0°.

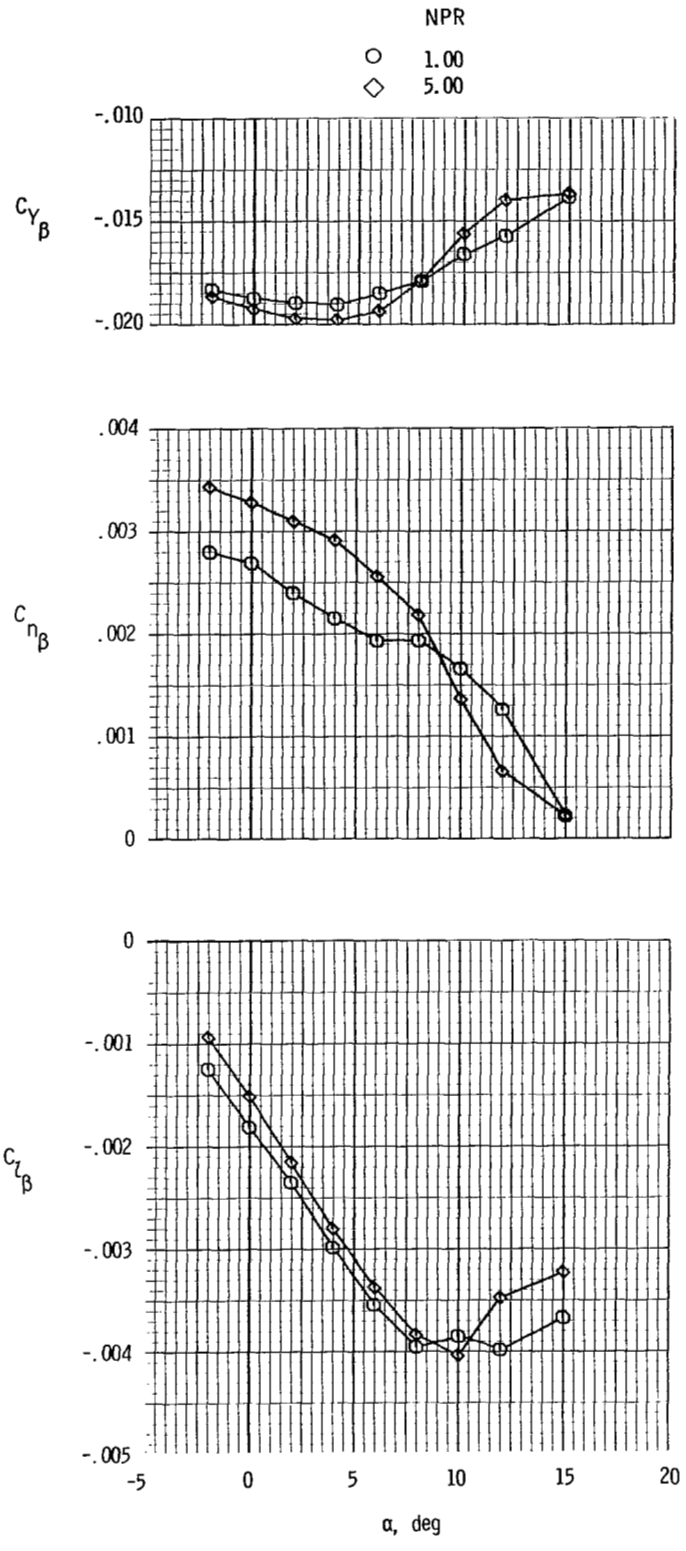

(b) M = 0.90.

Figure 32.- Concluded.

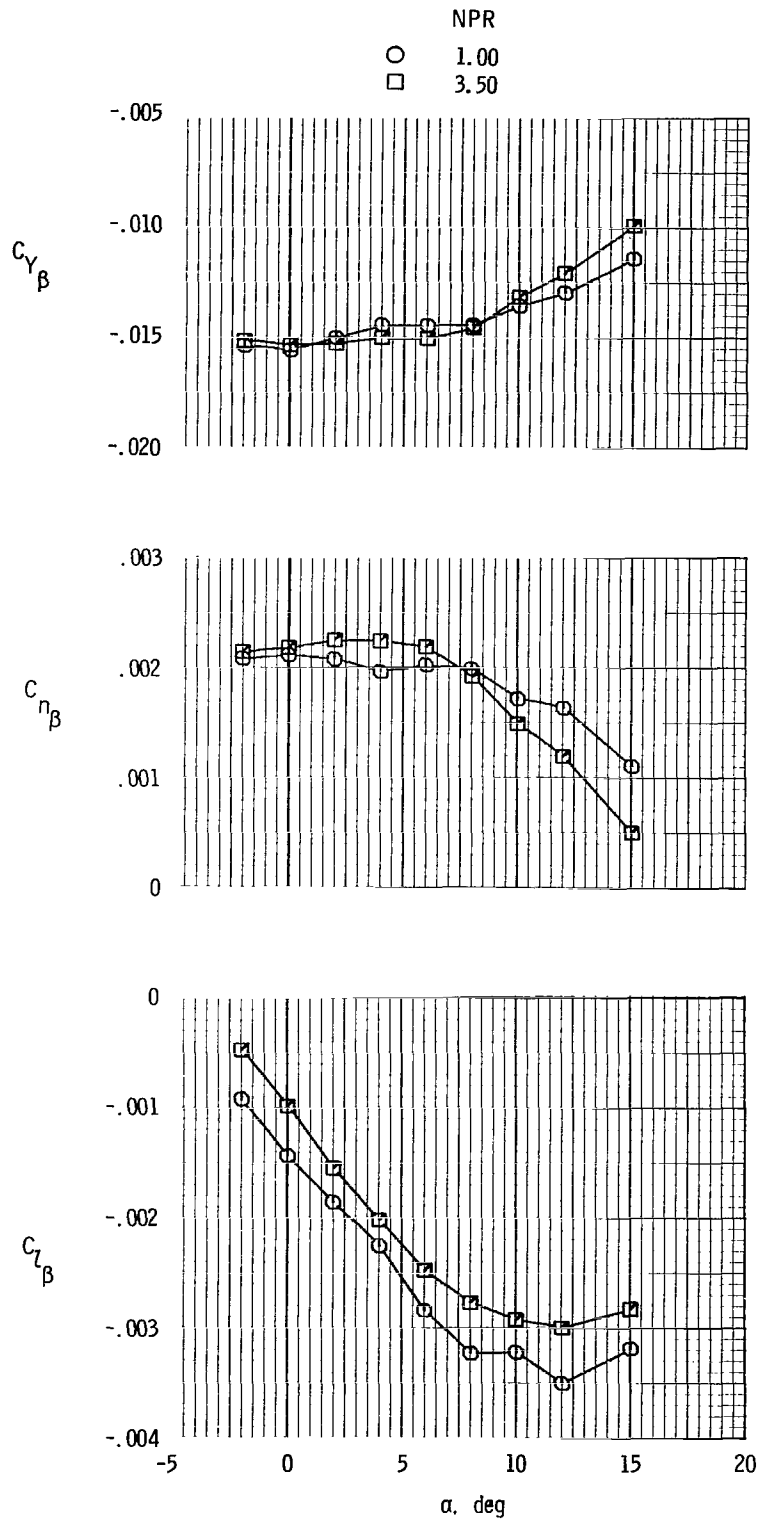

(a) M = 0.60.

Figure 33.- Static stability derivatives of configuration with 2-D C-D nozzles, reversers fully deployed (δ_{REV} = 130°) and δ_R = 0°.

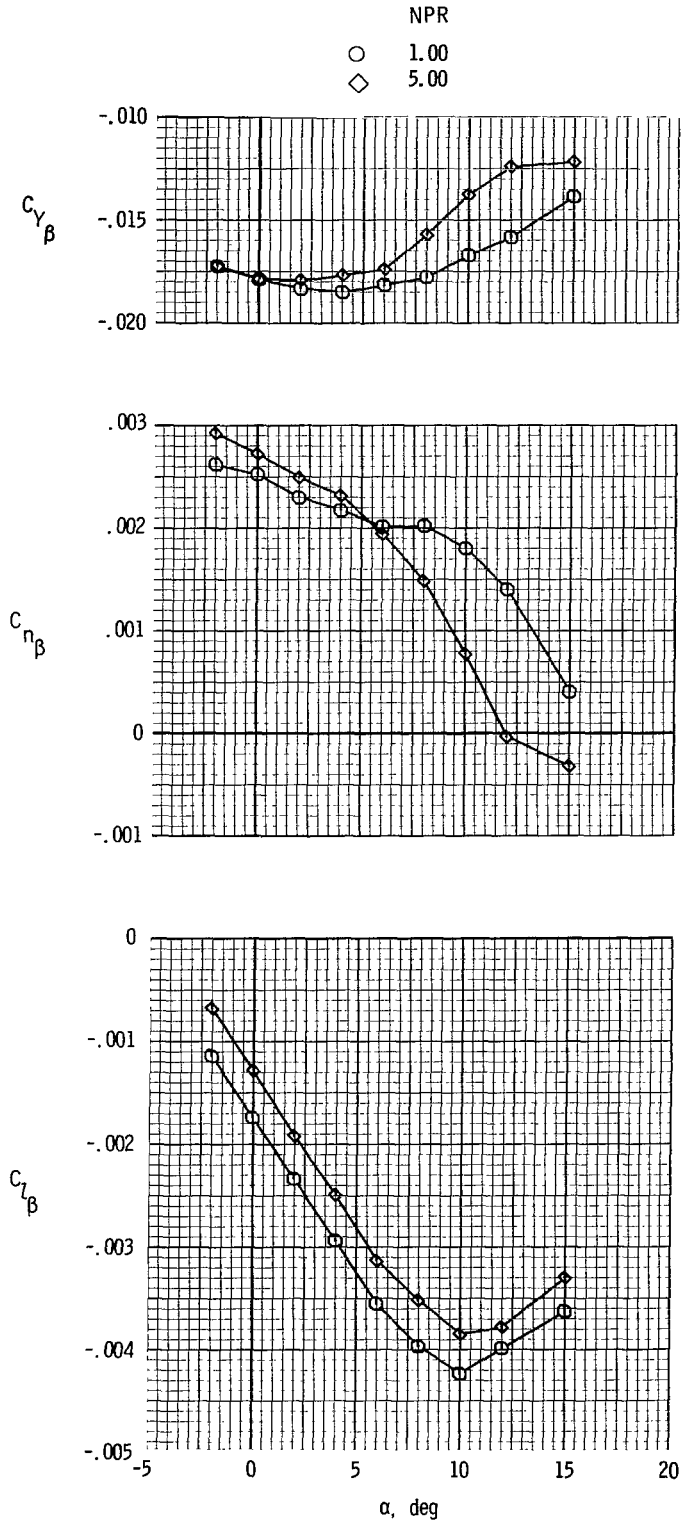

(b) M = 0.90.

Figure 33.- Concluded.

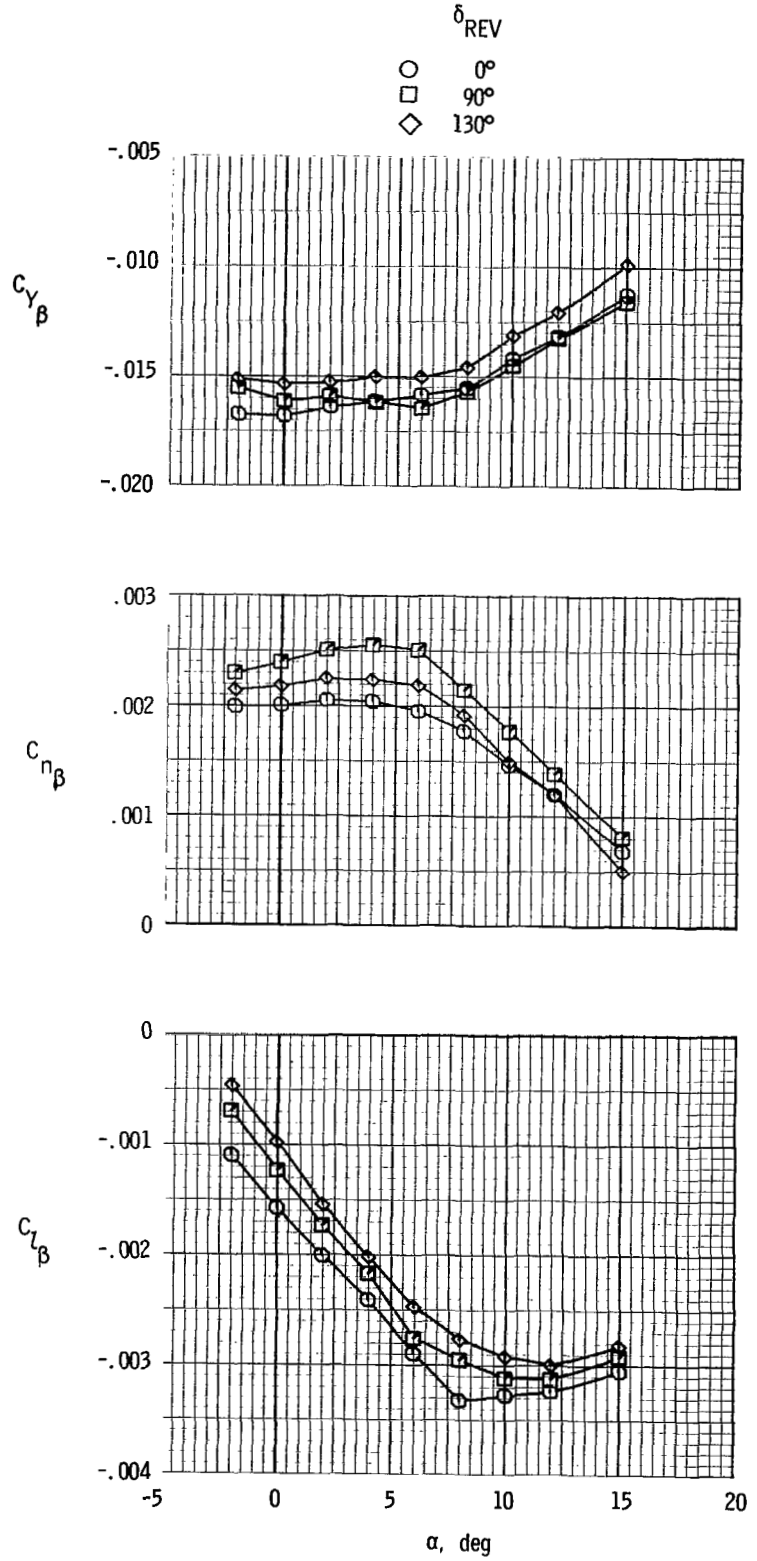

(a) M = 0.60; NPR = 3.50.

Figure 34.- Effect of thrust reversers on static stability derivatives of configuration with 2-D C-D nozzles and $\delta_R = 0°$.

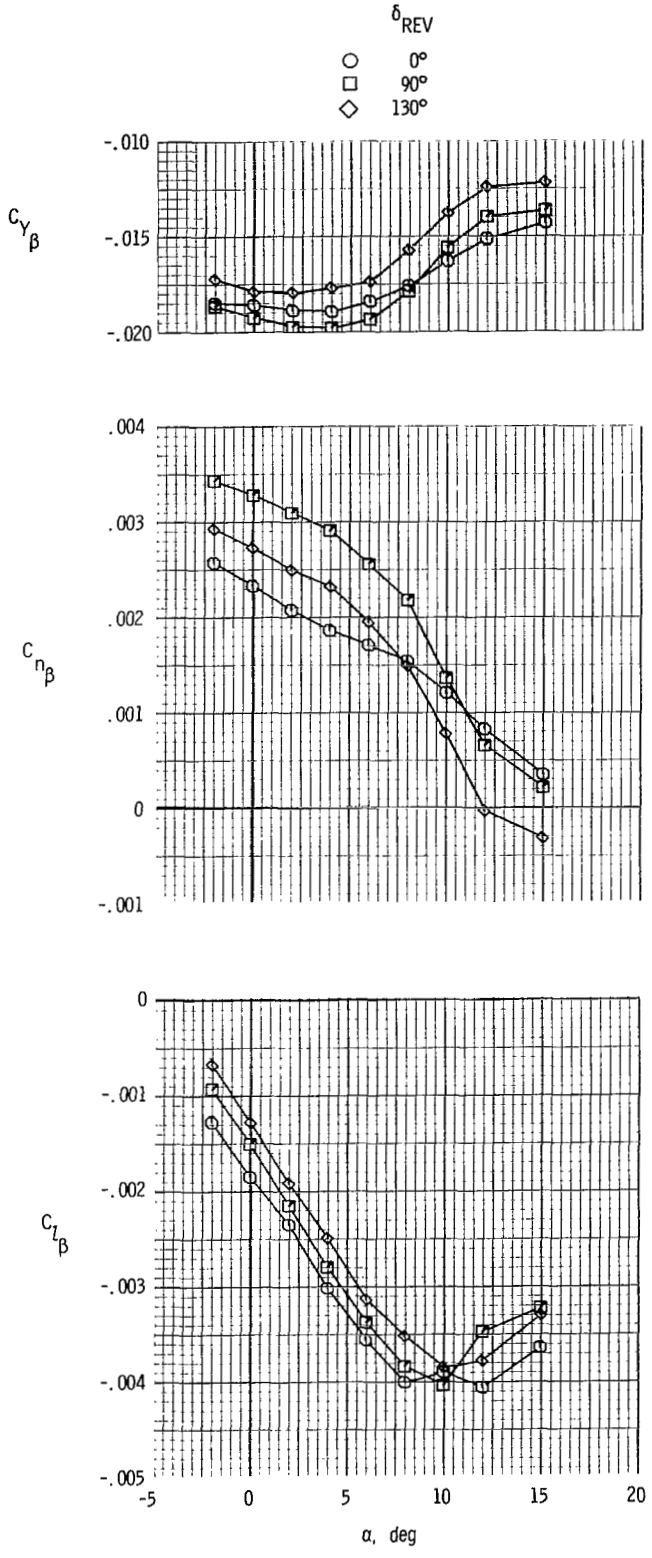

(b) M = 0.90; NPR = 5.00.

Figure 34.- Concluded.

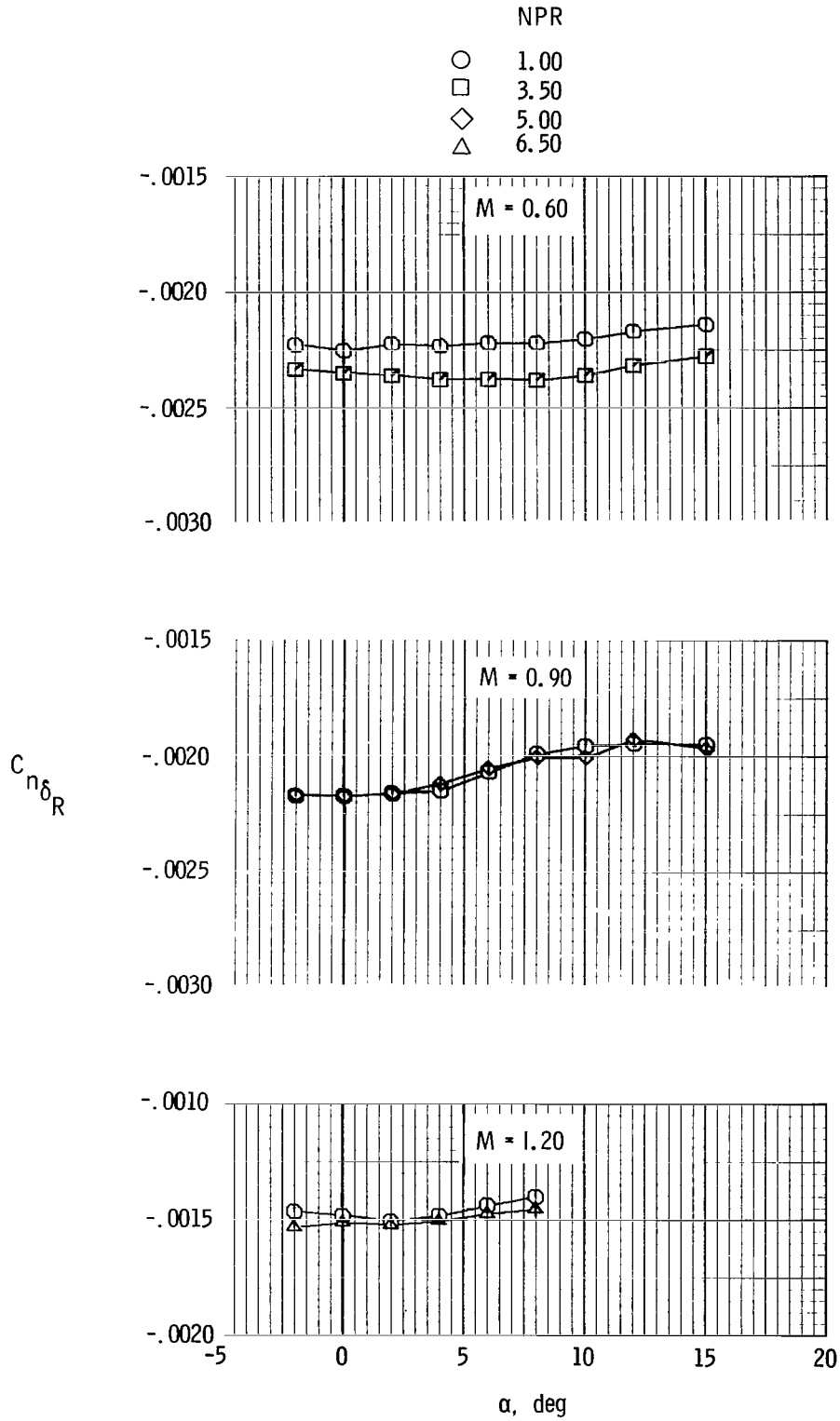

Figure 35.- Rudder power for configuration with 2-D C-D nozzles, $\beta = 0°$, and $\delta_{REV} = 0°$.

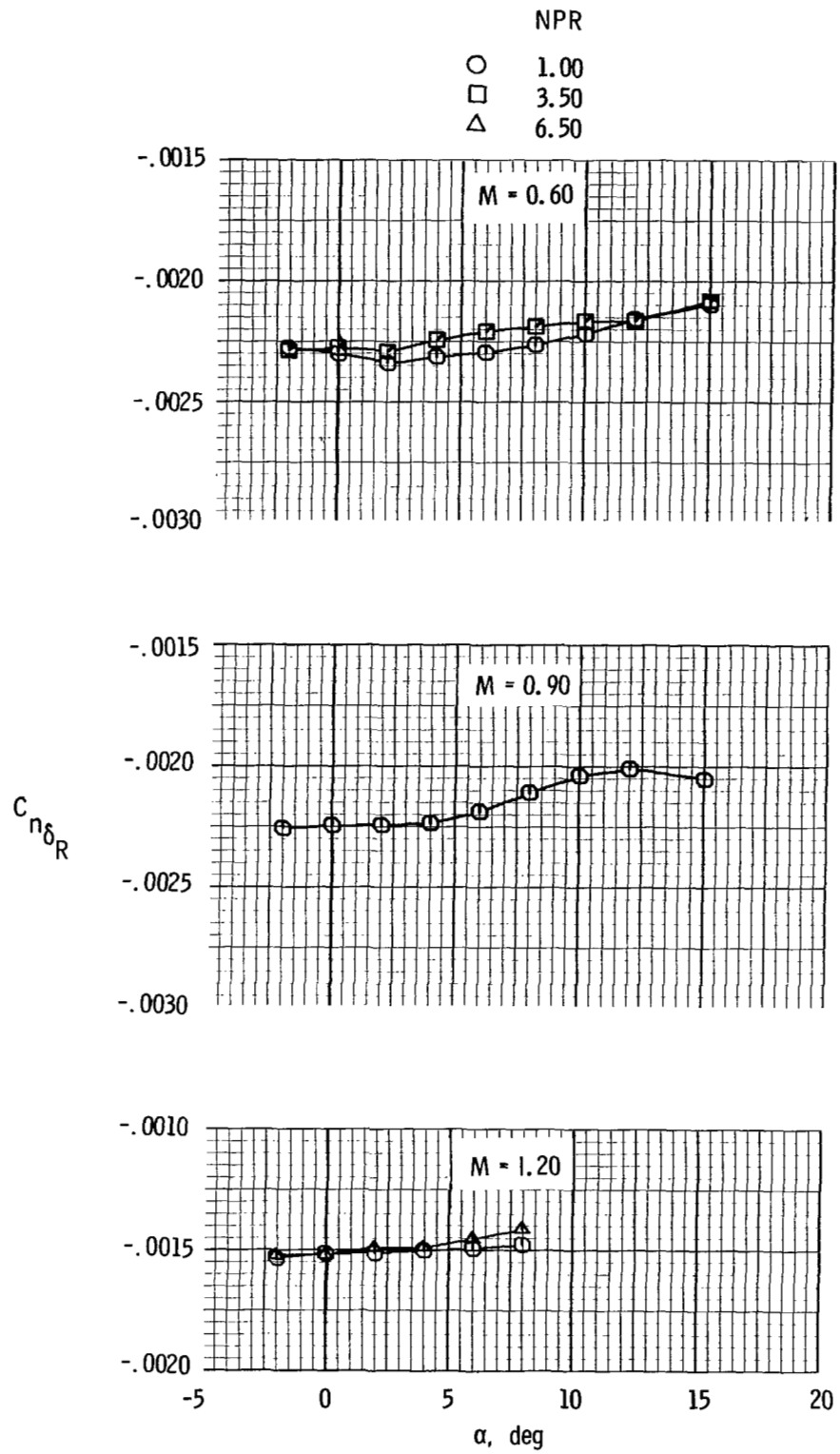

Figure 36.- Rudder power for configuration with 2-D C-D nozzles, $\beta = 0°$, and $\delta_{REV} = 90°$.

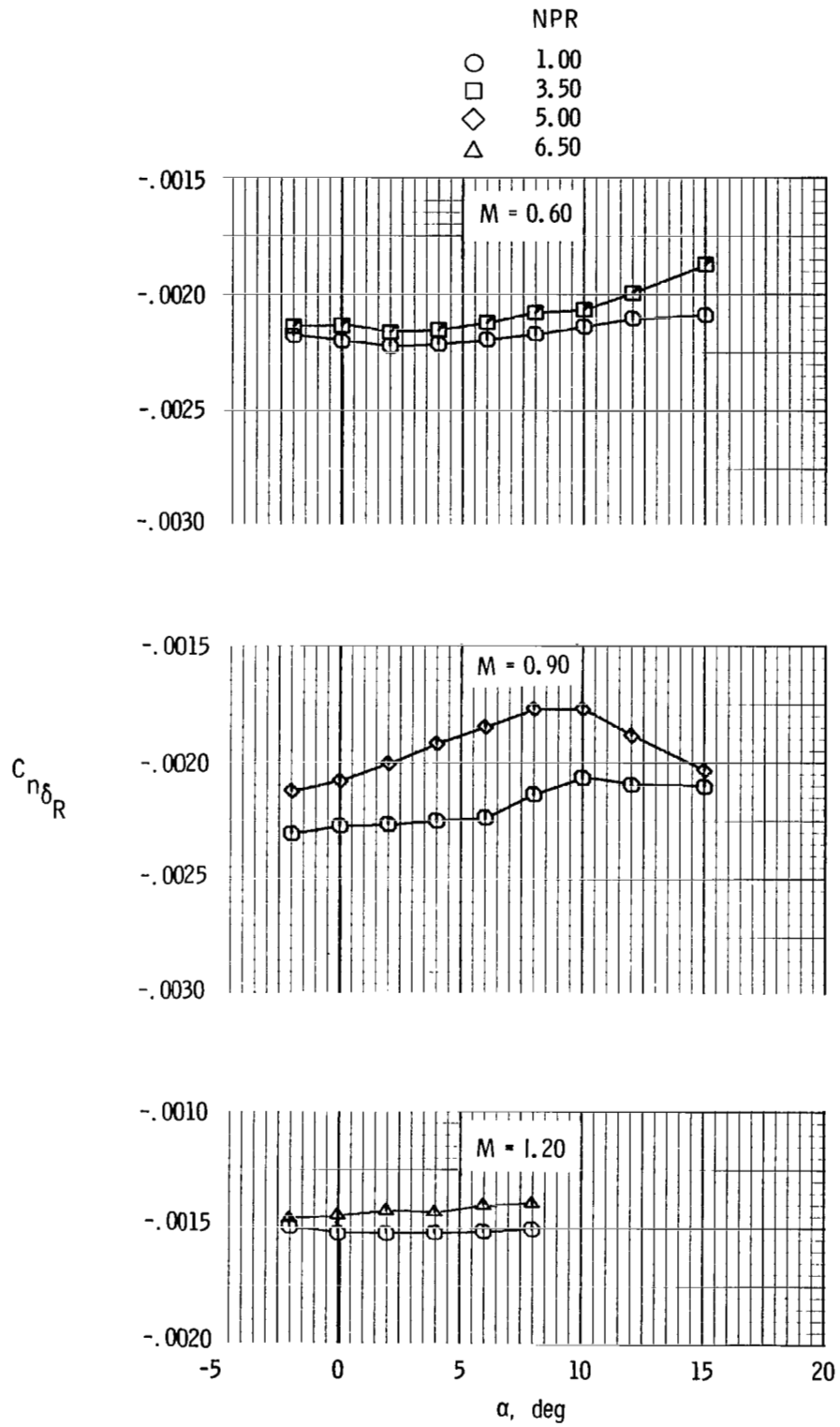

Figure 37.- Rudder power for configuration with 2-D C-D nozzles, $\beta = 0°$, and $\delta_{REV} = 130°$.

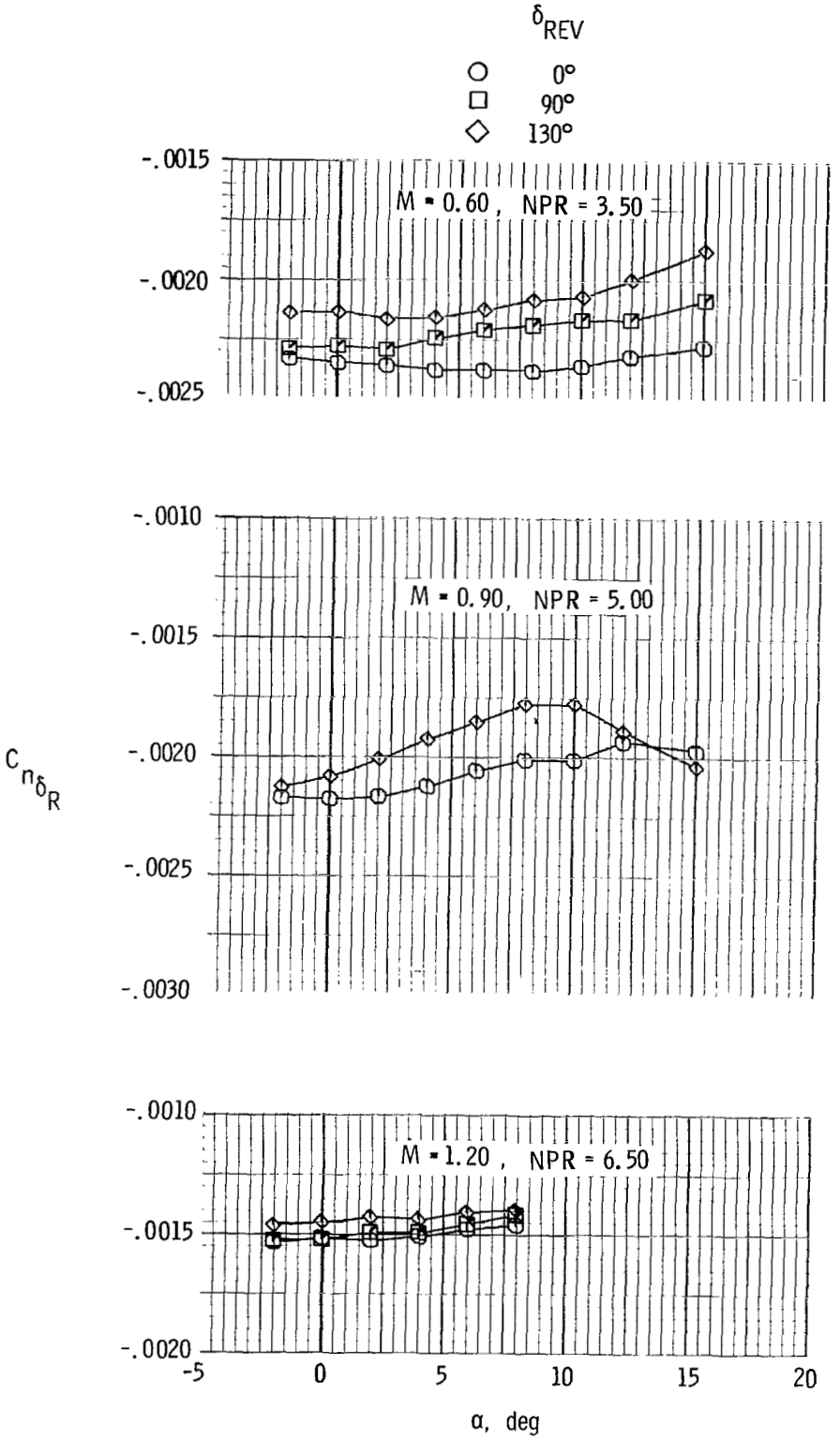

Figure 38.- Effect of thrust reversers on directional control of configuration with 2-D C-D nozzles, and $\beta = 0°$.

1. Report No.	2. Government Accession No.	3. Recipient's Catalog No.
NASA TP-2234		

4. Title and Subtitle	5. Report Date
EFFECT OF THRUST REVERSER OPERATION ON THE LATERAL-DIRECTIONAL CHARACTERISTICS OF A THREE-SURFACE F-15 MODEL AT TRANSONIC SPEEDS	December 1983
	6. Performing Organization Code 505-43-23-01
7. Author(s) E. Ann Bare and Odis C. Pendergraft, Jr.	8. Performing Organization Report No. L-15648
	10. Work Unit No.
9. Performing Organization Name and Address NASA Langley Research Center Hampton, VA 23665	11. Contract or Grant No.
	13. Type of Report and Period Covered Technical Paper
12. Sponsoring Agency Name and Address National Aeronautics and Space Administration Washington, DC 20546	14. Sponsoring Agency Code

15. Supplementary Notes

16. Abstract

An investigation was conducted in the Langley 16-Foot Transonic Tunnel to determine the lateral-directional aerodynamic characteristics of a fully metric 0.047-scale model of the F-15 three-surface configuration (canards, wing, horizontal tails) with twin two-dimensional (2-D) nozzles and twin axisymmetric nozzles installed. The effects of 2-D nozzle in-flight thrust reversing and rudder deflection were also determined. Test data were obtained at static conditions and at Mach numbers from 0.60 to 1.20 over an angle-of-attack range from -2° to 15°. Reynolds number varied from 2.6×10^6 to 3.8×10^6. Angle of sideslip was set at approximately 0° and -5° for all configurations and at -10° for selected configurations.

17. Key Words (Suggested by Author(s))	18. Distribution Statement
Two-dimensional nozzles Thrust reversers Propulsion effects Rudder effectiveness Twin vertical tails	Unclassified - Unlimited Subject Category 02

19. Security Classif. (of this report)	20. Security Classif. (of this page)	21. No. of Pages	22. Price
Unclassified	Unclassified	89	A05

For sale by the National Technical Information Service, Springfield, Virginia 22161

NASA-Langley, 1983

D 1 IJ.A, 831207 S00903DS
DEPT OF THE AIR FORCE
AF WEAPONS LABORATORY
ATTN: TECHNICAL LIBRARY (SUL)
KIRTLAND AFB NM 87117